Article

Not peer-reviewed version

Techno-Economic Assessment (TEA) and Sensitivity Analysis of Geothermal Power in Oman Using SAM (System Advisor Model)

Osama A. Marzouk *

Posted Date: 5 May 2026

doi: 10.20944/preprints202605.0188.v1

Keywords: Oman; geothermal; system advisor model; levelized cost of energy; techno-economic

 doi:10.20944/preprints202605.0188.v1

Article

Techno-Economic Assessment (TEA) and Sensitivity Analysis of Geothermal Power in Oman Using SAM (System Advisor Model)

Osama A. Marzouk

College of Engineering, University of Buraimi, Al Buraimi, Postal Code 512, Sultanate of Oman; osama.m@uob.edu.om

Abstract

The Sultanate of Oman enjoys plenty of solar energy and wind energy; both have been exploited successfully in the country. However, geothermal energy has not been exploited yet in Oman. This natural heat source deserves more studies to assess its technical potential and economic feasibility compared to other electricity generation technologies in Oman. The current study fills this gap by presenting a techno-economic assessment (TEA) of a small 30-MW geothermal power plant in Oman, operating on a binary (two-fluid) cycle, with a drilling depth of 2 km. The analysis was performed using the renowned software tool SAM (System Advisor Model) of the United States National Renewable Energy Laboratory (NREL). The current results suggest a levelized cost of energy (LCOE) of 8.68 cents/kWh (0.0868 US$/kWh) or 33.4 baisa/kWh (0.0334 OMR/kWh). When compared with electricity tariff or solar photovoltaic (PV) power purchase agreement (PPA) rates in Oman, it was found that geothermal-based electricity is too expensive. Furthermore, the estimated geothermal LCOE is more than three times the LCOE value of self-owned photovoltaic (PV) power systems in Oman, which is around 10 baisa/kWh (0.010 OMR/kWh). The estimated first-year electricity generation for the geothermal power plant model is 261.268 GWh/year, leading to a specific electricity generation of 8,709 kWh/kW/year. This is about five times the specific power generation from PV power plants. The study is augmented by sensitivity analyses and regression models to help understand the impact of multiple input parameters. The study provides novel results regarding decision-making for geothermal power investment in Oman.

Keywords: Oman; geothermal; system advisor model; levelized cost of energy; techno-economic

---

1. Nomenclature (In Alphabetical Order)

¢	American cent (100 ¢ = 1 US$)
AC	Alternating current (of electricity)
atm	Standard atmosphere (a pressure unit) [1,2]
baisa	One-thousandth of an Omani rial (1,000 baisa = 1 Omani rial)
BP	Boiling point (boiling temperature) [3,4]
Bz	Abbreviation for baisa
CAD	Computer-aided design
CAE	Computer-aided engineering
CBO	Central Bank of Oman
CF	Capacity factor
CFD	Computational fluid dynamics
CRT	Cost reflective tariff
DOE	United States Department of Energy
EAR	East African Rift [5,6]
EC	European Commission
EPC	Engineering, procurement, and construction

 doi:10.20944/preprints202605.0188.v1

epw	EnergyPlus [7–14] Weather (file format)
EU	European Union
GCR	Ground coverage ratio [15–17]
GDP	Gross domestic product
GEM	Global Energy Monitor
GETEM	Geothermal Electricity Technology Evaluation Model
GGPT	Global Geothermal Power Tracker
GHG	Greenhouse gas
GMT	Greenwich Mean Time
GTO	Geothermal Technologies Office (under the United States Department of Energy)
HT	High tension
HV	High voltage (same as HT)
ISA	International Standard Atmosphere
JRC	Joint Research Centre [18,19]
kV	kilovolt
LCOE	Levelized cost of electricity or energy [20–27]
LT	Low tension
LV	Low voltage (same as LT)
MSL	Mean sea level
MT	Medium tension
MV	Medium voltage (same as MT)
OMR	Omani rial
PDO	Petroleum Development Oman
PES	Primary energy supply [28–32]
pp	Percentage point
PPA	Power purchase agreement [33–37]
ppm	Part per million (for water salinity, by mass)
PV	Photovoltaic
PVGIS	Photovoltaic Geographical Information System
NREL	United States National Renewable Energy Laboratory
SAM	System Advisor Model
SOR	Secondary oil recovery
TDS	Total dissolved solids
TEA	Techno-economic assessment
TEG	Thermoelectric generator
TMY	Typical meteorological year [38–42]
WOR	Water-oil-ratio

2. Introduction

2.1. Geothermal Energy as a Natural Heat Source

Volcanoes can cause significant geophysical and environmental impacts. Yet, volcanoes are reminders of a colossal source of geothermal heat [43] available in the underground layers of the Earth [44]. The hot lava erupting from a volcano onto the Earth's surface are no more than molten rocks (magma) that were able to find an opening in the Earth’s surface to come out [45], with high temperatures (exceeding 1,100 °C) [46], as a viscous flow of molten minerals, moving slowly over the ground until it cools and solidifies as rocks [47].

The geothermal heat stems from the molten Earth’s core, with energy released due to the decay of unstable radioactive elements [48], which lose mass in the form of energy [49]. This heat is transferred toward the Earth’s surface by both heat conduction and heat convection [50]. This leads to a natural shallow temperature gradient radially [51], causing subsurface temperature to increase when drilling deep beneath the Earth’s surface. This heating process occurs so slowly (over billions

 doi:10.20944/preprints202605.0188.v1

of years) and involves relatively abundant long-lived radioactive isotopes, especially ^{40}K, ^{232}Th, ^{235}U, and ^{238}U. Therefore, geothermal heat energy is treated as a renewable energy source [52].

Rainwater is collected in underground reservoirs (upon meeting an impermeable geological layer that impedes further seepage through sands, porous or fractured rocks, and small holes) [53]. This trapped underground water is heated due to the conduction heat transfer, and this heating can be sufficient to transform this water into very hot liquid water or even to vaporize a fraction of it to be in the form of hot water vapor (steam) [54], with temperatures exceeding 300 °C (depending on the depth below the Earth's surface). This process establishes a hydrothermal resource (a natural geothermal resource) of energy in the form of hot liquid water and/or steam [55].

Geothermal energy is among the minor renewable energy sources [56], which are those sources not widely exploited (such as wave energy [57], crop-based biofuels [58], and tidal energy [59]). Compared to the three major renewable energy sources (photovoltaic solar energy [60], wind energy [61], and hydroelectric energy [62]), geothermal energy is much underutilized globally. However, there are promising examples of countries that heavily invest in geothermal energy. For example, Kenya in 2022 had the largest percentage share of geothermal-based electricity generation, which was about 45% [63]. This can be attributed to the high capacity factor (above 95%) and the reliability [64] of geothermal power in Kenya. Kenya is located along the East African Rift (EAR) [65], which is the most active and largest continental rift in the world [66]. This location enables the formation of hot shallow geothermal reservoirs [67–70]. This geological feature of Kenya offers ideal subsurface conditions for extracting underground steam near the surface. As a result, exploration and development are relatively feasible economically.

Iceland is another admirable example where geothermal energy is a sizeable contributor to the country's energy mix [71]. The country depends strongly on renewable energy [72]. In 2014, 66% of Iceland's primary energy use came from geothermal sources [73]. In 2015, renewable energy accounted for nearly all the electricity generation in Iceland, with about 27% of this generation coming from geothermal power, and 73% coming from hydropower [74]. In 2023, the electricity generation mix in Iceland had a share of 70.3% from hydropower and a share of 29.7% from geothermal power. Thus, it was 100% from a renewable primary energy supply (PES) [75].

2.2. Advantages of Geothermal Energy

Carbon dioxide (CO_2) emissions from geothermal power systems are possible, and these emissions contribute to the greenhouse gas (GHG) effect by absorbing reflected radiation from the Earth [76], in a phenomenon known as downwelling radiation [77]. However, they are still generally low when compared to traditional baseload (continuously running at approximately a steady output) thermal power systems that involve the combustion of fossil fuels [78].

Geothermal resources have advantages compared to other natural energy resources. Compared to solar radiation [79], winds [80], and thermally-induced draft; geothermal reservoirs are constantly available during the 24 hours of the day. This means that a geothermal power plant may operate with a high capacity factor (CF) in excess of 90% [81]. This is much higher than typical capacity factors in wind power, which are around 30% [82], and also much higher than typical capacity factors in solar photovoltaic (PV) power, which are around 20% [83]. Baseload hydropower plants can achieve high capacity factors like geothermal power plants [84], although some hydropower units can also have low capacity factors comparable to those of wind power units [85].

The capacity factor is defined as [86]

$$\mathrm{CF} = \frac{\text{electric energy generated during one year (kWh/year)}}{\text{nameplate capacity (kW)} \times 8{,}760\ \text{(hours/year)}} \tag{1}$$

Compared to hydropower [87], geothermal reservoirs are local sources of energy, instead of depending on a river whose source can be in another country or a faraway domestic territory that is located outside local control and direct management. This is another advantage of geothermal power.

Because geothermal power systems utilize a heat source located deeply beneath the ground surface, these systems have smaller footprints and less impact on surface ecosystems compared to

 doi:10.20944/preprints202605.0188.v1

many other power systems of either the renewable energy category or the conventional fossil-fuel-based category [88]. Table 1 compares the estimated required land area per generated gigawatt-hour (GWh) of electricity using different electricity generation technologies. It can be seen that a geothermal power plant may demand only 30.3% (1/3.30) of what a wind power plant demands, only 12.5% (1/8.01) of what a solar photovoltaic (PV) power plant demands, only 11.1% (1/9.01) of what a coal-fired thermal power plant demands, and only 5.05% (1/19.80) of what a gas-fired thermal power plant demands.

Table 1. Comparison of power plant technologies in terms of land needs per unit energy (1 GWh) of electricity produced.

Power plant type	Needed land per GWh annually	Land needs of other technologies relative to geothermal plants	Geothermal land use as % of other technologies	Reference
Geothermal	404 m^2	1.00	100%	[89]
Wind	1,335 m^2	3.30	30.3%	[89]
Solar photovoltaic	3,237 m^2	8.01	12.5%	[89,90]
Coal-fired	3,642 m^2	9.01	11.1%	[89]
Natural gas	8,000 m^2	19.80	5.05%	[91]

To further explain the meaning of the above table, a solar photovoltaic (PV) array with a specific power generation of 2,000 kWh/kW/year [92] is considered as an example. Because each kW occupies a module area of about 4.5 m^2 (assuming a module efficiency of 22.2%), this specific power generation can be converted approximately into 444 kWh/m^2(module area)/year. Assuming a ground coverage ratio (GCR) of 0.68, then this specific power generation becomes about 300 kWh/m^2(land)/year or 3×10^{-4} GWh/m^2(land). Inverting this factor gives 3,333 m^2(land)/GWh/year. This is close to the figure in the above table, which is 3,237 m^2(land)/GWh/year.

2.3. Drawbacks of Geothermal Energy

Geothermal energy utilization is not considered a significant source of greenhouse gas (GHG) emissions that cause global warming. Small amounts of carbon dioxide (CO_2) may be released from geothermal power plants during the energy conversion process due to the presence of dissolved gases contained in geothermal fluids [93]. Although geothermal emissions of carbon dioxide (CO_2) to the atmosphere do not involve combustion of a combustible fuel, they are still undesirable radiatively active gases [94] regardless of their clean origin.

Geothermal power plants may release hydrogen sulfide [95] (hydrogen sulphide) gas (H_2S), which is toxic.

Another limitation of geothermal energy is that it is geographically preferred in (but not restricted to) areas near tectonic plate boundaries [96].

The size of the geothermal reservoir (the amount of contained hot liquid water and/or steam) imposes a constraint regarding the duration over which it can actually be exploited [97]. Therefore, while geothermal energy can be described globally and theoretically as a renewable, sustainable source of heat; locally and practically, a naturally existing geothermal resource has a lifetime [98] like other groundwater sites [99], oil fields [100], and natural gas fields [101].

 doi:10.20944/preprints202605.0188.v1

One of the major concerns about geothermal power plants is the large upfront capital costs that need to be paid before any production [102]. These initial costs include the well drilling in order to access the deep geothermal reservoir [103], and such drilling costs are not present in photovoltaic (PV) solar power systems and wind power systems, for example. This is a major barrier against the wide deployment of geothermal power technology.

2.4. Status of Geothermal Energy in the World

It can be useful to describe the utilization level of the global geothermal energy. The source of data here is the Global Geothermal Power Tracker (GGPT) dataset [104–107] of the Global Energy Monitor (GEM) portal [108]. The data correspond to March 2025, and they were the latest available records at the time of preparing this text (December 2025). The dataset covers all geothermal units having a capacity of 1 MW and higher.

Figure 1 shows the Pareto chart representation of the geothermal power capacity of operating geothermal units in all countries with such operational geothermal units (total 27 countries having a total of 480 operating geothermal units). The global operational capacity is 16,173.41 MW. The top ten countries investing in the geothermal energy are: (1) United States, (2) Indonesia, (3) Philippines, (4) Türkiye, (5) New Zealand, (6) Mexico, (7) Italy, (8) Kenya, (9) Iceland, and (10) Japan. They together have an operational capacity of 15,194.31 MW (93.95% of the global operational capacity).

It should be noted that these data from the Global Geothermal Power Tracker (GGPT) dataset of the Global Energy Monitor (GEM) portal are not targeting geothermal energy potential, but actual geothermal power units (electricity generation from exploited geothermal energy). This explains why a country like India is not among the dataset countries, although there are several studies related to its geothermal resources and hot springs [109–112]. While India developed a plan for establishing its first geothermal power plant [113], this is not yet an "operational capacity", and this is not listed in the figure.

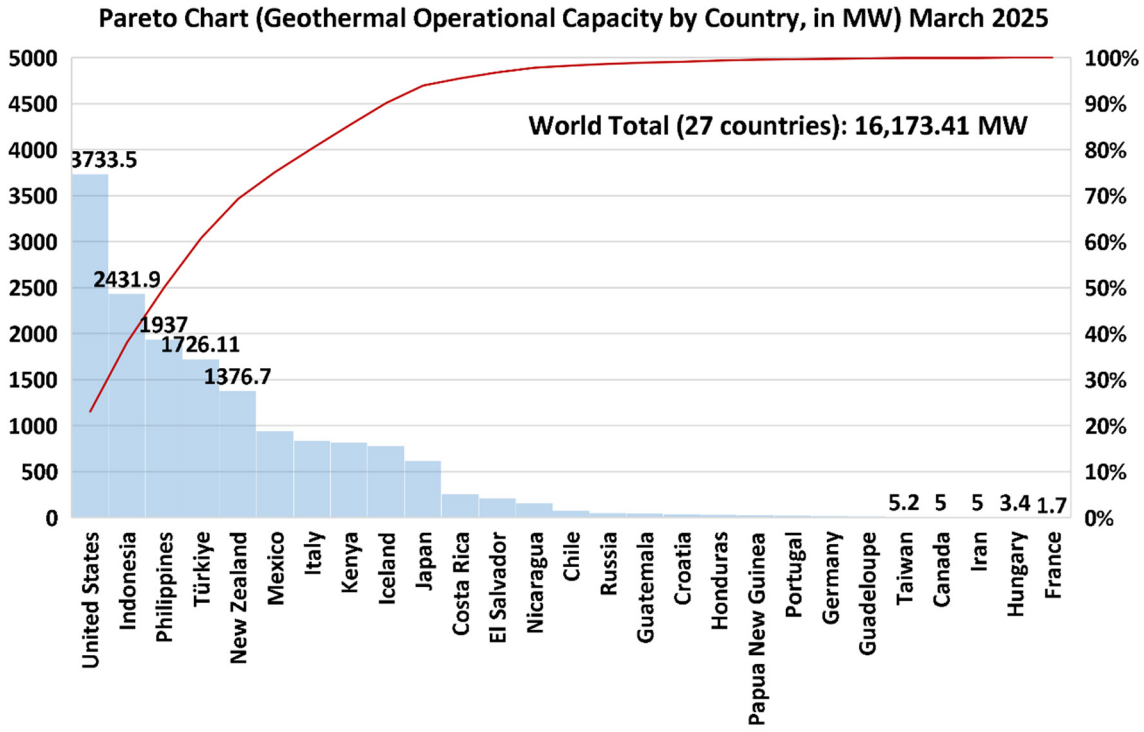

Figure 1. Distribution of geothermal power by country (operational capacity).

Table 2 augments the previous figure by listing the geothermal capacity for each of the 27 countries having one or more operating geothermal units, along with the number of these units in

 doi:10.20944/preprints202605.0188.v1

each county, and the average capacity per unit in each country. Overall (globally), the average capacity of the operating geothermal units is 33.69 MW/unit.

Table 2. Distribution of geothermal power by country (operational capacity and number of operational geothermal units).

Index	Country (descending order by capacity)	Operational Capacity (MW)	Number of Units	Average Capacity per Unit (MW/unit)
1	United States	3733.5	118	31.64
2	Indonesia	2431.9	50	48.64
3	Philippines	1937	39	49.67
4	Türkiye	1726.11	68	25.38
5	New Zealand	1376.7	32	43.02
6	Mexico	941	23	40.91
7	Italy	834	32	26.06
8	Kenya	816.5	16	51.03
9	Iceland	779.4	24	32.48
10	Japan	618.2	30	20.61
11	Costa Rica	253	7	36.14
12	El Salvador	211.2	8	26.40
13	Nicaragua	158.6	6	26.43
14	Chile	81	3	27.00
15	Russia	50	1	50.00
16	Guatemala	46	2	23.00
17	Croatia	36.1	4	9.03
18	Honduras	35	1	35.00
19	Papua New Guinea	30	1	30.00
20	Portugal	24	3	8.00
21	Germany	18.9	4	4.73
22	Guadeloupe	15	2	7.50
23	Taiwan	5.2	2	2.60
24	Canada	5	1	5.00
25	Iran	5	1	5.00
26	Hungary	3.4	1	3.40
27	France	1.7	1	1.70
	World	16173.41	480	33.69

Figure 2 shows the Pareto chart representation of the geothermal power capacity of prospective geothermal units in all countries with such prospective (expected) geothermal units (total 35

 doi:10.20944/preprints202605.0188.v1

countries having a total of 224 prospective geothermal units). The term "prospective" here refers to geothermal units that are either under construction or pre-construction or have been announced. The 224 prospective geothermal units are categorized as 52 in the construction phase, 111 in the pre-construction phase, and 61 announced. The global prospective capacity is 15,357.3 MW. The top ten countries in terms of planned installations in the geothermal energy are: (1) United States, (2) Indonesia, (3) Laos, (4) Kenya, (5) Philippines, (6) Türkiye, (7) Ethiopia, (8) Canada, (9) New Zealand, and (10) Dominica. They together have a prospective capacity of 14,308.5MW (93.17% of the global prospective capacity).

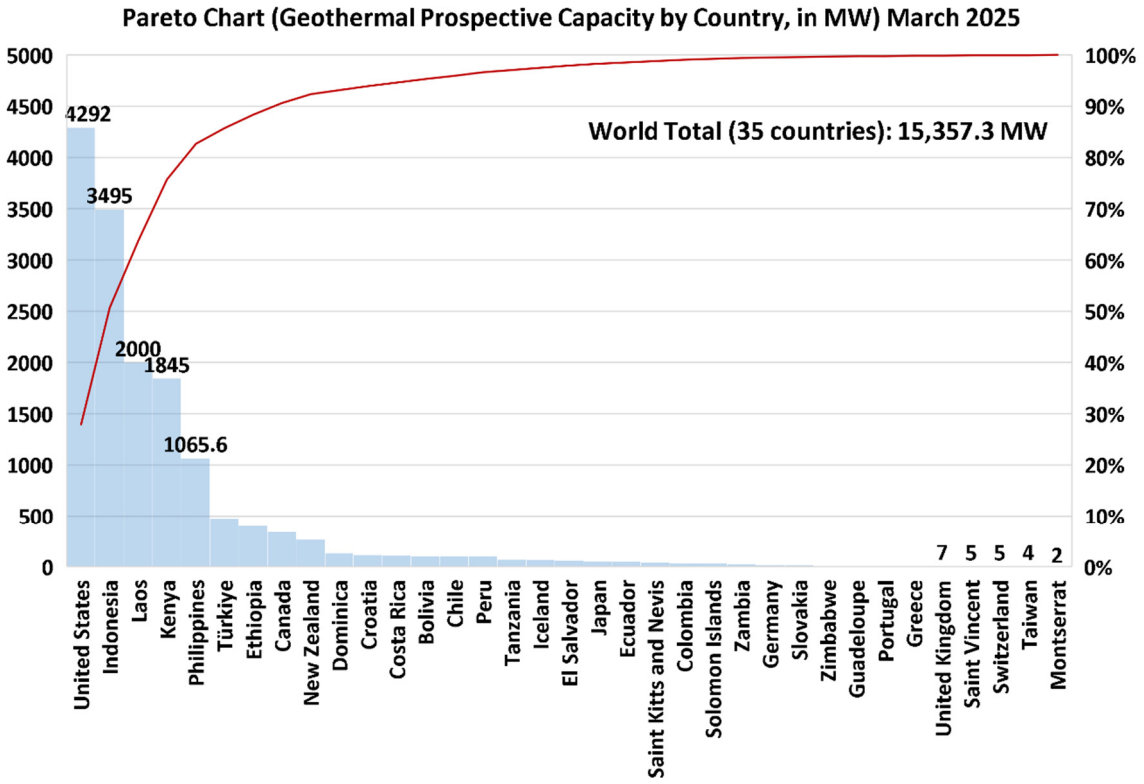

Figure 2. Distribution of geothermal power by country (prospective capacity).

Table 3 augments the previous figure by listing the geothermal capacity for each of the 35 countries having one or more prospective geothermal units, along with the number of these units in each county, and the average capacity per unit in each country. Overall (globally), the average capacity of the prospective geothermal units is 68.56 MW/unit, which is approximately twice the average value of operating geothermal units.

Table 3. Distribution of geothermal power by country (prospective capacity and number of prospective geothermal units).

Index	Country (descending order by capacity)	Prospective Capacity (MW)	Number of Units	Average Capacity per Unit (MW/unit)
1	United States	4292	40	107.30
2	Indonesia	3495	52	67.21
3	Laos	2000	2	1000.00
4	Kenya	1845	25	73.80
5	Philippines	1065.6	23	46.33

 doi:10.20944/preprints202605.0188.v1

6	Türkiye	473.9	16	29.62
7	Ethiopia	400	5	80.00
8	Canada	340	10	34.00
9	New Zealand	267	5	53.40
10	Dominica	130	2	65.00
11	Croatia	116	4	29.00
12	Costa Rica	110	2	55.00
13	Bolivia	100	2	50.00
14	Chile	100	2	50.00
15	Peru	100	1	100.00
16	Tanzania	70	2	35.00
17	Iceland	67	2	33.50
18	El Salvador	64	4	16.00
19	Japan	55.3	3	18.43
20	Ecuador	50	1	50.00
21	Saint Kitts and Nevis	40	2	20.00
22	Colombia	30	1	30.00
23	Solomon Islands	30	1	30.00
24	Zambia	23	3	7.67
25	Germany	20	2	10.00
26	Slovakia	12.5	2	6.25
27	Zimbabwe	10	1	10.00
28	Guadeloupe	10	1	10.00
29	Portugal	10	1	10.00
30	Greece	8	1	8.00
31	United Kingdom	7	2	3.50
32	Saint Vincent	5	1	5.00
33	Switzerland	5	1	5.00
34	Taiwan	4	1	4.00
35	Montserrat	2	1	2.00
	World	15357.3	224	68.56

2.5. Electricity Mix in Oman

According to the latest (2023 edition) annual report of the Central Bank of Oman (CBO) [114], oil and gas revenues have typically occupied more than half of the total country's revenues between 2019 and 2023. This is illustrated in Table 4. These data reveal the historical heavy reliance of Oman on fossil fuels, and show a lack of energy diversification as well as economic vulnerability due to exposure to the volatility of the global fossil fuel market [115,116].

 doi:10.20944/preprints202605.0188.v1

Table 4. Fiscal indicators for Oman.

Indicator	2019	2020	2021	2022	2023 (estimated)	Reference
Share of oil and gas in total revenues	57.6%	46.3%	50.1%	52.7%	57.0%	[117]
Total revenues as a percentage of GDP	31.3%	29.1%	33.3%	33.6%	30.0%	[117]
Oil and gas revenues as a percentage of GDP	18.0%	13.5%	16.7%	17.7%	17.1%	[117]

As of 2024, the electricity generation in Oman remains overwhelmingly dominated by fossil fuels, particularly natural gas [118]. Natural gas is still the primary energy source for electricity generation in Oman, approximately contributing 93% of the total electricity production. In 2024, renewable energy sources in Oman accounted for 4.2% (3.9% solar photovoltaic, and 0.3% wind), only [119]. The share of electricity generation from renewables in Oman was 0.00% up to 2016, as shown in Table 5.

Table 5. Share of renewables in electricity generation in Oman (data from Reference [120]).

2016	2017	2018	2019	2020	2021	2022	2023	2024
0.00%	0.06%	0.13%	0.15%	0.80%	1.91%	3.79%	4.04%	4.20%

Despite this traditional penetration of natural gas into the electricity sector in Oman, this is expected to drastically change, with big strides toward renewable energy [121], particularly in solar photovoltaic (PV) power plants and onshore wind farms. The anticipated capacity additions of renewable electricity in Oman are not only to meet increasing demand (both average and peak) on electric capacity [122] for residential consumption [123] and electrification [124–127]. In fact, a major driver for this huge planned investment in renewable electricity in Oman is the national determination to be a pioneer in producing green hydrogen [128] and green hydrogen derivatives (such as green ammonia). This requires proportional generation of renewable electricity to power the water electrolyzers that split water into oxygen and green hydrogen. Hydrogen and its derived fuels and industrial feedstocks [129] are nontraditional energy carriers that recently attracted global attention [130] as zero-carbon alternatives (in the case of green hydrogen) [131] or low-carbon (when considering both green hydrogen and blue hydrogen) alternatives [132] to fossil fuels. The revolutionary advancement in Oman's electricity sector is not in isolation from other sectors. The country is undergoing noticeable progress in multiple aspects in accordance with Oman Vision 2040, such as sustainable life [133], economic diversification [134], higher education [135–137], an attractive labor market [138], protected environment [139], innovation and novel technologies [140], green urban development, flexible government, and globalization [141].

It is useful to add here that Oman has an official national net-zero target by 2050 [142]. In addition, the country took measures toward installing about 70 GW of renewables in 2040, which is expected to increase to nearly 180 GW in 2050 [143].

2.6. Geothermal Energy in Oman and a Binary Geothermal Plant

Geothermal energy has never been exploited in Oman, and it is not among the near-future possibilities of the large-scale renewable energy installations. The two technologies of renewable

 doi:10.20944/preprints202605.0188.v1

energy that have been successfully installed and are expected to dominate renewable energy projects in Oman are ground-mounted solar PV module arrays and onshore wind farms [144].

The potential of geothermal energy in Oman is not clear, and deserves further investigation.

One study [145] analyzed temperature maps for existing borehole locations at depths varying between 500 m and 1500 m. These boreholes were within the concession area of the Petroleum Development Oman (PDO) company, which is the leading company in Oman for oil and gas exploration and production. PDO is jointly owned by the Omani government (60% share), Shell plc (34% share), Total (4% share), and Partex (2% share). The analysis showed that the highest temperature is 174 °C, which is below the temperature required for running a steam power plant directly using underground steam. In another subsequent study, the same research team concluded that geothermal energy in Oman does not have any potential use [146]. This was attributed to their opinion in the earlier study, which considered the temperatures in the examined boreholes not high enough.

The aforementioned conclusion is considered inaccurate and unnecessarily inauspicious. The reason for this judgment is given as follows: It is admitted that the temperature of the geothermal resource predominantly decides the suitability of this resource for electricity generation through a steam power plant [147]. However, temperatures exceeding 150 °C are still sufficient for electricity generation, but a flashing stage [148] is then required to convert hot liquid water into vapor by a sudden reduction of the pressure. Even without flashing, geothermal resources with lower temperatures (as low as 95 °C) can still be used to generate electricity using a steam power plant, but through a binary (two-fluid) cycle [149]. In such a binary-cycle power system, the geothermal hot liquid water extracted from the reservoir is used as a heat source only and is not converted into steam that is sent to a steam turbine within a steam power plant. Instead, a different working fluid with a low boiling point (BP), such as butane (C_4H_{10}, normal BP −0.5 °C) [150] or the hydrofluorocarbon refrigerant R134a ($C_2H_2F_4$, normal BP −26.1 °C) [151], is heated and evaporated as superheated vapor that is then expanded in the turbine to produce mechanical rotary shaft energy according to an organic Rankine cycle (ORC) than drives an electric generator [152,153].

In thermodynamic terms, the geothermal binary cycle involves two cycles and two different fluids that do not come into contact with each other. First, there is an open single-phase (liquid only) primary cycle for the geothermal fluid (hot water) that is withdrawn from the underground reservoir and then injected back into another injection reservoir. Second, there is a closed two-phase [154] (liquid and vapor) secondary cycle for the working fluid (having a lower boiling temperature than water) that changes phase between liquid and vapor, and repeatedly circulates through an expansion turbine, condenser, pump, and heat exchanger. In the heat exchanger (also called evaporator as in refrigeration applications), the working fluid absorbs heat from the geothermal hot water such that the working fluid vaporizes and becomes superheated compressed vapor suitable for expansion and energy extraction inside the turbine.

The primary cycle is easier to analyze because it has an incompressible fluid [155], with no moving mechanical parts. On the other hand, the secondary cycle includes a compressible gas during parts of it, and also includes work extraction (via a turbine) and work addition (via a pump); these features make this cycle more difficult to analyze. It is pointed out that the resilience offered by the binary cycle in terms of its tolerance for low temperatures comes with a penalty of reduced energy conversion efficiency (such as 15%) [156], which is implied by the second law of thermodynamics.

Figure 3 illustrates the components and operation of the binary-cycle geothermal power plant.

 doi:10.20944/preprints202605.0188.v1

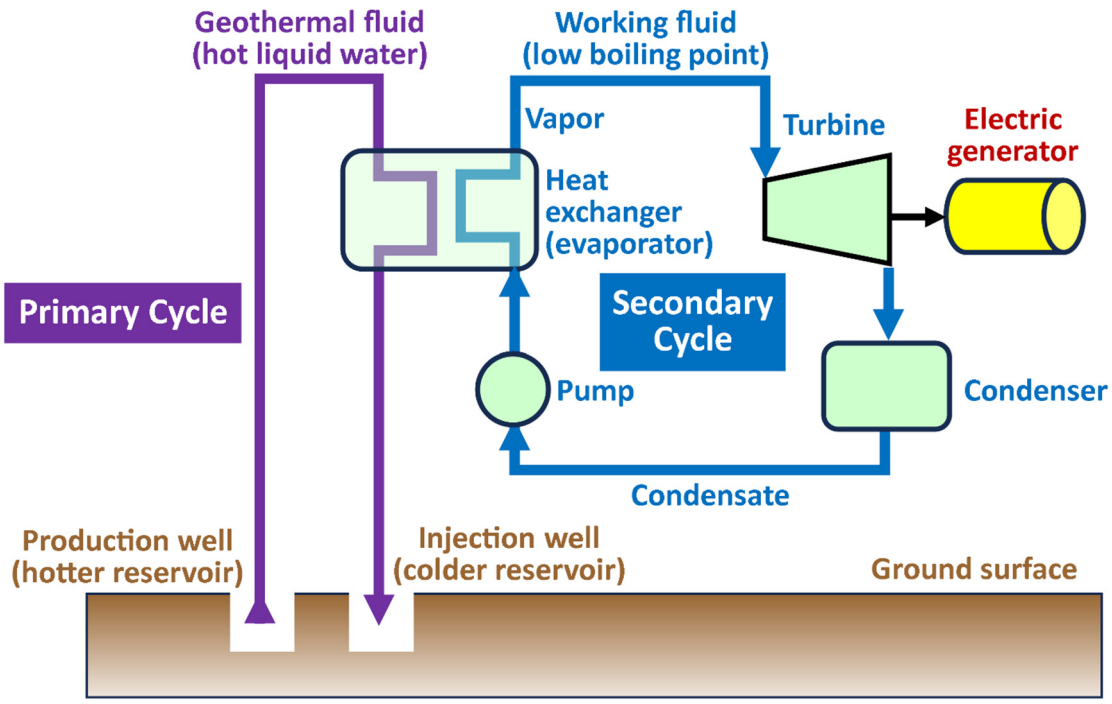

Figure 3. A sketch for the working principles of a binary-cycle geothermal power plant (this sketch is self-made; it is not taken from an external source).

In addition, the reported conclusion about the uselessness of geothermal power in Oman was based on surveying existing boreholes in specific sites, with a maximum depth of 1.5 km. Deeper drilling and exploring additional sites for geothermal applications can lead to better outcomes due to the effect of geothermal temperature gradients, such as 30 °C/km [157].

Another study reported water temperatures in the range of 68–137 °C in more than 55 boreholes in Oman, and suggested a limited possibility of investing in geothermal power plants for electricity generation compared to solar and onshore wind power plants [158]. Despite that, the mentioned study still assessed geothermal power plants in Oman as being feasible.

A study listed 53 boreholes of PDO (in the block 6 concession area in Oman) that have a water temperature beyond 100 °C. The maximum recorded temperature was 174 °C [159]. The mentioned study thus proposed that a binary cycle geothermal power plant can be used for power generation in Oman, given that this binary cycle is achievable at temperatures above 85 °C. It is helpful to add here that, during the time of the mentioned study, PDO was operating more than 5,000 well drillings in Oman for exploration in more than 120 oil fields. It is also helpful to add that PDO oil production yields approximately seven volumes of well water per volume of crude oil, giving a water-oil-ratio (WOR) of seven [160]. The majority of this byproduct oil well water is reinjected into the same well or new wells, as a process of secondary oil recovery (SOR), which improves the oil recovery by maintaining the reservoir pressure and by displacing hydrocarbons toward the wellbore. The oil well produced water is not potable, but typically contains a high level of dissolved solids and other contaminants, reaching, for example, a TDS salinity level of 8,000 ppm [161]. It is worth mentioning here that 1 ppm water salinity means that each liter of water has 1 milligram of salt. Drinking water (potable water) is generally restricted to a maximum limit of 1,000 ppm (0.1%), while seawater (oceans) has approximately a salinity of 35,000 ppm (3.5%) [162].

Another study was conducted to assess the temperature distribution, as well as hydraulic properties and heat transfer, within the sedimentary cover of northern Oman [163]. The findings of the mentioned study support the presence of a geothermal potential, where geothermal heat can be used for energy-intensive applications other than power generation, such as thermally driven cooling (driven by an absorption chiller) [164] or water desalination.

 doi:10.20944/preprints202605.0188.v1

Despite the lack of comprehensive geological details about geothermal energy sources in Oman, preliminary work suggests that the country hosts several geothermal reservoirs that have not been explored, especially in the northern part of Oman along the Omani Mountains. These reservoirs are primarily classified as low-enthalpy type (70–90 °C) and medium-enthalpy type (100–174 °C) [165,166]. Geothermal energy potential is particularly attractive in pre-identified locations within the area between the town of Fanja (23.461° N, 58.109° E) in the Wilayat (province) of Bidbid within Ad Dakhiliyah governorate (state) and Al Ansab village (23.538° N, 58.349° E) in the Wilayat (province) of Bausher in Muscat. The biggest known hot spring resource in Oman is Al Rustaq Hot Springs, which is also called Al Kasfah Hot Spring (23.393° N, 57.411° E), located in South Al Batinah governorate. It is a cluster of hot springs with the water temperature approaching 50 °C. The hottest known hot spring in Oman is Ayn Al Hammam (23.529° N, 58.383° E), located in the Ghala region of Muscat. The temperature of this surface spring reaches about 65 °C.

The highest recorded temperature for the borehole data of the Petroleum Development Oman (PDO) is 174 °C (more precisely 173.68 °C), corresponding to the Makarem-I well (21.705° N, 56.464° E), which is part of the broader Makarem Oil and Gas Field [167]. This location is within the giant Khazzan oil and gas complex, in the western Ad Dhahirah governorate (state) of Oman [168]. The Khazzan field is operated by BP (British Petroleum), while jointly owned by BP (60% share), OQ Exploration and Production or OQEP (30% share), and PC Oman Ventures Limited, which is a subsidiary of the Malaysian oil and gas company PETRONAS (10% share) [169]. This temperature is high enough to mark the site as a candidate for geothermal power exploitation. In addition, 53 nearby boreholes had temperatures exceeding 100 °C. On the other hand, the temperature of surface hot springs in Oman usually ranges from 40 °C to 65 °C.

Regarding the tectonic framework of geothermal resources in Oman, the primary geothermal activity is linked to the Frontal Range Fault (FRF), which is a major tectonic structure that was formed during the obduction process of the Samael Ophiolite over the Arabian continental margin [163].

Unlike many geothermal zones, the geothermal heat in Oman is believed to be primarily driven by deep circulation. In this heating mechanism, rainwater descends through fault lines, where it is heated by the Earth's crustal gradient, and then rises back to the surface [170]. Another geothermal heating mechanism is believed to be the serpentinization of ultramafic rocks. In this case, an exothermic chemical reaction occurs when water comes into contact with specific rock types in the ophiolite.

2.7. Primary Objective of the Current Study (Addressed Research Gap)

The primary objective of the current study is to provide data-driven recommendations regarding whether or not geothermal power is feasible in Oman as a commercial source of electricity that can successfully compete with existing power plants. A clear view regarding such a recommendation seems to be unavailable in the current literature, as shown in the previous subsection. Thus, there is apparently a research gap that the current study aims to fill.

The answer to this question clarifies the expected status of this kind of renewable energy in the country's electricity sector. The findings of the current study constitute informed advice to policymakers in Oman, as well as corporate investors (locally or foreign) in the electricity sector, by which strategic decisions can be taken to divert the national focus toward geothermal power as a novel technology or away from it toward the two mature and proven technologies of solar photovoltaic panels and onshore wind turbines. For example, in an earlier study, a similar research work for thermoelectric generators (TEG) was performed, leading to the conclusion that they cannot compete with photovoltaic (PV) modules as large-scale electricity generation units because of both technical and financial challenges [171]. This did not mean that thermoelectric generators are totally useless. Instead, it meant that their domain of applicability is not large-scale centralized power plants, but small-scale decentralized energy harvesting, especially that is if free from moving mechanical parts [172].

 doi:10.20944/preprints202605.0188.v1

The current study has additional secondary objectives, such as reporting sensitivity analysis outcomes for a binary geothermal power plant in Oman while exploring the influence of the resource depth and the power capacity.

The current study also aims to present an example of using the SAM (System Advisor Model) software to perform techno-economic assessment (TEA) for a geothermal binary power plant, which can be performed for other geographic locations worldwide.

While the results of the current study focus on Oman (particularly Muscat), it can be viewed as an archetypal example that can be insightful for other regions sharing similar climatic, energy, and developmental scenarios.

3. Research Method

3.1. SAM (System Advisor Model)

The current study implements computational techno-economic assessment for an exemplary binary-cycle geothermal power plant in Oman. The software program used here is System Advisor Model (SAM) [173] by the United States National Renewable Energy Laboratory (NREL) [174].

The System Advisor Model™ (SAM™) is a free desktop application for conducting a technical and financial feasibility study of renewable energy projects. SAM can be used with different renewable energy technologies, such as solar photovoltaic (PV) arrays, concentrated solar power (CSP), wind turbines, and geothermal plants. SAM can also model solar heat for industrial processes (SHIP) [175] and battery storage [176]. SAM is a robust program that is backed by many years of development and upgrades. The first public version was targeting solar energy professionals, and it was released in August 2007 under the name (Solar Advisor Model Version 1), where it enabled computer-aided design (CAD) [177] and computer-aided engineering (CAE) [178] of photovoltaic systems and concentrated solar power systems (parabolic troughs) [179,180]. In 2010, the program was renamed from (SAM: Solar Advisor Model) to (SAM: System Advisor Model) to reflect the broader scope of this software, which became no longer limited to solar energy applications.

The SAM version used here is 2025.4.16 (16/April/2025), which was the latest release at the time of initiating this study. SAM is available as a binary installation file and as open-source code.

Because SAM is developed and maintained by a reputable specialized research entity such as NREL, which also developed many other free software programs in the fields of power and renewable energy [181]; including desktop applications [182], web-based services [183], open-source repositories [184], properties estimators [185], and computational fluid dynamics (CFD) packages; SAM is a popular and widely adopted tool. SAM has been utilized in several studies in the literature [186–193]. This testifies to its success and accuracy. SAM has been validated for geothermal power output prediction in key example cases [194].

The computations of SAM (System Advisor Model) can be divided into two areas, namely performance modeling and financial modeling.

The performance modeling in SAM is based on a timestep-by-timestep estimation of the electric power output from the modeled system (modeled project). This results in time series data that represent the system's electricity generation over one year (the initial year of operation). The simulation timestep is determined internally based on the temporal resolution of the data in the required weather file (this can be selected from a built-in database or can be imported as an external computer file), which can be hourly or subhourly.

The financial modeling in SAM is optional (can be deactivated). It estimates financial metrics of the simulated project based on the project's cash flows over the analysis period that the user specifies. The financial model uses the estimated project's electric outputs according to the performance model to predict annual cash flows. Thus, the performance modeling is a prerequisite for the financial modeling.

 doi:10.20944/preprints202605.0188.v1

A simulation in SAM involves calculating the electric output of the power project for each hourly or subhourly timestep in a year, and also involves calculating the project's cash flow over a multi-year period.

The SAM simulations allow conducting studies that involve parametric modeling (sensitivity analysis) to investigate the impact of variations and uncertainty in adopted assumptions (such as performance parameters and financial parameters) on the model results, and this permits design optimization [195–197].

The computations of the System Advisor Model software (SAM) are based on integral system-level analysis, without the need for sophisticated multi-dimensional geometric representations [198,199], turbulence modeling [200], structural modeling [201], or computational fluid dynamics (CFD) techniques [202–204]. Instead, the computational core behind the SAM's user interface for geothermal power projects is an Excel-based model called GETEM (Geothermal Electricity Technology Evaluation Model), developed by the United States Department of Energy (DOE) [205]. Earlier, before being transformed into a model within SAM, GETEM was a standalone Microsoft Excel workbook [206–208]. This spreadsheet modeling is an advantage to make the simulation relatively fast [209,210], without requiring specialized computational resources, advanced computational skills [211], or specialized data processing dealing with extensive volumes of results [212,213].

3.2. Weather Data File

The capital of Oman (Muscat) is selected as the representative site for performing the simulation of the binary-cycle geothermal power plant in Oman. This choice is justified by the availability of more data about it relative to other, less politically important cities in Oman, the concentrated population (thus, high electricity demand and more access to skilled labor), and the proximity to existing infrastructures as well as large corporations and service providers.

Because the built-in weather database in SAM (System Advisor Model) did not have a location in Oman, it was necessary to import an external weather data file for Muscat. This weather file was obtained using the Photovoltaic Geographical Information System (PVGIS) web tool [214] for modeling solar power systems and for meteorological data. PVGIS is developed by the Joint Research Centre (JRC) [215,216], which is the science and knowledge service of the European Commission (EC), carrying out research in various areas to provide independent advice to policymakers of the European Union (EU). PVGIS version 5.3 [217] was accessed. It was released on 25/September/2024 as an upgrade of the previous version PVGIS 5.2.1, and it was the latest at the time of initiating the current study.

Searching for a location by the word "Muscat" in PVGIS, the following point was retrieved as described in Table 6.

Table 6. Muscat data in PVGIS 5.3.

Property	Value
Latitude	23.483° North
Longitude	58.592° East
Elevation	411 m

The typical meteorological year (TMY) records were downloaded using the database PVGIS-SARAH3: 2005-2023 [218]. Weather data were downloaded in the epw (EnergyPlus Weather) file format [219,220]. The downloaded epw file contained a total of 8,768 lines, including eight header lines. The data lines covered hourly points, from 1/January to 31/December, with a total of 8,760 lines (365 days and 24 hours per day). Each line of weather data included information about [221]

1. date (year, month, day)

 doi:10.20944/preprints202605.0188.v1

2. time (hour)
3. air temperature at 2-m height (dry bulb temperature)
4. relative humidity
5. global horizontal irradiance
6. direct (beam) normal irradiance
7. diffuse horizontal irradiance
8. long-wave downwelling (from the atmosphere) infrared radiation
9. wind speed at 10-m height
10. wind direction at 10-m height
11. air (atmospheric) pressure

The term (dry bulb temperature) refers to the ordinary temperature as measured by a regular thermometer, without imposing artificial humidification.

The time zone of Muscat and the entire Oman is GMT 4 (four hours ahead of Greenwich Mean Time) [222].

According to the PVGIS algorithm, the TMY weather file is produced by choosing the most "typical" month out of the full period available for each month (19 years for the range 2005-2020). The three variables used to determine the "typical" month are:

(1) global horizontal irradiance
(2) air temperature
(3) relative humidity.

For the downloaded weather data, the mapping of year-month was as shown in Table 7:

Table 7. Selected year for defining the most typical month in PVGIS weather data.

Index	Month	Year
1	January	2014
2	February	2021
3	March	2017
4	April	2006
5	May	2021
6	June	2006
7	July	2005
8	August	2012
9	September	2013
10	October	2005
11	November	2015
12	December	2016

3.3. SAM Modeling Parameters

In addition to the weather data, the SAM simulation for a binary geothermal power plant requires specifying a large number of inputs (operational conditions or assumptions). In the current subsection, some of these inputs are listed. They are largely based on reasonable choices as well as recommended/default settings in SAM. Table 8 summarizes some of the conditions used in the simulation of the binary geothermal power plant in Muscat.

 doi:10.20944/preprints202605.0188.v1

Table 8. Some inputs used in the SAM simulation of a geothermal power plant in Muscat.

Index	Input	Value	Reference
1	Power plant electric output capacity	30,000 kW (30.00 MW)	[223]
2	Power plant type	Binary	[224,225]
3	Geothermal resource temperature	200 °C	[226]
4	Temperature decline	0.5% per year	[227]
5	Geothermal resource depth	2,000 m	[228]
6	Rock density	2,600 kg/m^3	[229,230]
7	Rock specific heat	950 J/kg/K	[231–233]
8	Rock thermal conductivity	3.0 W/m/K	[234–237]
9	Subsurface water loss (of injected water)	2%	[238,239]
10	Well pump efficiency	67.5%	[240]
11	Pressure drop within the binary plant (hydrodynamic loss)	2.7579 bar (40 psi)	[241]
12	Cycle design inlet temperature	200 °C	[242]
13	Cycle design outlet temperature	90 °C	[243]
14	Evaporator operating pressure	2 bar	[244,245]
15	Blowdown fraction	1.3%	[246]
16	Ratio of injection wells to production wells	0.5	[247]
17	Drilling success rate	76%	[248–250]
18	Well type	Vertical open hole	[251,252]
19	Plant baseline cost	1,800 US$/kW	[253–255]
20	EPC cost	16% of the direct cost	[256]
21	Contingency	10%	[257–260]
22	Fixed annual operating cost	6,087,700 US$/year	[261,262]
23	Analysis period	20 years	[263–265]
24	Inflation rate	2.5%/year	[266–269]

4. Results

4.1. Scalar Results

The System Advisor Model (SAM) program provides a comprehensive set of numerical and graphical results at the level of hours, months, and the entire year. It also allows the user to make customized visualizations of selected results.

In the current section, selected scalar results (the word "scalar" here means a single overall value for the entire geothermal project, rather than a series of values such as an array of monthly records) for the performed simulation are presented, as computed by SAM.

First, year-round average weather values computed by SAM are presented in Table 9, based on the imported weather data for Muscat.

 doi:10.20944/preprints202605.0188.v1

Table 9. Averaged weather variables as computed by SAM from the PVGIS weather file.

Index	Variable	Year-average
1	Global horizontal irradiance	6.14 kWh/m²/day
2	Direct normal (beam) irradiance	6.05 kWh/m²/day
3	Diffuse horizontal irradiance	1.98 kWh/m²/day
4	Air temperature at 2-m height	28.0 °C
5	Wind speed at 10-m height	2.2 m/s

Then, additional outputs are listed in Table 10 related to the modeled geothermal power plant. These are either performance outputs (such as the annual electricity generation) or internally-computed design variables (such as the number of wells).

Table 10. Some performance outputs or internally-computed design variables as reported by the SAM simulation of a geothermal power plant in Muscat.

Index	Output	Value
1	Annual AC energy (first year)	261,267,936 kWh (261.268 GWh)
2	Capacity factor (first year)	99.4%
3	LCOE	8.68 ¢/kWh (33.4 baisa/kWh at 0.260 ¢ per baisa [270,271])
4	Pressure change across the reservoir	24.077 bar (349.212 psi)
5	Average reservoir temperature	200.00 °C (392.00 °F)
6	Production well bottom hole pressure	162.910 bar (2,362.812 psi)
7	Number of wells in analysis	4.232
8	Actual plant efficiency	9.225 W/(lb/hr)
9	Gross plant electric output	34.078 MW
10	Net plant electric output	30.000 MW
11	Plant design temperature	200 °C
12	Well pump depth	342.327 m (1,123.120 ft)
13	Well pump power	4.078 MW
14	Production well pump size	539.596 kW (733.646 hp)
15	Injection well pump size	1,739.264 kW (2,364.741 hp)
16	Number of production wells to be drilled	5.568
17	Number of injection wells to be drilled	2.109
18	Total number of wells to be drilled	7.677
19	Cost per well	US$ 4,310,562
20	Total drilling cost	US 33,341,087
21	Production pump cost per well	187,653.749 US$/well
22	Injection pump cost per well	341,258.814 US$/well

 doi:10.20944/preprints202605.0188.v1

23	Total capital cost	US$ 108,672,755
24	Total installed cost (sum of direct and indirect costs)	US$ 138,895,952 (OMR 53,421,520 at 2.60 US$/OMR)
25	Total installed cost per unit net capacity	4,630 US$/kW (1,781 OMR/kW at 2.60 US$/OMR)

In order to contrast the electricity generation capability of this modeled geothermal technology and the solar photovoltaic technology [272], a normalized performance metric is used, which is the electricity generated (in the first year) per unit of capacity power. From the above table, this normalized performance metric (in Muscat) becomes 261,267,936 kWh/year ÷ 30,000 kW = 8,709 kWh/kW/year. Based on earlier work, the counterpart value (in Muscat also) in the case of monofacial solar photovoltaic (PV) arrays with an optimized fixed tilt [273,274] of 23.6° is 1,586 kWh/kW/year. Therefore, per unit capacity, a geothermal plant can produce more than five times the electricity that a PV plant can.

4.2. Monthly Results

In the current subsection, the computed monthly data points of four key variables as estimated by the System Advisor Model (SAM) program are presented in Table 11. These monthly values correspond to the first 365-day year of operation, which is assumed to start on 1/January (12:00 am) and to end on 31/December (11:00 pm).

Table 11. Monthly variations of four key variables as estimated by the SAM simulation of a geothermal power plant in Muscat.

Month	Air (ambient) temperature (°C)	Air (ambient) pressure (atm)	Geothermal resource temperature (°C)	Monthly AC electricity generation (GWh)	Monthly net capacity (MW)
Jan	18.2984	0.984152	200.000	22.3200	30.0000
Feb	22.4492	0.982892	199.917	20.1388	29.9684
Mar	25.0894	0.978741	199.833	22.2730	29.9368
Apr	28.9648	0.974816	199.750	21.5318	29.9052
May	33.0837	0.972363	199.667	22.2259	29.8736
Jun	33.8049	0.966698	199.584	21.4862	29.8419
Jul	33.7718	0.964331	199.501	22.1788	29.8102
Aug	33.1972	0.965389	199.417	22.1552	29.7785
Sep	31.1863	0.970421	199.334	21.4177	29.7468
Oct	27.9454	0.977709	199.251	22.1080	29.7150
Nov	24.7315	0.980728	199.168	21.3719	29.6833
Dec	22.6024	0.982646	199.085	22.0607	29.6515

The resource temperature's decline from 200.000 °C in January to 199.085 °C in December is consistent with the assumption of a 0.5% drop per year (thus, per 12 months). This can be explained as follows. A 0.5% year-wise drop in the initial 200 °C is exactly 1 °C/year. This is assumed to occur

 doi:10.20944/preprints202605.0188.v1

at a constant rate during the year, leading to a monthly decline of 1/12 or 0.0833 °C/month. Furthermore, the drop in the resource's temperature is approximated as a piecewise constant function, with the drop occurring at the transition between two successive months. This algorithm in SAM means that the resource's temperature in December experiences 11 (not 12) incidents of monthly drops since the initial operation. Therefore, the resource's temperature in December should be computed as

$$T_{December} = T_{January} - \frac{11}{12}\Delta T_{year} \quad (2)$$

where ($T_{December}$) is the temperature of the liquid hot water in the geothermal reservoir during December; ($T_{January}$) is this reservoir's temperature, but at an earlier stage in January; and (ΔT_{year}) is the total annual decrement in the reservoir's temperature. In the current simulation, $T_{January} = 200$ ℃, and $\Delta T_{year} = 1$ ℃. Therefore, Equation (2) gives

$$T_{December} = 200 - \frac{11}{12} \times 1 = 199.083 \text{ ℃} \quad (3)$$

The idealized value of 199.083 °C obtained by Equation (3) is slightly lower than the one reported by SAM (199.085 °C). This is an insignificant deviation (only 0.001%), which can arise as a result of applied convergence tolerance during the solution process in SAM.

4.3. Graphical Results

In the current subsection, graphical forms of the results obtained from the SAM (System Advisor Model) simulation of the binary-cycle geothermal power plant in Oman are presented and discussed.

Figure 4 shows the weak decline in the net electric capacity from the power plant during its first year of operation, starting from the initial nominal value of 30,000 kW. The capacity decline is attributed to the assumed drop in the reservoir's temperature, from the initial value of 200 °C, at a rate of 0.5%/year. This is a natural decline due to extracting the hot liquid water from the production reservoir, which is then injected at a lower temperature in an injection reservoir after losing some heat through heat exchange with the working fluid in the binary cycle.

Although the displayed line curve decreases continuously. However, in the SAM simulation, this drop occurs as discrete small decrements at the end of each month. The electric capacity becomes 29,651.5 kW at the end of the first year of operation in December; which means after 11 monthly decrements.

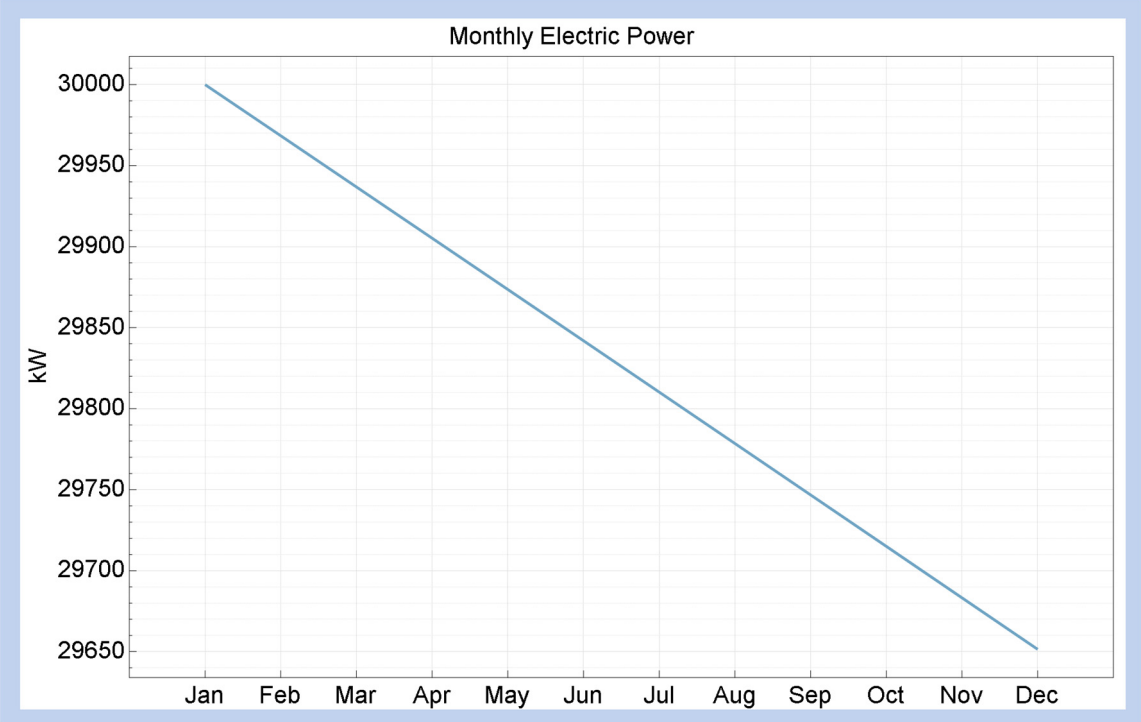

 doi:10.20944/preprints202605.0188.v1

Figure 4. The estimated monthly profile of the net output electric power capacity for the binary geothermal power plant in Muscat during its first year of operation.

Figure 5 visualizes the net electric capacity during the first year of operation in the form of a two-dimensional heat map, which allows portraying the variation across months (horizontal axis) as well as across hours (vertical axis). This figure is an extended version of the previous one-dimensional figure. There is no change in the capacity during the same month; thus, each vertical color band in the shown figure has a uniform color (uniform value). Again, this net electric capacity drops from 30,000 kW in January (the first month) to 29,651.5 kW in December (the twelfth month).

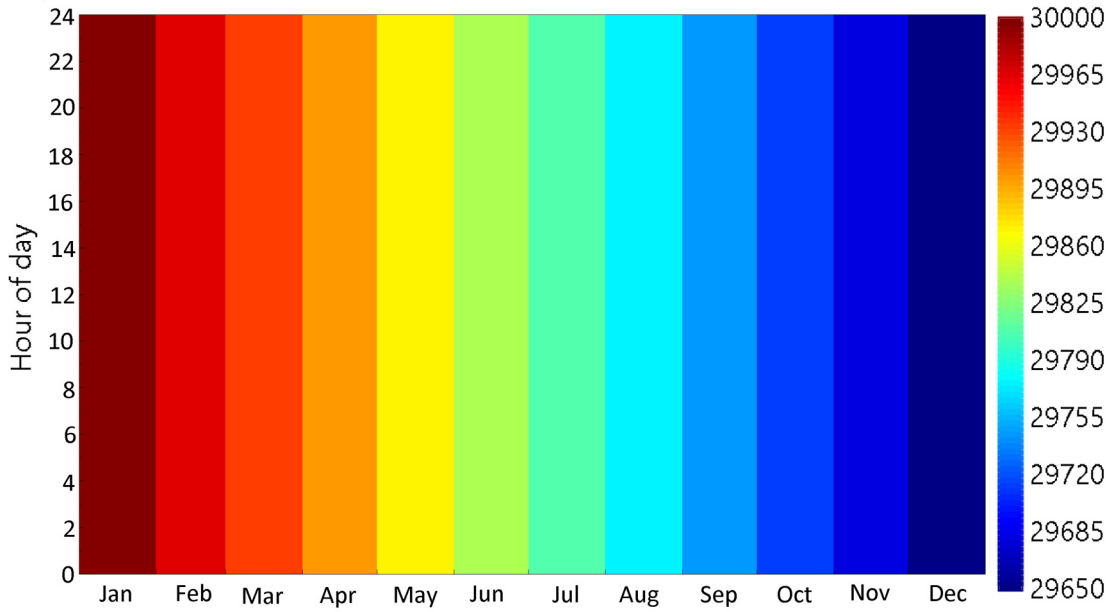

Figure 5. The estimated monthly and hourly profile of the net output electric power capacity for the binary geothermal power plant in Muscat during its first year of operation.

Figure 6 shows the alternating-current (AC) electricity generation per month during the first year of operation. The shown profile manifests three combined effects that influence the electricity generation. First, there is the effect of different numbers of days per month. This is a primary source of variability in the displayed figure, and it explains why February (28 days) has noticeably less electricity generation than all other months. In addition, months with 31 days have more electricity generation than months with 30 days. Second, there is the effect of the slow decline in the power capacity, which was discussed earlier. Third, there is the effect of the variations in the monthly ambient conditions.

Figure 7 shows the drop in the reservoir's temperature due to withdrawing the hot liquid water from it during the first year of operation. The temperature of the geothermal resource drops slowly from the initial value of 200 °C (January, the 1st month of operation) to 199.085 °C (December, the 12th month of operation). While the line plot here gives an impression of a smooth, gradual decrease at an annual or even hourly decrements; actually, the temperature drop is implemented as monthly decrements. The span of the total drop in temperature is within 1 °C only. It is useful to add here that in SAM, it is possible to set a threshold gross drop in the resource's temperature (such as 30 °C), beyond which the reservoir should be replaced.

 doi:10.20944/preprints202605.0188.v1

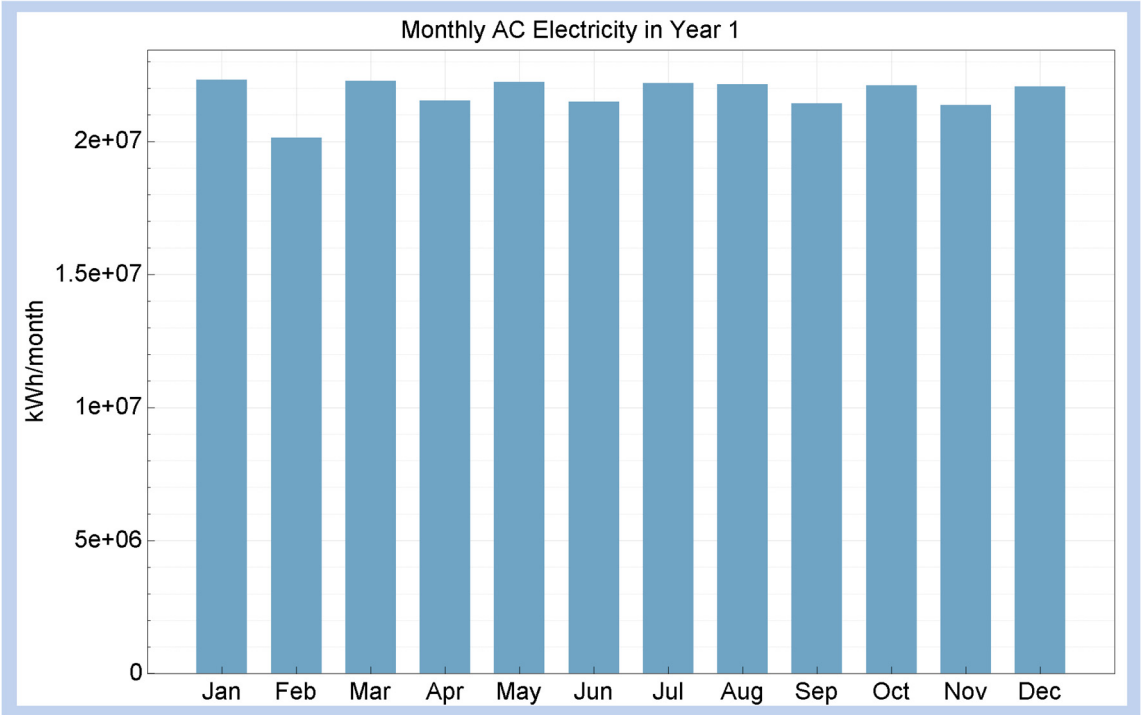

Figure 6. The estimated monthly profile of the net output electricity (alternating current) for the binary geothermal power plant in Muscat during its first year of operation.

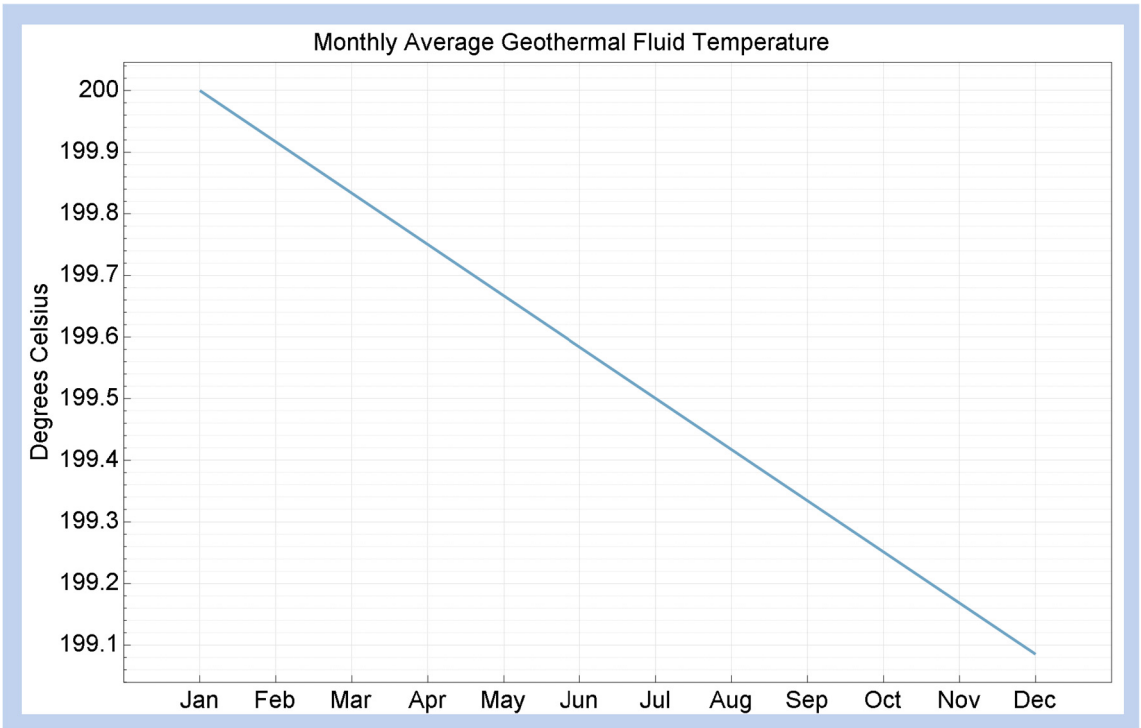

Figure 7. The estimated monthly profile of the geothermal reservoir's temperature for the binary geothermal power plant in Muscat during its first year of operation.

Figure 8 shows a monthly profile of the atmospheric pressure in Muscat, as estimated by SAM after processing the weather file. The unit is standard atmosphere (atm), where

$$1 \text{ atm} = 101{,}325 \text{ Pa} = 1.01325 \text{ bar} = 14.696 \text{ psi} \quad (4)$$

 doi:10.20944/preprints202605.0188.v1

The sea-level normal atmospheric pressure is 1 atm, according to the ISA (International Standard Atmosphere) model [275–278]. However, the atmospheric (ambient) pressure in the location selected for siting the geothermal power plant in Muscat is mildly below this reference pressure throughout the year. This can be explained by the elevation of the site selected above the mean sea level (MSL). Near sea level, for each 10 m of elevation, the air pressure drops approximately by 1%. Thus, a height of 411 m roughly leads to a decline of 0.04 atm. These explain the small decrease in pressure. Also, there is a seasonality pattern in the atmospheric pressure curve, which is smaller in the summer than in the winter [279]. This is also logical because the air density decreases in the summer (at higher temperatures) in accordance with the ideal gas law [166,280], which leads to reduced weight of the overhead air column, and thus reduced air pressure [281].

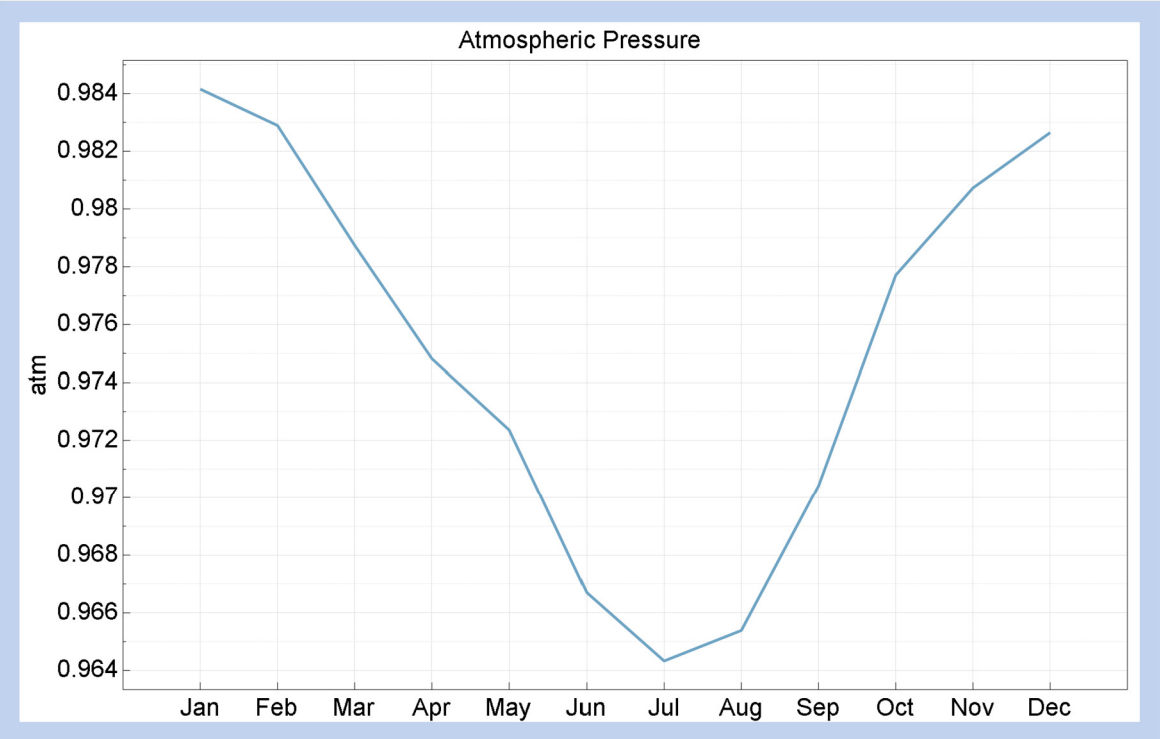

Figure 8. The estimated monthly profile of the atmospheric pressure for the binary geothermal power plant in Muscat during a typical year.

Figure 9 shows monthly profiles of the dry bulb and wet bulb temperatures in Muscat, as estimated by SAM from the weather file. The wet bulb temperature is the lower temperature that is measured after imposing a condition of evaporative cooling [282]. The wet bulb temperature is the minimum attainable temperature to which air can be cooled as a result of evaporating water into it (the evaporation heat is partly extracted from the air), while the pressure remains constant [283]. The difference between the dry bulb temperature and the wet bulb temperature is an important quantity in psychrometry, where it indicates the moisture level in air [284]. While both temperatures increase in the summer; as expected, the gap between them also increases in the summer. This indicates the elevated humidity in Muscat during the summer months.

 doi:10.20944/preprints202605.0188.v1

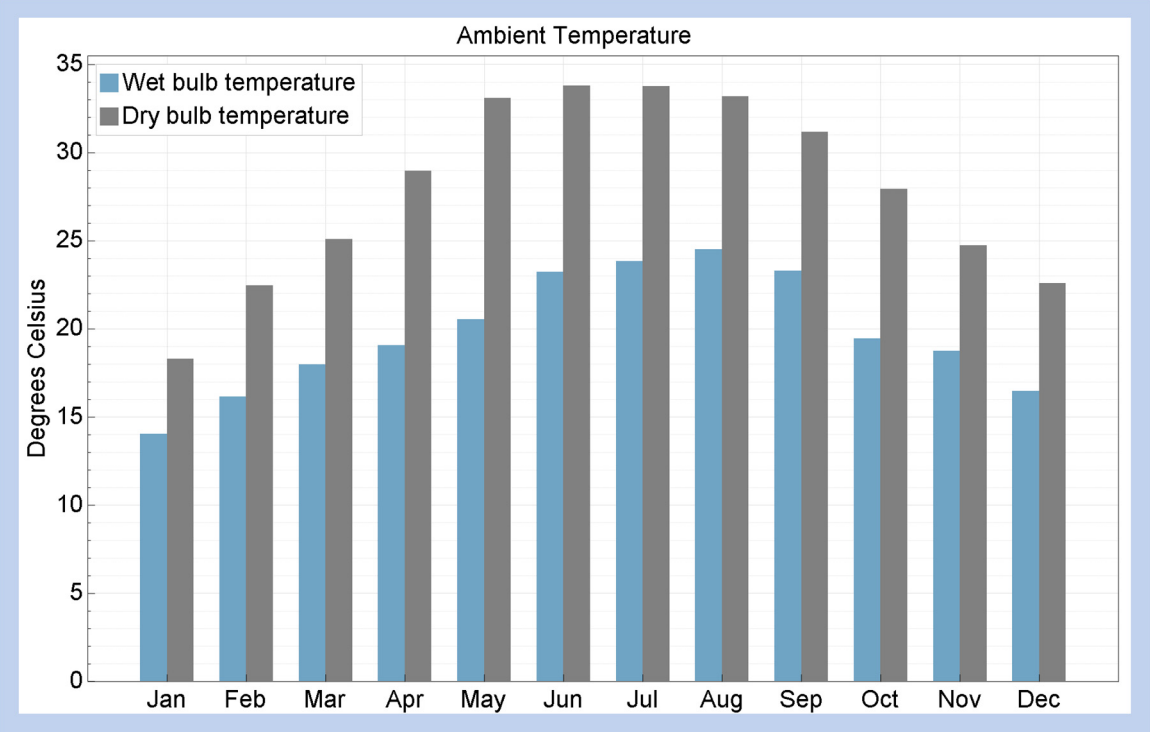

Figure 9. The estimated monthly profile of the dry bulb temperature and wet bulb temperature for the binary geothermal power plant in Muscat during a typical year.

To validate the above-shown temperature profiles reported by SAM, equivalent monthly profiles of these dry bulb temperatures [285] and wet bulb temperatures [286] in Muscat are constructed using independent external data sources. The external validation temperature profiles are shown in Figure 10. When compared with the SAM-reported profiles in the previous figure, good agreement can be inferred. This successful validation gives more confidence in the overall modeling process.

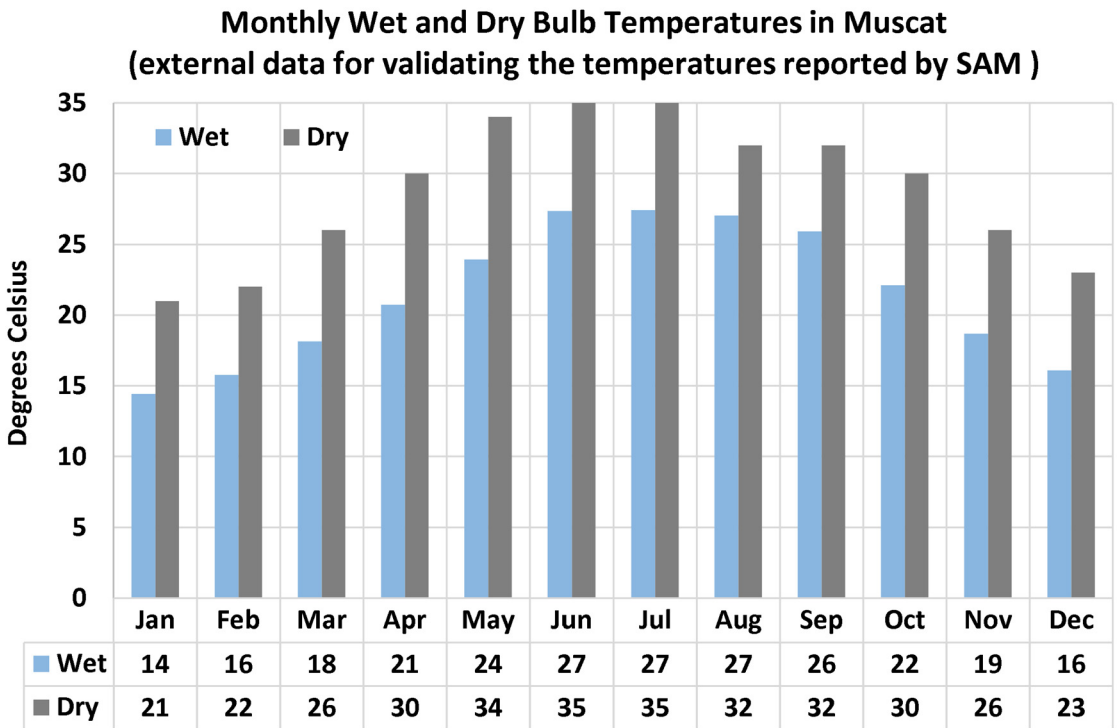

	Jan	Feb	Mar	Apr	May	Jun	Jul	Aug	Sep	Oct	Nov	Dec
Wet	14	16	18	21	24	27	27	27	26	22	19	16
Dry	21	22	26	30	34	35	35	32	32	30	26	23

 doi:10.20944/preprints202605.0188.v1

Figure 10. Externally (not from the SAM program) reported monthly profile of the dry bulb temperature and wet bulb temperature in Muscat.

4.4. Sensitivity Analyses (Selected Inputs and Outputs)

After completing the simulation of the 30-MW binary-cycle geothermal power plant in Oman at the selected base-point condition; in the current section, an auxiliary parametric study (sensitivity analysis) is performed using this built-in capability in the SAM (System Advisor Model) software. Such a parametric study allows for the identification of which parameters are more influential in controlling the technical and financial aspects of the geothermal power plant. Such a parametric study also mitigates [287] the uncertainty involved in some assumptions, by exploring the situations if an assumed parameter is shifted up or down within an interval.

Although there are many input and output variables in the simulated geothermal power plant, one key output performance metric and one key financial metric were selected for further investigation of their variability in response to changes in certain input parameters. These are:

1. the levelized cost of energy (LCOE)
2. the AC electricity generation during the first year

Likewise, there are many input parameters whose influence can be explored in the sensitivity analysis. However, four key input parameters for exploration as independent variables were selected. These are:

1. the plant's nameplate net electric power capacity (the base-point value was 30 MW or 3,000 kW)
2. the drilling depth to access the geothermal resource (the base-point value was 2 km or 2,000 m)
3. the ratio or percentage of geothermal injection wells relative to the number of geothermal production wells (the base-point value was 0.5 or 50%)
4. the pump efficiency of the geothermal production wells (the base-point value was 0.675 or 67.5%)

4.5. Rationale for the Selected Output Variables for Sensitivity Analysis

The techno-economic simulation of a binary-cycle geothermal power plant involves a large number of input parameters (or assumptions) and output results that are related nonlinearly through comprehensive relationships [288]. Therefore, it is not reasonable to perform a sensitivity analysis (parametric analysis) to reveal how each input quantity affects each output quantity. Otherwise, this study becomes a massive report with large amounts of insignificant components.

Instead, only two important output quantities are selected, which are the AC electricity generation during the first year and the levelized cost of energy (LCOE).

The first selected output quantity is in an absolute form (not normalized), such as GWh/year. It is important to reveal the generation size of the geothermal plant. It can easily be normalized and expressed as electricity per unit net capacity (kWh/kW/year) by dividing by the net plant capacity of 30,000 kW and converting the electricity unit from GWh to kWh by multiplying by 10^6. For example, the base-value annual absolute electricity generation of 261.268 GWh/year can be easily converted into a scaled performance metric of 8,709 kWh/kW/year. Such scaling (effectively dividing the GWh/year value by 0.03 to obtain the corresponding kWh/kW/year value) helps in performing subsequent comparative studies to compare the electricity generation capability of this geothermal power plant to other electricity generation technologies, in terms of how much electricity can be generated during one year after installation per kW of installed capacity. So, as shown in this example, the first output quantity selected for the sensitivity analyses is a useful metric that can be transformed into other helpful performance metrics easily, making it a justified choice.

The second selected output quantity (the levelized cost of energy or LCOE) is in a normalized form. Therefore, it is readily suitable for comparison with other electricity generation technologies. The levelized cost of energy (LCOE) is defined as the minimum cost (expressed in net present value) at which energy or electricity should be sold in order to regain investment (both initial investment in

 doi:10.20944/preprints202605.0188.v1

the construction and running investment in the operation) of an energy generation unit during its lifetime [289]. The LCOE quantity is typically used by investors in the power sector, making it also a justified choice for further sensitivity analyses.

4.6. Rationale for the Selected Input Variables for Sensitivity Analysis

Again, the techno-economic simulation of a binary-cycle geothermal power plant involves a large number of coupled input and output variables. Thus, it is compulsory to select a subset of input variables to explore their effect on the techno-economic assessment.

Four input variables are selected for the sensitivity analyses. These are the plant's nameplate net electric power capacity, the drilling depth, the ratio or percentage of geothermal injection wells relative to the number of geothermal production wells, and the pump efficiency of the geothermal production wells.

The first selected input variable (the net power capacity) is a key way to quantify the size of an electricity generation unit. Therefore, it is very justifiable.

The second and third input variables are directly related to the drilling costs of the geothermal power plant. These are also useful, given that the drilling is a major budget element for geothermal plants, and it can account for up to 50% of the total investment cost of a hydrothermal geothermal project [290–293].

The fourth selected input variable (pump efficiency) seems to lack sufficient understanding of its role in a geothermal power plant [294]. By including it in the sensitivity analysis, the contribution of the current study is largely boosted. Therefore, this selection is beneficial.

4.7. Sensitivity Analyses (Criteria for the Selected Ranges of Input Variables)

For each of the selected input sensitivity variables, the range explored of that variable is from 50% (half) of the base-point value to twice (200%) of the base-point value. This establishes consistency in the sensitivity analyses. These chosen ranges are favorably based on relative scaling (the ranges are decided in relation to the base-point values), rather than absolute range bounds. This takes into account the variations in the order of magnitude of these input variables and makes the sensitivity analyses more meaningful and robust.

4.8. Sensitivity Analyses (Criteria for the Plotting Ranges of Output Variables)

When the sensitivity response curves are plotted, care is taken in selecting the range of the vertical axis (representing the output sensitivity variable). The range for each output sensitivity variable is deliberately frozen in all its sensitivity analysis plots (irrespective of the input sensitivity variable). More precisely, the plotting range for the levelized cost of energy (LCOE) is from 0.075 US$/kWh to 0.120 US$/kWh, and the plotting range for the AC electricity generation during the first year is from 100 GWh to 400 GWh. These ranges were selected carefully such that all obtained values for either output sensitivity variable fit well within the same fixed range. This allows for efficient recognition of the qualitative and quantitative variations in the output sensitivity variable as a result of altering the input sensitivity variable.

4.9. Sensitivity to Plant Net Capacity

The current subsection is dedicated to presenting and discussing the portion of the sensitivity analyses that is related to the influence of the first input parametric quantity (first input control variable), which is the plant capacity.

The range over which the power plant capacity was varied is from 15 MW to 45 MW. As discussed earlier, the criterion for adopting this range is that it corresponds to a 50% decrease and a 50% increase away from the design-point capacity of 30 MW, respectively.

A total of 11 capacity data points were used in the parametric study, which included the base capacity (30 MW), plus five additional lower capacities and five additional higher capacities.

 doi:10.20944/preprints202605.0188.v1

The 11 capacity points are equally spaced with a step of 3 MW, starting from 15 MW. Thus, the 11 electric net capacities explored are:

1. 15 MW
2. 18 MW
3. 21 MW
4. 24 MW
5. 27 MW
6. 30 MW (base or reference value)
7. 33 MW
8. 36 MW
9. 39 MW
10. 42 MW
11. 45 MW

Figure 11 shows the response curve of the levelized cost of energy (LCOE) to the net power plant capacity. This curve suggests a strong and nonlinear impact of the plant capacity on LCOE, which favorably drops as the capacity increases. For example, the base-point LCOE of 8.67875 ¢/kWh at 30 MW drops by 11.24% and reaches 7.70302 ¢/kWh at 45 MW, while this base-point LCOE increases by 33.52% and reaches 11.5877 ¢/kWh at 15 MW.

The rate of decline decelerates as the capacity increases. This means that the same absolute increment in the plant capacity has a larger improvement (larger reduction in LCOE) when the plant is small compared to when it is large. This is a reasonable behavior given that the smaller plant is more affected by the same upgrade of capacity compared to a larger plant.

As shown in the figure, the nonlinear dependence of LCOE on the plant capacity can be described well by a cubic function. In such a third-degree polynomial fitting, the R-squared goodness-of-fit metric is very high (0.9994), close to the ideal value of 1.0 [295,296].

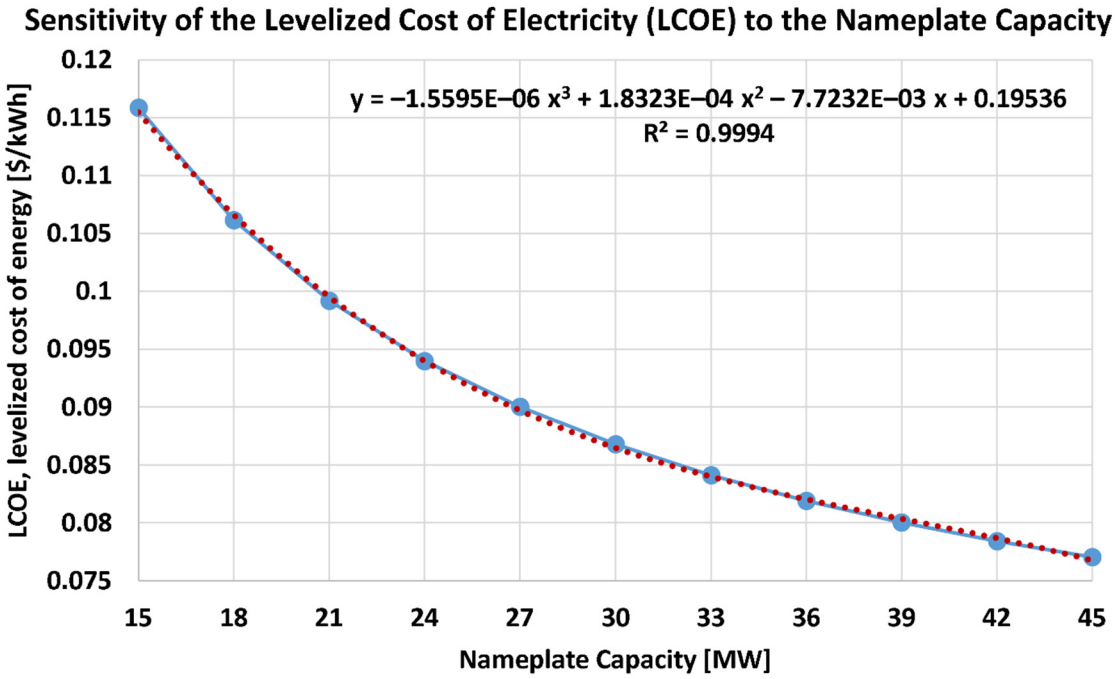

Figure 11. The estimated variation of LCOE with the net capacity for the binary geothermal power plant in Muscat. The base-point capacity is 30 MW.

Figure 12 shows the dependence of the first-year electric yield on the plant capacity. Unlike the influence on LCOE, the plant capacity has a direct linear influence on the annual electric yield. This is noticeable visually, and also numerically through the perfect R-squared value of 1.0000. According

 doi:10.20944/preprints202605.0188.v1

to the linear fit model shown in the figure, each MW increase in the capacity results in 8.7089 GWh of additional electric output. This linearity is explained by the continuous operation of the plant during the year (almost 100% capacity factor in the current model).

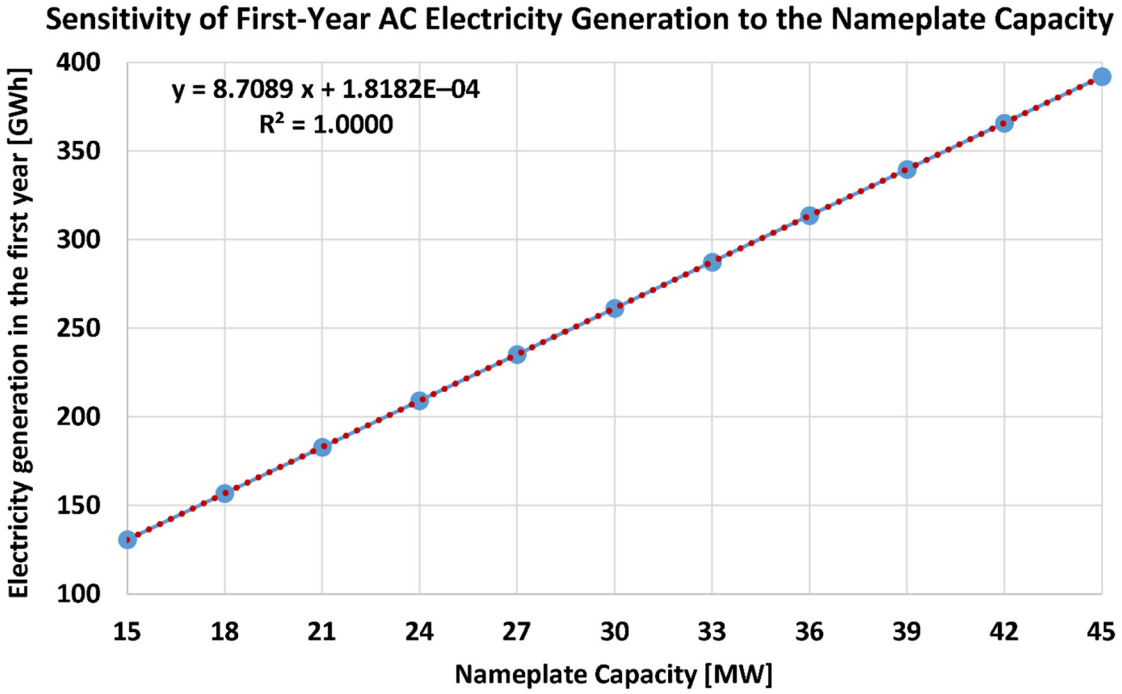

Figure 12. The estimated variation of the first-year generated electricity with the net capacity for the binary geothermal power plant in Muscat. The base-point capacity is 30 MW.

4.10. Sensitivity to Geothermal Resource Depth

The current subsection is dedicated to presenting and discussing the portion of the sensitivity analyses that is related to the influence of the second input parametric quantity (second input control variable), which is the depth of the geothermal resource. This input sensitivity variable determines the drilling overhead.

The range over which the depth was varied is from 1 km to 3 km. The criterion for adopting this range is that it corresponds to a 50% decrease and a 50% increase away from the design-point depth of 2 km, respectively. This is consistent with the criterion adopted earlier for the exploratory range of the net capacity.

Eleven depth data points were used in the parametric study, which are the base depth (2 km), plus five additional lower depths and five additional higher depths.

The 11 depth points are equally spaced with a step of 0.2 km, starting from 1 km. Thus, the 11 reservoir depths explored are:

1. km
2. km
3. km
4. 1.6 km
5. 1.8 km
6. MW (base or reference value)
7. km
8. MW
9. 2.6 MW
10. 2.8 MW
11. MW

 doi:10.20944/preprints202605.0188.v1

Figure 13 shows the response curve of the levelized cost of energy (LCOE) to the resource depth. This curve suggests a strong and weakly-linear impact of the depth on LCOE, which monotonically increases as the depth increases (thus, the drilling costs increase). For example, the base-point LCOE of 8.67875 ¢/kWh at 2 km increases by 12.36% and reaches 9.75182 ¢/kWh at 3 km, while this base-point LCOE decreases by 9.76% and reaches 7.83137 ¢/kWh at 1 km.

A quadratic polynomial is sufficient to capture the weak nonlinearity in the response curve of LCOE to the depth, with an R-squared value of 1.0000. In fact, an attempted linear approximation (not displayed here) still gave a high R-squared value of 0.9957.

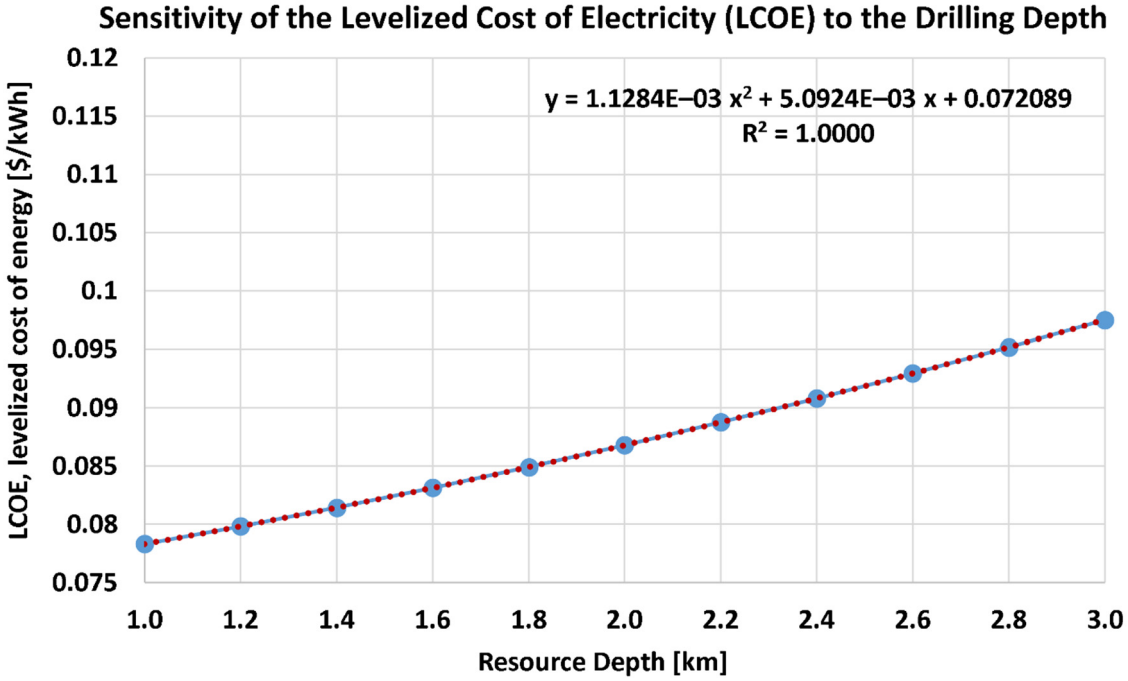

Figure 13. The estimated variation of LCOE with the depth of the geothermal resource for the binary geothermal power plant in Muscat. The base-point depth is 2 km.

Figure 14 shows the dependence of the first-year electric yield on the resource depth. It is apparent that the depth of the geothermal resource does not strongly affect the annual electric yield. This is noticeable visually through the nearly flat response curve. Despite this qualitative behavior, further detailed quantitative analysis showed very small gains in the electric yield as the depth increases, at a rate of about 0.0269 GWh/km. This gain is indicated by the regression model displayed in the figure. The R-squared value with a linear regression model is not exactly 1.0000 (but 0.9985), which is explained by imperfect linearity in the electricity–depth relationship. For each increment of the depth (0.2 km), the resultant gain in the electricity yield is not uniform, but varies between 0.005 GWh and 0.006 GWh. The small gains in the yield at larger depths can be explained by the updated well pumping conditions, making the self-consumption to run these pumps lower, and thus freeing some power to be shifted to the net capacity. Regardless of these details, the very shallow profile of the response curve makes it acceptable to consider the depth and the annual electricity yield as independent variables.

 doi:10.20944/preprints202605.0188.v1

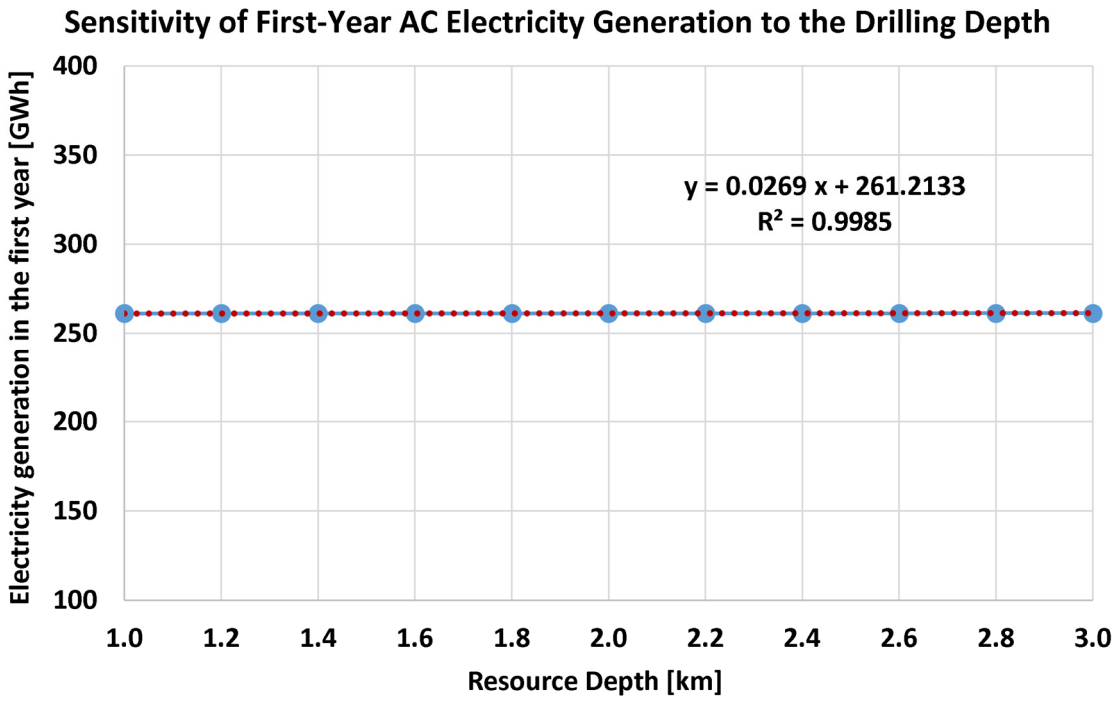

Figure 14. The estimated variation of the first-year generated electricity with the depth of the geothermal resource for the binary geothermal power plant in Muscat. The base-point depth is 2 km.

4.11. Sensitivity to Injection-to-Production Well Ratio

The current subsection is dedicated to presenting and discussing the portion of the sensitivity analyses that is related to the influence of the third input parametric quantity (third independent control variable), which is the ratio of the number of geothermal injection wells to the number of geothermal production wells.

The range over which the injection-to-production well ratio was varied is from 0.25 (or 25%) to 0.75 (or 75%). The criterion for adopting this range is that it corresponds to a 50% decrease and a 50% increase away from the design-point injection-to-production well ratio of 0.50 (or 50%), respectively. This is consistent with the criterion adopted for all other input sensitivity variables.

Eleven injection-to-production well ratios were used in the parametric study, which included the base ratio (0.50), plus five additional lower ratios and five additional higher ratios.

The 11 injection-to-production well ratios are equally spaced with a step of 0.05, starting from 0.25. Thus, the 11 injection-to-production well ratios explored are:

1. 0.25
2. 0.30
3. 0.35
4. 0.40
5. 0.45
6. 0.50
7. 0.55
8. 0.60
9. 0.65
10. 0.70
11. 0.75

Figure 15 shows the response curve of the levelized cost of energy (LCOE) to the injection-to-production well ratio. This curve shows that two contradicting influences coexist. One influence boosts LCOE as the injection-to-production well ratio increases (the flow rates within the injection

 doi:10.20944/preprints202605.0188.v1

wells decrease, which reduces the pump load and its power consumption), while the other reduces LCOE as the injection-to-production well ratio increases (initial drilling costs increase). At lower values of the injection-to-production well ratio, the reducing influence is stronger; while at higher values of the injection-to-production well ratio, the boosting influence is stronger, but it is relatively slow or weak. As a result, an optimum value for the injection-to-production well ratio exists, where LCOE is minimized. This optimum injection-to-production well ratio is 0.55 (given the incremental resolution of 0.05), at which LCOE becomes 8.67583 ¢/kWh. This is very close to the base-point LCOE of 8.67875 ¢/kWh at a 0.50 injection-to-production well ratio. Relative to the optimized minimum LCOE, the LCOE value increases by 6.29% and reaches 9.2215 ¢/kWh at 0.25 injection-to-production well ratio, while it increases by 1.31% and reaches 8.78958 ¢/kWh at 0.75 injection-to-production well ratio.

A cubic polynomial is necessary to model the reversing trend in the response curve of LCOE to the injection-to-production well ratio. A high R-squared value of 0.9902 can be attained under this cubic polynomial regression.

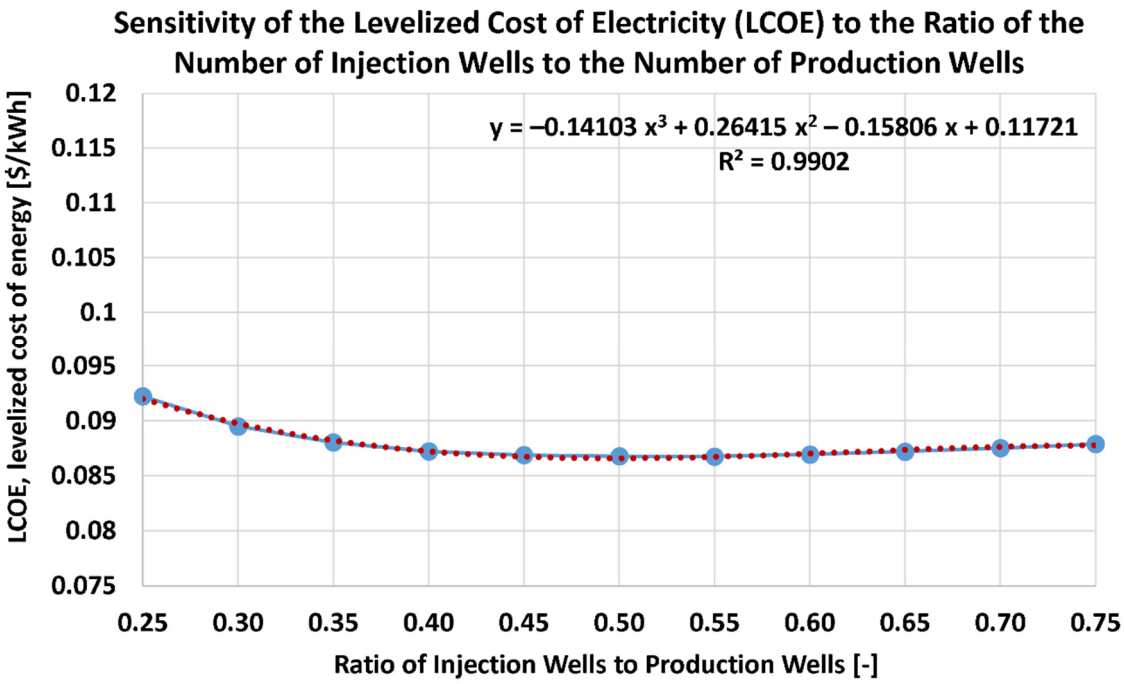

Figure 15. The estimated variation of LCOE with the injection-to-production well ratio for the binary geothermal power plant in Muscat. The base-point injection-to-production well ratio is 0.5.

Figure 16 shows the dependence of the first-year electric yield on the injection-to-production well ratio. Similar to the previous input sensitivity variable (the depth of the geothermal resource), the injection-to-production well ratio does not nearly affect the annual electric yield. Quantitative analysis of the shown almost-flat response curve showed that there are actually small gains in the electric yield as the injection-to-production well ratio increases, with a nonlinear, monotonic trend. This gain is indicated by the suggested cubic regression model displayed in the figure. The R-squared value with this cubic regression model is high (0.9979). The first-year electricity yield increased from 261.035 GWh at the lower-bound of 0.25 injection-to-production well ratio to 261.268 GWh at the base-value of 0.50 injection-to-production well ratio, and increased further to 261.325 GWh at the upper-bound of 0.75 injection-to-production well ratio. These values show that the gain in the first-year electricity yield becomes smaller as the injection-to-production well ratios increase (a decelerating gain trend). Despite this present gain, the shallow profile of the response curve makes it practical to consider the injection-to-production well ratio and the annual electricity yield as being approximately independent. To emphasize this finding, it is useful to add that over the entire

 doi:10.20944/preprints202605.0188.v1

explored range of the injection-to-production well ratio (from 0.25 to 0.75), the gain in the first-year electric yield was 0.290 GWh, which is only 0.11% of the base value of 261.268 GWh.

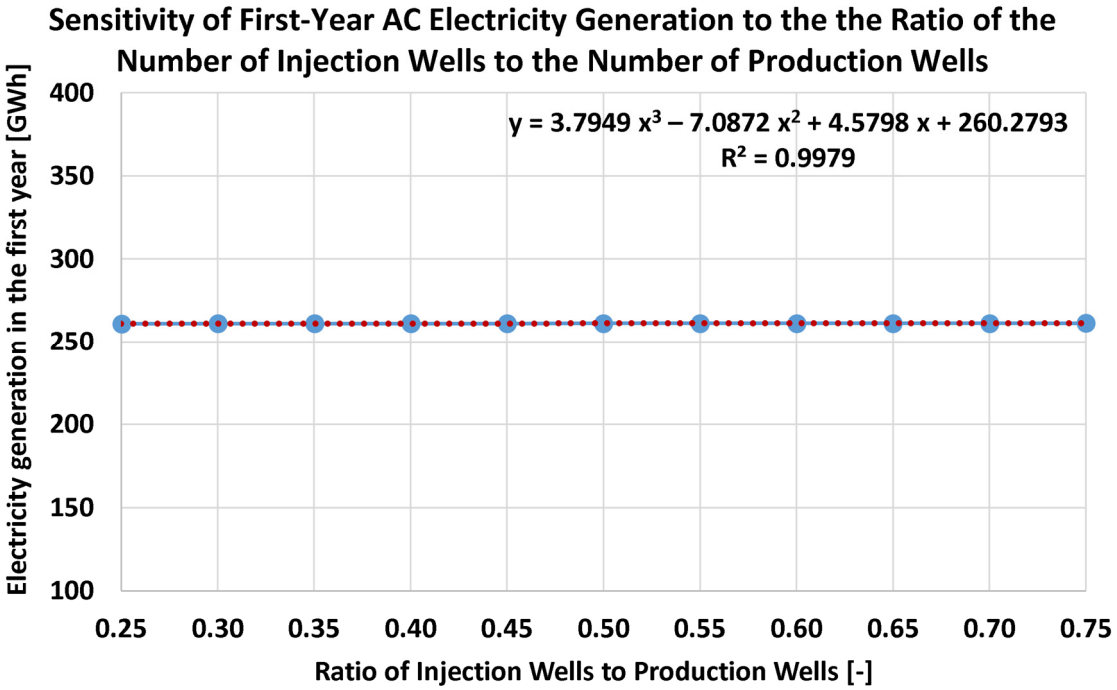

Figure 16. The estimated variation of the first-year generated electricity with the injection-to-production well ratio for the binary geothermal power plant in Muscat. The base-point injection-to-production well ratio is 0.5.

4.12. Sensitivity to Well Pump Efficiency

The current subsection is dedicated to presenting and discussing the portion of the sensitivity analyses that is related to the influence of the fourth input parametric quantity (fourth independent control variable), which is the efficiency of the pumps used in the production wells and injection wells.

The range over which the well pump efficiency was varied is from 45.0% to 90.0%. As discussed earlier, this range is selected as a result of imposing a 50% decrease and a 50% increase away from the design-point well pump efficiency of 67.5%, respectively.

Eleven well pump efficiencies were used in the parametric study, which included the base efficiency (67.5%), plus five additional lower efficiencies and five additional higher efficiencies.

The 11 well pump efficiencies are equally spaced with a step of 4.5% percentage points (pp), starting from 45.0%. Thus, the 11 well pump efficiencies explored are:

1. 45.0%
2. 49.5%
3. 54.0%
4. 58.5%
5. 63.0%
6. 67.5%
7. 72.0%
8. 76.5%
9. 81.0%
10. 85.5%
11. 90.0%

Figure 17 shows the response curve of the levelized cost of energy (LCOE) to the well pump efficiency. This curve suggests a favorable monotonic decline in LCOE, which decreases as the well

 doi:10.20944/preprints202605.0188.v1

pump efficiency increases (thus, the operational costs for powering the pumps decrease). For example, the base-point LCOE of 8.67875 ¢/kWh at 67.5% efficiency decreases by 2.45% and reaches 8.46577 ¢/kWh at 90.0% efficiency, while this base-point LCOE increases by 5.19% and reaches 9.12932 ¢/kWh at 45.0% efficiency.

A quadratic polynomial is sufficient to excellently capture the weak nonlinearity in the response curve of LCOE to the well pump efficiency, with an R-squared value of 0.9978. It should be noted that the displayed quadratic regression equation treats the well pump efficiency as a fraction (thus, having a valid range between 0.45 and 0.90, not between 45 and 90).

An attempted linear approximation (not displayed here) gave a lower R-squared value of 0.9567. That more approximate linear regression model suggested a steady drop in LCOE as the well pump efficiency increases, at the rate of 0.014139 US$/kWh (or 1.4139 ¢/kWh) per unit of efficiency. Thus, over the varied efficiency range of 0.45 (between 0.45 and 0.90), the linear regression model predicted an overall drop of 0.0063626 US$/kWh or 0.63626 ¢/kWh (computed as 0.45 times the rate of 0.014139 US$/kWh or 1.4139 ¢/kWh). The actual overall drop was 0.663550 ¢/kWh, which is slightly above the linear-regression estimation.

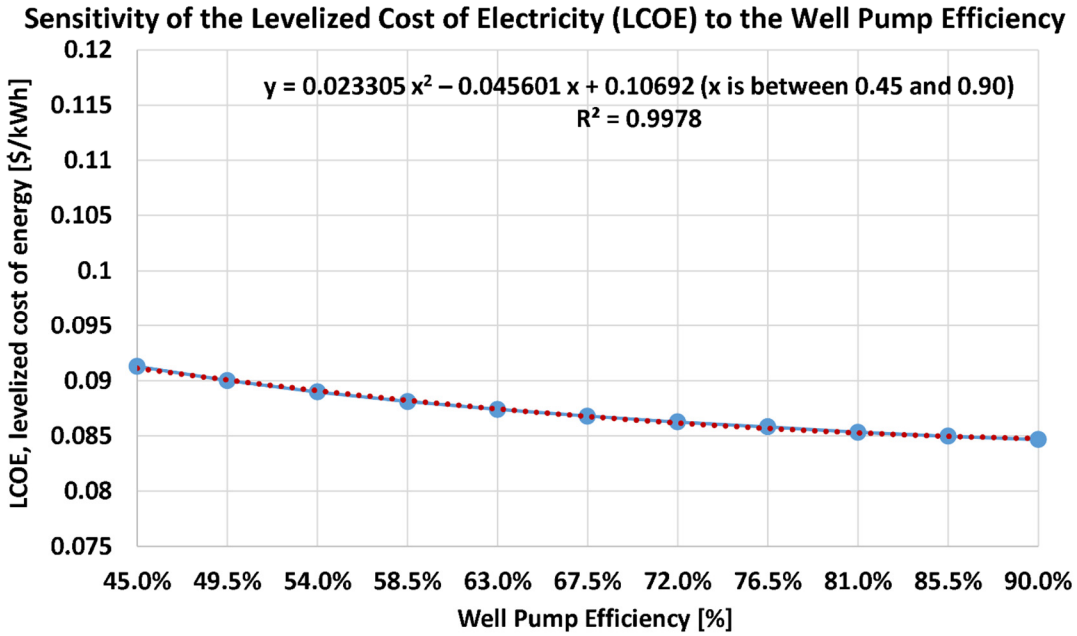

Figure 17. The estimated variation of LCOE with the well pump efficiency for the binary geothermal power plant in Muscat. The base-point well pump efficiency is 67.5%.

Figure 18 shows the dependence of the first-year electric yield on the well pump efficiency. It is apparent that the well pump efficiency does not have a big effect on the annual electric yield. Deeper analysis revealed a small monotonic gain in the first-year electric yield as the well pump efficiency increases. This is logical, due to the decreased power penalty when the pump becomes more efficient. This gain is from 261.156 GWh at 45% efficiency to 261.318 GWh at 90.0% efficiency. Thus, the overall gain (considering the overall explored range of well pump efficiency) is 0.162 GWh only, which is 0.062% of the base-point first-year electric yield of 261.268 GWh at 67.5% efficiency. The profile of this gain in the first-year electric yield can be represented by a quadratic regression model, with a high R-squared value of 0.9979. As found in the case of the injection-to-production well ratio, the profile of the gain due to the improved well pump efficiency is decelerating, with progressively smaller gain increments achieved at higher efficiencies. As found in the case of the injection-to-production well ratio, it is reasonable to neglect the effect of the well pump efficiency on the annual electricity yield.

 doi:10.20944/preprints202605.0188.v1

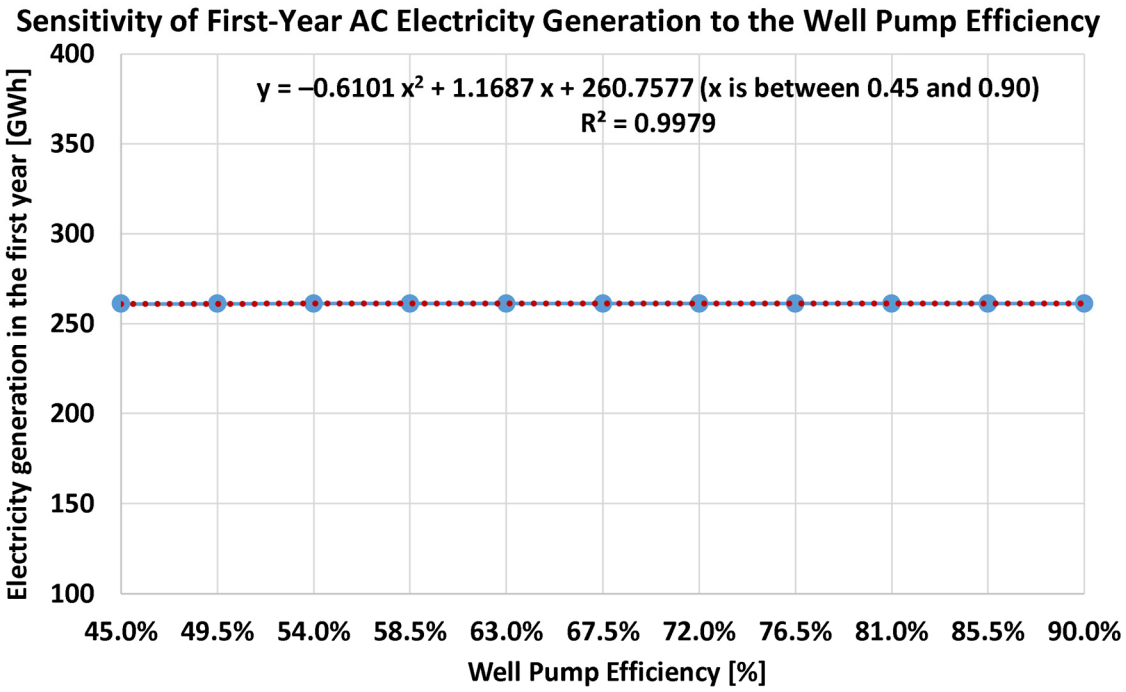

Figure 18. The estimated variation of the first-year generated electricity with the well pump efficiency for the binary geothermal power plant in Muscat. The base-point well pump efficiency is 67.5%.

4.13. Competitiveness of Geothermal Electricity in Oman

The presented results (electric generation performance and economic metrics) for the imagined geothermal power plant in Muscat, Oman, are useful but insufficient to draw a conclusion regarding the primary objective of the current study, which is to make a recommendation regarding whether geothermal power in Oman is attractive or not.

In order to address this inquiry, a comparison is needed between the estimated geothermal LCOE and the existing electricity tariffs in Oman. It is admitted that this criterion is merely financial, and does not take into account several factors; such as environmental gains, technology maturity, and social acceptance. While these factors establish valid inputs for making a generic decision about the potential of geothermal power in Oman, relying on a single measurable factor (electricity cost) simplifies the analysis and makes it easier to defend. In addition, the electricity cost is de facto a crucial factor when deciding on the viability and success of a geothermal project. If the project is profitable, minor technical or environmental challenges may be coped with. However, if the project is not financially successful, then it becomes difficult to implement, even if it has several environmental or societal advantages.

For competitiveness testing in Oman, the design-point LCOE estimation of the SAM simulation (8.68 cents/kWh or 33.4 Bz/kWh) is adopted as a hypothetical tariff for geothermal power. This is intentionally a conservative assumption, giving an advantage to the geothermal power technology when compared to other electricity generation technologies in Oman, because a profit margin is not imposed on top of the estimated LCOE.

While the commercially sold grid electricity in Oman is subsidized [297] for small consumers (such as residential electricity consumers with a monthly consumption within 6 MWh) [298], large corporate consumers or institutional consumers with an annual consumption beyond 100 MWh pay the unsubsidized tariffs, known in Oman as the cost reflective tariffs (CRT) [299].

According to the 2025 announced CRT (which was the latest edition at the time of initiating this study), there is an option of a flat tariff (year-round constant, no peak period, no seasonal variation) according to the level of electric connection [300]. These are summarized in Table 12.

 doi:10.20944/preprints202605.0188.v1

Table 12. Flat-rate version of the cost reflective tariffs (CRT) in Oman, 2025 edition.

Connection level (voltage)	HV/HT (132 kV, 220 kV, 400 kV)	MV/MT (33 kV)	MV/MT (11 kV)	LV (0.415 kV or 415 V)
Tariff (Bz/kWh)	21	25	26	33

With this, comparing the SAM's estimated LCOE of 33.4 Bz/kWh to the cheapest selling price of 21 Bz/kWh shows that the geothermal plant is not an advantageous alternative technology compared to the existing power generation technologies that supply electricity to the electric grid in Oman.

Considering photovoltaic (PV) systems in Oman, a power purchase agreement (PPA) [301,302] may be used to purchase solar electricity at a flat rate of about 25 Bz/kWh. This is well below the SAM's LCOE estimation for geothermal power.

From first-hand recent experience in Oman, it was found that a self-owned photovoltaic power system (without battery storage) can have an LCOE value of approximately 10 Bz/kWh. This is much below (much more attractive) than the SAM's LCOE estimation for geothermal power.

With these remarks, it is evident that geothermal power is more expensive than conventional (natural gas) power or PV power. When adding to this finding the simplicity in installing PV systems [303–305] compared to a geothermal system, the maturity and widespread of PV systems in Oman [306–308], the direct conversion to electricity in the case of PV systems (little maintenance needed other than cleaning), and the possibility of retrofitting existing parking lots with rooftop PV modules for solar carport [309,310], especially for charging electric vehicles [311], without occupying new land footprints; one can judge that geothermal power is not expected to be exploited in Oman unless new incentivizing factors appear.

5. Discussion of the Limitations

After presenting information about the modeling performed here for geothermal power generation and presenting results obtained through this modeling, it is important to admit that the current study still has some limitations. This section is devoted to discussing this matter.

However, it should be noted first that the primary goal of this study is to identify the feasibility of geothermal power in Oman, rather than to provide a precise and comprehensive design of a particular geothermal power plant. Thus, the results of the current study should be viewed with tolerance, accepting that some uncertainty in the assumptions made does not harm the overall aim of the study. Even with small variations in the quantitative results, the main outcome (which is answering the question of "is commercial geothermal-based electricity generation in Oman competitive or not?") remains valid.

1. The first limitation to mention here is the reliance on the SAM (System Advisor Model) tool for performing the techno-economic assessment, without performing benchmarking of its predictions. While this limitation is true, it is alleviated by the implied robustness and accuracy of SAM. This is supported by its wide use by researchers and professionals in the sector of renewable and sustainable technologies [312–314] and by the third-party validation performed by the SAM development team [315] or independent researchers [316]. Also, SAM enjoys an extended history of development and improvement provided by NREL. In addition, it is worth mentioning that the open-course code package behind the SAM computations is available in a public GitHub repository [317–323]. This allows for transparency and continuous handling of any identified issues.
2. The second limitation to mention here is the large number of assumptions made, through specified input parameters, to perform either the technical part of the simulation or the economic part. However, this is an inevitable situation in simulation studies in general. Many of the assumptions made here are guided by recommendations from reliable sources in the literature,

 doi:10.20944/preprints202605.0188.v1

as well as professional judgment. Also, sensitivity analyses are performed to explore the influence of possible variations of some assumptions.

3. The third limitation to add is the adoption of built-in cost elements in SAM for estimations in belonging to Oman. Some of the geothermal financial data in SAM are based on the Geothermal Vision Study (GeoVision Study) of the Geothermal Technologies Office (GTO) at the United States Department of Energy (DOE) [324]. This means that a similarity of certain costs (like drilling labor rates) in the United States and Oman encourages the assumption that reasonable predictions can be made for Oman. The fact that both Oman and the United States are in the same economic category of high-income countries makes this assumption plausible [325].
4. The fourth limitation that might be noticed in the current study is its focus on Oman, rather than being of wide coverage. While this remark is correct, it does not mean that the study is only useful to readers within Oman. The study contains many pieces of information that are transferable to other regions. For example, information provided about the use of SAM in modeling geothermal power systems can be applied when using SAM in other locations. This study can be viewed as a case study for Oman, which can be replicated for other countries. Especially, readers in countries sharing similar energy sources with Oman, with ambitions to explore their geothermal potential in the power sector, can find this study beneficial.
5. The fifth limitation to state here is that the adopted geothermal resource temperature of 200 °C is not based on direct measurement. However, this assumption seems realistic given that temperatures as high as 174 °C were measured at depths of up to 1.5 km in Oman (as described in subsection "2.5 Geothermal Energy in Oman and Binary Geothermal Plant"). Therefore, reaching a mildly higher temperature of 200 °C at a deeper point of 2 km appears to be attainable.

6. Conclusions

In the current study, the System Advisor Model (SAM) modeling tool was used to perform techno-economic assessment (TEA) and sensitivity analysis of a 30-MW geothermal power plant in Muscat, Oman. Based on literature data, it was found that the binary cycle is an adequate choice. Compared to other electricity generation sources in Oman, particularly natural gas power stations and solar photovoltaic arrays, geothermal power was not an attractive alternative due to economic considerations.

The performed parametric studies showed that the power plant capacity is an influential method to improve the feasibility of geothermal power, where the economy of scale (through a larger plant) leads to appreciable nonlinear reductions in the levelized cost of energy (LCOE).

The current study neither anticipates nor recommends that the government of the Sultanate of Oman or non-governmental corporations invest in a geothermal power plant when better alternatives (particularly solar photovoltaic arrays) are available.

The study concludes that the main barrier against the deployment of geothermal power plants in Oman is the presence of much better (cheaper and proven) alternatives.

Funding: Not applicable (this research received no funding).

Data Availability Statement: Data sharing is not applicable to this article as no datasets were generated or analysed during the current study.

Declaration of Competing Interests Statement: The author declares that they have no known competing financial interests or personal relationships that could have appeared to influence the work reported in this paper.

References

1. G. Yushin, R. Dash, J. Jagiello, J.E. Fischer, Y. Gogotsi, Carbide-Derived Carbons: Effect of Pore Size on Hydrogen Uptake and Heat of Adsorption, Advanced Functional Materials 16 (2006) 2288–2293. https://doi.org/10.1002/adfm.200500830.

 doi:10.20944/preprints202605.0188.v1

2. T. Ebina, F. Mizukami, Flexible Transparent Clay Films with Heat-Resistant and High Gas-Barrier Properties, Advanced Materials 19 (2007) 2450–2453. https://doi.org/10.1002/adma.200700162.
3. D. Mackay, R.S. Boethling, eds., Handbook of Property Estimation Methods for Chemicals: Environmental Health Sciences, CRC Press, Boca Raton, 2000. https://doi.org/10.1201/9781420026283.
4. H. Chang, The Myth of the Boiling Point, Science Progress 91 (2008) 219–240. https://doi.org/10.3184/003685008X360632.
5. Introduction to the East African Rift System, in: Geoscience of Rift Systems—Evolution of East Africa, American Association of Petroleum Geologists, 1999: pp. 1–18. https://doi.org/10.1306/St44623C1.
6. D.S. Stamps, E. Calais, E. Saria, C. Hartnady, J. Nocquet, C.J. Ebinger, R.M. Fernandes, A kinematic model for the East African Rift, Geophysical Research Letters 35 (2008) 2007GL032781. https://doi.org/10.1029/2007GL032781.
7. R. Zhang, K.P. Lam, S. Yao, Y. Zhang, Coupled EnergyPlus and computational fluid dynamics simulation for natural ventilation, Building and Environment 68 (2013) 100–113. https://doi.org/10.1016/j.buildenv.2013.04.002.
8. D. Esteves, J. Silva, L. Martins, J. Teixeira, S. Teixeira, Building Energy Performance: Comparison Between EnergyPlus and Other Certified Tools, in: O. Gervasi, B. Murgante, S. Misra, C. Garau, I. Blečić, D. Taniar, B.O. Apduhan, A.M.A.C. Rocha, E. Tarantino, C.M. Torre (Eds.), Computational Science and Its Applications – ICCSA 2021, Springer International Publishing, Cham, 2021: pp. 493–503. https://doi.org/10.1007/978-3-030-86653-2_36.
9. D. Zhu, T. Hong, D. Yan, C. Wang, A detailed loads comparison of three building energy modeling programs: EnergyPlus, DeST and DOE-2.1E, Build. Simul. 6 (2013) 323–335. https://doi.org/10.1007/s12273-013-0126-7.
10. H.B. Gunay, W. O'Brien, I. Beausoleil-Morrison, Implementation and comparison of existing occupant behaviour models in EnergyPlus, Journal of Building Performance Simulation 9 (2016) 567–588. https://doi.org/10.1080/19401493.2015.1102969.
11. K.W.D.K.C. Dahanayake, C.L. Chow, Studying the potential of energy saving through vertical greenery systems: Using EnergyPlus simulation program, Energy and Buildings 138 (2017) 47–59. https://doi.org/10.1016/j.enbuild.2016.12.002.
12. N. Fumo, P. Mago, R. Luck, Methodology to estimate building energy consumption using EnergyPlus Benchmark Models, Energy and Buildings 42 (2010) 2331–2337. https://doi.org/10.1016/j.enbuild.2010.07.027.
13. G. Ramos, E. Ghisi, Analysis of daylight calculated using the EnergyPlus programme, Renewable and Sustainable Energy Reviews 14 (2010) 1948–1958. https://doi.org/10.1016/j.rser.2010.03.040.
14. D.B. Crawley, L.K. Lawrie, F.C. Winkelmann, W.F. Buhl, Y.J. Huang, C.O. Pedersen, R.K. Strand, R.J. Liesen, D.E. Fisher, M.J. Witte, J. Glazer, EnergyPlus: creating a new-generation building energy simulation program, Energy and Buildings 33 (2001) 319–331. https://doi.org/10.1016/S0378-7788(00)00114-6.
15. R. Evans, B. Yildiz, J. Bilbao, Capturing Photons Using High Ground Coverage Ratio (GCR) approaches, in: 2020 47th IEEE Photovoltaic Specialists Conference (PVSC), IEEE, Calgary, AB, Canada, 2020: pp. 2296–2299. https://doi.org/10.1109/PVSC45281.2020.9301029.
16. C. Dupraz, Assessment of the ground coverage ratio of agrivoltaic systems as a proxy for potential crop productivity, Agroforest Syst 98 (2024) 2679–2696. https://doi.org/10.1007/s10457-023-00906-3.
17. L. Narvarte, E. Lorenzo, Tracking and ground cover ratio, Progress in Photovoltaics: Research and Applications 16 (2008) 703–714. https://doi.org/10.1002/pip.847.
18. A.P. Worth, C.J. Van Leeuwen, T. Hartung, The prospects for using (Q)SARs in a changing political environment--high expectations and a key role for the european commission's joint research centre, SAR and QSAR in Environmental Research 15 (2004) 331–343. https://doi.org/10.1080/10629360412331297371.
19. M. Pavan, A.P. Worth, Publicly-accessible QSAR software tools developed by the Joint Research Centre, SAR and QSAR in Environmental Research 19 (2008) 785–799. https://doi.org/10.1080/10629360802550390.
20. R.P. Shea, Y.K. Ramgolam, Applied levelized cost of electricity for energy technologies in a small island developing state: A case study in Mauritius, Renewable Energy 132 (2019) 1415–1424. https://doi.org/10.1016/j.renene.2018.09.021.

 doi:10.20944/preprints202605.0188.v1

21. K. Hansen, Decision-making based on energy costs: Comparing levelized cost of energy and energy system costs, Energy Strategy Reviews 24 (2019) 68–82. https://doi.org/10.1016/j.esr.2019.02.003.
22. X. Ouyang, B. Lin, Levelized cost of electricity (LCOE) of renewable energies and required subsidies in China, Energy Policy 70 (2014) 64–73. https://doi.org/10.1016/j.enpol.2014.03.030.
23. K. Branker, M.J.M. Pathak, J.M. Pearce, A review of solar photovoltaic levelized cost of electricity, Renewable and Sustainable Energy Reviews 15 (2011) 4470–4482. https://doi.org/10.1016/j.rser.2011.07.104.
24. O. Schmidt, S. Melchior, A. Hawkes, I. Staffell, Projecting the Future Levelized Cost of Electricity Storage Technologies, Joule 3 (2019) 81–100. https://doi.org/10.1016/j.joule.2018.12.008.
25. M. Obi, S.M. Jensen, J.B. Ferris, R.B. Bass, Calculation of levelized costs of electricity for various electrical energy storage systems, Renewable and Sustainable Energy Reviews 67 (2017) 908–920. https://doi.org/10.1016/j.rser.2016.09.043.
26. W. Shen, X. Chen, J. Qiu, J.A. Hayward, S. Sayeef, P. Osman, K. Meng, Z.Y. Dong, A comprehensive review of variable renewable energy levelized cost of electricity, Renewable and Sustainable Energy Reviews 133 (2020) 110301. https://doi.org/10.1016/j.rser.2020.110301.
27. C.S. Lai, M.D. McCulloch, Levelized cost of electricity for solar photovoltaic and electrical energy storage, Applied Energy 190 (2017) 191–203. https://doi.org/10.1016/j.apenergy.2016.12.153.
28. K.J. Chalvatzis, A. Ioannidis, Energy supply security in the EU: Benchmarking diversity and dependence of primary energy, Applied Energy 207 (2017) 465–476. https://doi.org/10.1016/j.apenergy.2017.07.010.
29. M. Akai, Primary energy supply, IEEJ Transactions Elec Engng 2 (2007) 17–21. https://doi.org/10.1002/tee.20110.
30. J. Vehmas, J. Kaivo-oja, J. Luukkanen, Energy efficiency as a driver of total primary energy supply in the EU-28 countries – incremental decomposition analysis, Heliyon 4 (2018) e00878. https://doi.org/10.1016/j.heliyon.2018.e00878.
31. A. Deka, H. Ozdeser, M. Seraj, The impact of primary energy supply, effective capital and renewable energy on economic growth in the EU-27 countries. A dynamic panel GMM analysis, Renewable Energy 219 (2023) 119450. https://doi.org/10.1016/j.renene.2023.119450.
32. H. Farzaneh, Energy Supply Models, in: Energy Systems Modeling, Springer Singapore, Singapore, 2019: pp. 81–105. https://doi.org/10.1007/978-981-13-6221-7_4.
33. N. Noorfatima, J. Koh, J. Jung, A. Onen, Trading mechanism for improved interoperability in virtual power purchase agreement towards 100% renewable energy, Journal of Cleaner Production 520 (2025) 146065. https://doi.org/10.1016/j.jclepro.2025.146065.
34. K. Fedorová, T. Ábelová, M. Kvasnica, Dynamic Power Purchase Agreement, in: 2023 24th International Conference on Process Control (PC), IEEE, Strbske Pleso, Slovakia, 2023: pp. 156–161. https://doi.org/10.1109/PC58330.2023.10217697.
35. K. Kapral, K. Soetaert, R. Castro, An Off-Site Power Purchase Agreement (PPA) as a Tool to Protect against Electricity Price Spikes: Developing a Framework for Risk Assessment and Mitigation, Energies 17 (2024) 2161. https://doi.org/10.3390/en17092161.
36. F. Isaza Cuervo, C.A. Arredondo-Orozco, G.C. Marenco-Maldonado, Photovoltaic power purchase agreement valuation under real options approach, Renewable Energy Focus 36 (2021) 96–107. https://doi.org/10.1016/j.ref.2020.12.006.
37. L. Mendicino, D. Menniti, A. Pinnarelli, N. Sorrentino, Corporate power purchase agreement: Formulation of the related levelized cost of energy and its application to a real life case study, Applied Energy 253 (2019) 113577. https://doi.org/10.1016/j.apenergy.2019.113577.
38. T. Lhendup, S. Lhundup, Comparison of methodologies for generating a typical meteorological year (TMY), Energy for Sustainable Development 11 (2007) 5–10. https://doi.org/10.1016/S0973-0826(08)60571-2.
39. Y. Jiang, Generation of typical meteorological year for different climates of China, Energy 35 (2010) 1946–1953. https://doi.org/10.1016/j.energy.2010.01.009.
40. D. Pissimanis, G. Karras, V. Notaridou, K. Gavra, The generation of a “typical meteorological year” for the city of Athens, Solar Energy 40 (1988) 405–411. https://doi.org/10.1016/0038-092X(88)90095-3.
41. A.L.S. Chan, T.T. Chow, S.K.F. Fong, J.Z. Lin, Generation of a typical meteorological year for Hong Kong, Energy Conversion and Management 47 (2006) 87–96. https://doi.org/10.1016/j.enconman.2005.02.010.

 doi:10.20944/preprints202605.0188.v1

42. T. Cebecauer, M. Suri, Typical Meteorological Year Data: SolarGIS Approach, Energy Procedia 69 (2015) 1958–1969. https://doi.org/10.1016/j.egypro.2015.03.195.
43. P. Stelling, L. Shevenell, N. Hinz, M. Coolbaugh, G. Melosh, W. Cumming, Geothermal systems in volcanic arcs: Volcanic characteristics and surface manifestations as indicators of geothermal potential and favorability worldwide, Journal of Volcanology and Geothermal Research 324 (2016) 57–72. https://doi.org/10.1016/j.jvolgeores.2016.05.018.
44. T.W. Heggie, Geotourism and volcanoes: Health hazards facing tourists at volcanic and geothermal destinations, Travel Medicine and Infectious Disease 7 (2009) 257–261. https://doi.org/10.1016/j.tmaid.2009.06.002.
45. O.K. Zakharova, V.V. Spichak, Geothermal fields of Hengill Volcano, Iceland, J. Volcanolog. Seismol. 6 (2012) 1–14. https://doi.org/10.1134/S074204631201006X.
46. R.T. Helz, C.R. Thornber, Geothermometry of Kilauea Iki lava lake, Hawaii, Bull Volcanol 49 (1987) 651–668. https://doi.org/10.1007/BF01080357.
47. [Woods Hole Oceanographic Institution] WHOI, WHOI | Lava Flows, (2025). https://divediscover.whoi.edu/hot-topics/lavaflows (accessed June 27, 2025).
48. A.G.E. Abbady, Evaluation of heat generation by radioactive decay of sedimentary rocks in Eastern Desert and Nile Valley, Egypt, Applied Radiation and Isotopes 68 (2010) 2020–2024. https://doi.org/10.1016/j.apradiso.2010.03.023.
49. W.R.V. Schmus, Radioactivity Properties of Minerals And Rocks, in: Handbook of Physical Properties of Rocks (1984), CRC Press, 1984.
50. C. Clauser, Heat Transport Processes in the Earth's Crust, Surv Geophys 30 (2009) 163–191. https://doi.org/10.1007/s10712-009-9058-2.
51. M. Nathenson, M. Guffanti, Geothermal gradients in the conterminous United States, Journal of Geophysical Research: Solid Earth 93 (1988) 6437–6450. https://doi.org/10.1029/JB093iB06p06437.
52. W.E. Glassley, Geothermal Energy: Renewable Energy and the Environment, Second Edition, 2nd ed., CRC Press, New York, USA, 2014. https://books.google.com.om/books?id=hPCsBAAAQBAJ (accessed June 27, 2025).
53. Y. Li, Y. Chen, Q. Jiang, R. Hu, C. Zhou, Performance assessment and optimization of seepage control system: A numerical case study for Kala underground powerhouse, Computers and Geotechnics 55 (2014) 306–315. https://doi.org/10.1016/j.compgeo.2013.09.013.
54. O.A. Marzouk, Condenser Pressure Influence on Ideal Steam Rankine Power Vapor Cycle using the Python Extension Package Cantera for Thermodynamics, Engineering, Technology & Applied Science Research 14 (2024) 14069–14078. https://doi.org/10.48084/etasr.7277.
55. G. Cui, Z. Niu, D. Zhao, Y. Kong, B. Feng, High-temperature hydrothermal resource exploration and development: Comparison with oil and gas resource, Gondwana Research 122 (2023) 306–314. https://doi.org/10.1016/j.gr.2022.09.015.
56. EDF Energy, EDF | Renewable Energy - Types, Forms & Sources, (2025). https://www.edfenergy.com/energywise/renewable-energy-sources (accessed June 27, 2025).
57. A.F. de O. Falcão, Wave energy utilization: A review of the technologies, Renewable and Sustainable Energy Reviews 14 (2010) 899–918. https://doi.org/10.1016/j.rser.2009.11.003.
58. O.A. Marzouk, *Jatropha Curcas* as Marginal Land Development Crop in the Sultanate of Oman for Producing Biodiesel, Biogas, Biobriquettes, Animal Feed, and Organic Fertilizer, Reviews in Agricultural Science 8 (2020) 109–123. https://doi.org/10.7831/ras.8.0_109.
59. C. Shetty, A. Priyam, A review on tidal energy technologies, Materials Today: Proceedings 56 (2022) 2774–2779. https://doi.org/10.1016/j.matpr.2021.10.020.
60. [International Energy Agency] IEA, IEA | Share of renewable electricity generation by technology, 2000-2030, IEA (2023). https://www.iea.org/data-and-statistics/charts/share-of-renewable-electricity-generation-by-technology-2000-2030 (accessed July 1, 2025).
61. O.A. Marzouk, Wind Speed Weibull Model Identification in Oman, and Computed Normalized Annual Energy Production (NAEP) From Wind Turbines Based on Data From Weather Stations, Engineering Reports 7 (2025) e70089. https://doi.org/10.1002/eng2.70089.

 doi:10.20944/preprints202605.0188.v1

62. E.F. Moran, M.C. Lopez, N. Moore, N. Müller, D.W. Hyndman, Sustainable hydropower in the 21st century, Proceedings of the National Academy of Sciences 115 (2018) 11891–11898. https://doi.org/10.1073/pnas.1809426115.
63. I.K. Rotich, H. Chepkirui, P.K. Musyimi, G. Kipruto, Geothermal energy in Kenya: Evaluating health impacts and environmental challenges, Energy for Sustainable Development 82 (2024) 101522. https://doi.org/10.1016/j.esd.2024.101522.
64. I.K. Rotich, H. Chepkirui, P.K. Musyimi, Renewable energy status and uptake in Kenya, Energy Strategy Reviews 54 (2024) 101453. https://doi.org/10.1016/j.esr.2024.101453.
65. J. Chorowicz, The East African rift system, Journal of African Earth Sciences 43 (2005) 379–410. https://doi.org/10.1016/j.jafrearsci.2005.07.019.
66. R.K. Upadhyay, Earth's Internal Dynamics and Landforms, in: R.K. Upadhyay (Ed.), Geology and Mineral Resources, Springer Nature, Singapore, 2025: pp. 139–212. https://doi.org/10.1007/978-981-96-0598-9_3.
67. P. Amatyakul, W. Siripunvaraporn, T. Rung-Arunwan, C. Vachiratienchai, K. Pirarai, N. Prommakorn, A decade of successful magnetotelluric surveys for delineating shallow geothermal reservoirs beneath nonvolcanic hot springs in Thailand, Geophysics 88 (2023) WB55–WB69. https://doi.org/10.1190/geo2022-0486.1.
68. L. Junrong, L. Wenqiang, W. Xingru, Z. Yaping, Numerical simulation of heat transfer phenomena and influencing factors between deep and shallow geothermal reservoirs, Applied Thermal Engineering 290 (2026) 130038. https://doi.org/10.1016/j.applthermaleng.2026.130038.
69. A.L. Brettschneider, L. Perković, Theoretical analysis of using multiple borehole heat exchangers for production of heating and cooling energy in shallow geothermal reservoirs with underground water flow, Applied Thermal Engineering 254 (2024) 123914. https://doi.org/10.1016/j.applthermaleng.2024.123914.
70. J.S. Figueira, A. García Gil, A. Vieira, A.K. Michopoulos, D.P. Boon, F. Loveridge, F. Cecinato, G. Götzl, J. Epting, K. Zosseder, M. Bloemendal, M. Woods, P. Christodoulides, P.J. Vardon, S.P. Borg, S. Erbs Poulsen, T.R. Andersen, Shallow geothermal energy systems for district heating and cooling networks: Review and technological progression through case studies, Renewable Energy 236 (2024) 121436. https://doi.org/10.1016/j.renene.2024.121436.
71. [Nordic Energy Research] NER, NER | World's highest share of geothermal power, (2025). https://www.nordicenergy.org/figure/two-thirds-renewable/worlds-highest-share-of-geothermal-power (accessed June 27, 2025).
72. K. Benediktsson, Conflicting imaginaries in the energy transition? Nature and renewable energy in Iceland, Moravian Geographical Reports 29 (2021) 88–100. https://doi.org/10.2478/mgr-2021-0008.
73. Government of Iceland, Government of Iceland | Geothermal, (2025). https://www.government.is/topics/business-and-industry/energy/geothermal (accessed June 27, 2025).
74. Government of Iceland, Government of Iceland | Energy, (2025). https://www.government.is/topics/business-and-industry/energy (accessed June 27, 2025).
75. [International Energy Agency] IEA, IEA | Iceland - Country Profile, (2025). https://www.iea.org/countries/iceland (accessed July 20, 2025).
76. O.A. Marzouk, Technical review of radiative-property modeling approaches for gray and nongray radiation, and a recommended optimized WSGGM for CO2/H2O-enriched gases, Results in Engineering 25 (2025) 103923. https://doi.org/10.1016/j.rineng.2025.103923.
77. L.R. Vargas Zeppetello, A. Donohoe, D.S. Battisti, Does Surface Temperature Respond to or Determine Downwelling Longwave Radiation?, Geophysical Research Letters 46 (2019) 2781–2789. https://doi.org/10.1029/2019GL082220.
78. T. Fridriksson, A.M. Merino, A.Y. Orucu,, P. Audinet, Greenhouse Gas Emissions from Geothermal Power Production, in: 2nd Workshop on Geothermal Reservoir Engineering, Stanford University, Stanford, California, USA, 2017: pp. 1–12. https://documents1.worldbank.org/curated/en/875761592973336676/pdf/Greenhouse-Gas-Emissions-from-Geothermal-Power-Production.pdf.

 doi:10.20944/preprints202605.0188.v1

79. O.A. Marzouk, Energy Generation Intensity (EGI) for Parabolic Dish/Engine Concentrated Solar Power in Muscat, Sultanate of Oman, IOP Conference Series: Earth and Environmental Science 1008 (2022) 012013. https://doi.org/10.1088/1755-1315/1008/1/012013.
80. S. Watson, Quantifying the variability of wind energy, WIREs Energy and Environment 3 (2014) 330–342. https://doi.org/10.1002/wene.95.
81. V. Stefánsson, Investment cost for geothermal power plants, Geothermics 31 (2002) 263–272. https://doi.org/10.1016/S0375-6505(01)00018-9.
82. C. Jung, D. Schindler, Development of onshore wind turbine fleet counteracts climate change-induced reduction in global capacity factor, Nat Energy 7 (2022) 608–619. https://doi.org/10.1038/s41560-022-01056-z.
83. L.M. Miller, D.W. Keith, Observation-based solar and wind power capacity factors and power densities, Environ. Res. Lett. 13 (2018) 104008. https://doi.org/10.1088/1748-9326/aae102.
84. [International Energy Agency - Energy Technology Systems Analysis Programme] IEA-ETSAP, [International Renewable Energy Agency] IRENA, IEA-ETSAP & IRENA | Hydropower - Technology Brief, IEA-ETSAP [International Energy Agency - Energy Technology Systems Analysis Programme] and IRENA [International Renewable Energy Agency], Paris, France, 2015. https://www.irena.org/-/media/Files/IRENA/Agency/Publication/2015/IRENA-ETSAP_Tech_Brief_E06_Hydropower.pdf (accessed June 30, 2025).
85. [United States National Renewable Energy Laboratory] NREL, NREL | 2024 ATB [Annual Technology Baseline] Electricity - Hydropower, (2025). https://atb.nrel.gov/electricity/2024/hydropower (accessed June 30, 2025).
86. B. Falahati, A. Kargarian, Y. Fu, Timeframe capacity factor reliability model for isolated microgrids with renewable energy resources, in: 2012 IEEE Power and Energy Society General Meeting, 2012: pp. 1–8. https://doi.org/10.1109/PESGM.2012.6345546.
87. A. Bartle, Hydropower potential and development activities, Energy Policy 30 (2002) 1231–1239. https://doi.org/10.1016/S0301-4215(02)00084-8.
88. V. Fthenakis, H.C. Kim, Land use and electricity generation: A life-cycle analysis, Renewable and Sustainable Energy Reviews 13 (2009) 1465–1474. https://doi.org/10.1016/j.rser.2008.09.017.
89. [United States Department of Energy] DOE, DOE | Geothermal Basics (and footprint comparison for different power technologies), (2025). https://www.energy.gov/eere/geothermal/geothermal-basics (accessed June 27, 2025).
90. E.R. Sanseverino, M. Cellura, L.Q. Luu, M.A. Cusenza, N. Nguyen Quang, N.H. Nguyen, Life-Cycle Land-Use Requirement for PV in Vietnam, Energies 14 (2021) 861. https://doi.org/10.3390/en14040861.
91. N.B. Desai, S. Bandyopadhyay, Sustainability in Power Generation Systems, in: M.A. Abraham (Ed.), Encyclopedia of Sustainable Technologies, Elsevier, Oxford, 2017: pp. 157–163. https://doi.org/10.1016/B978-0-12-409548-9.10045-4.
92. O.A. Marzouk, Land-Use competitiveness of photovoltaic and concentrated solar power technologies near the Tropic of Cancer, Solar Energy 243 (2022) 103–119. https://doi.org/10.1016/j.solener.2022.07.051.
93. A. Holm, D. Jennejohn, L. Blodgett, GEA | Geothermal Energy and Greenhouse Gas Emissions, GEA [Geothermal Energy Association], Washington, D.C., USA, 2012. https://geothermal.org/sites/default/files/2021-02/Geothermal_Greenhouse_Emissions_2012_0.pdf (accessed June 28, 2025).
94. O.A. Marzouk, Dataset of total emissivity for CO2, H2O, and H2O-CO2 mixtures; over a temperature range of 300-2900 K and a pressure-pathlength range of 0.01-50 atm.m, Data in Brief 59 (2025) 111428. https://doi.org/10.1016/j.dib.2025.111428.
95. H. Kimura, Hydrogen sulfide: its production, release and functions, Amino Acids 41 (2011) 113–121. https://doi.org/10.1007/s00726-010-0510-x.
96. D. Hasterok, J.A. Halpin, A.S. Collins, M. Hand, C. Kreemer, M.G. Gard, S. Glorie, New Maps of Global Geological Provinces and Tectonic Plates, Earth-Science Reviews 231 (2022) 104069. https://doi.org/10.1016/j.earscirev.2022.104069.

 doi:10.20944/preprints202605.0188.v1

97. TWI, What is Geothermal Energy? How Does it Work?, (2025). https://www.twi-global.com/technical-knowledge/faqs/geothermal-energy/home.aspx (accessed June 27, 2025).
98. J.F. Bauer, M. Krumbholz, E. Luijendijk, D.C. Tanner, A numerical sensitivity study of how permeability, porosity, geological structure, and hydraulic gradient control the lifetime of a geothermal reservoir, Solid Earth 10 (2019) 2115–2135. https://doi.org/10.5194/se-10-2115-2019.
99. J.L. McCallum, S. Dogramaci, A. Bai, P.G. Cook, N.B. Engdahl, C.T. Simmons, G. Skrzypek, P.F. Grierson, Assessing Temporal Changes in Groundwater Recharge Using Spatial Variations in Groundwater Ages, Water Resources Research 56 (2020) e2020WR027240. https://doi.org/10.1029/2020WR027240.
100. P. Owens, A.G. Ryder, N.J.F. Blamey, Frequency Domain Fluorescence Lifetime Study of Crude Petroleum Oils, J Fluoresc 18 (2008) 997–1006. https://doi.org/10.1007/s10895-008-0330-5.
101. J.W. Day, H.C. Clark, C. Chang, R. Hunter, C.R. Norman, Life Cycle of Oil and Gas Fields in the Mississippi River Delta: A Review, Water 12 (2020) 1492. https://doi.org/10.3390/w12051492.
102. H. Puppala, S. K Jha, A.P. Singh, R. Madurai Elavarasan, P. Elia Campana, Identification and analysis of barriers for harnessing geothermal energy in India, Renewable Energy 186 (2022) 327–340. https://doi.org/10.1016/j.renene.2022.01.002.
103. H.H. Thorsteinsson, J.W. Tester, Barriers and enablers to geothermal district heating system development in the United States, Energy Policy 38 (2010) 803–813. https://doi.org/10.1016/j.enpol.2009.10.025.
104. [Global Energy Monitor] GEM, GGPT [Global Geothermal Power Tracker], (2025). https://globalenergymonitor.org/projects/global-geothermal-power-tracker/ (accessed December 12, 2025).
105. [Global Energy Monitor] GEM, GGPT [Global Geothermal Power Tracker] - Tracker Map, (2025). https://globalenergymonitor.org/projects/global-geothermal-power-tracker/tracker-map/ (accessed December 12, 2025).
106. [Global Energy Monitor] GEM, GGPT [Global Geothermal Power Tracker] - Summary Tables, (2025). https://globalenergymonitor.org/projects/global-geothermal-power-tracker/summary-tables/ (accessed December 12, 2025).
107. [Global Energy Monitor] GEM, GGPT [Global Geothermal Power Tracker] - Methodology, (2025). https://globalenergymonitor.org/projects/global-geothermal-power-tracker/methodology/ (accessed December 12, 2025).
108. [Global Energy Monitor] GEM, About Us (GEM: Global Energy Monitor), (2024). https://globalenergymonitor.org/about (accessed August 7, 2024).
109. S. Goswami, A.K. Rai, An assessment of prospects of geothermal energy in India for energy sustainability, Renewable Energy 233 (2024) 121118. https://doi.org/10.1016/j.renene.2024.121118.
110. S. Goswami, A.K. Rai, S. Tripathy, Re-visiting Geothermal Fluid Circulation, Reservoir Depth and Temperature of Geothermal Springs of India, Journal of Hydrology 612 (2022) 128131. https://doi.org/10.1016/j.jhydrol.2022.128131.
111. S. Goswami, A.K. Rai, Groundwater and hot-spring interactions around Bakreswar geothermal spring, Sustain. Water Resour. Manag. 10 (2024) 44. https://doi.org/10.1007/s40899-023-01012-z.
112. S. Goswami, A.K. Rai, Assessment of hot-springs and geothermal prospects for sustainable energy goals, Journal of Cleaner Production 512 (2025) 145637. https://doi.org/10.1016/j.jclepro.2025.145637.
113. Drishti, Geothermal Power in Ladakh, (2022). https://www.drishtiias.com/daily-updates/daily-news-analysis/geothermal-power-in-ladakh (accessed February 4, 2026).
114. [Central Bank Of Oman] CBO, CBO | Annual Reports, (2025). https://cbo.gov.om/Pages/AnnualReport.aspx (accessed June 28, 2025).
115. A.K. Nassar, Strategic energy transition in the Gulf Cooperation Council: Balancing economic, social, political, and environmental dynamics for sustainable development, International Journal of Green Energy 22 (2025) 1570–1586. https://doi.org/10.1080/15435075.2024.2435434.
116. R. Karmakar, V. Tripathi, P. Kumar, N. Singh, R. Kumar, The Interplay of Fossil Fuels and Natural Disasters, in: N. Singh, S.A. Babu (Eds.), Climate Crisis and Sustainable Solutions: Strategies for Adaptation, Mitigation and Sustainable Development, Springer Nature, Singapore, 2024: pp. 91–106. https://doi.org/10.1007/978-981-97-7110-3_6.

 doi:10.20944/preprints202605.0188.v1

117. [Central Bank Of Oman] CBO, CBO | Annual Report 2023, Muscat, Sultanate of Oman, 2023. https://cbo.gov.om/sites/assets/Documents/English/Publications/AnnualReports/Annual%20Report%202023%20ENG.pdf (accessed June 27, 2025).
118. O.A. Marzouk, Estimated electric conductivities of thermal plasma for air-fuel combustion and oxy-fuel combustion with potassium or cesium seeding, Heliyon 10 (2024) e31697. https://doi.org/10.1016/j.heliyon.2024.e31697.
119. [Low-Carbon Power] LCP, LCP | Electricity in Oman in 2024, (2025). https://lowcarbonpower.org/region/Oman (accessed June 28, 2025).
120. H. Ritchie, M. Roser, P. Rosado, OWiD [Our World in Data] | Energy, (2022). https://ourworldindata.org/energy/country/oman (accessed June 28, 2025).
121. O.A. Marzouk, Summary of the 2023 (1st edition) Report of TCEP (Tracking Clean Energy Progress) by the International Energy Agency (IEA), and Proposed Process for Computing a Single Aggregate Rating, E3S Web of Conferences 601 (2025) 00048. https://doi.org/10.1051/e3sconf/202560100048.
122. [Nama Power and Water Procurement Company] NPWP, OPWP's 7-YEAR STATEMENT (2023 – 2029) (Issue 17), NPWP [Nama Power and Water Procurement Company], Muscat, Sultanate of Oman, 2023. https://omanpwp.om/PDF/7%20Year%20Statement%20Issue%2017%202023%20-%202029.pdf (accessed June 28, 2025).
123. O.A. Marzouk, Evolution of the (Energy and Atmosphere) credit category in the LEED green buildings rating system for (Building Design and Construction: New Construction), from version 4.0 to version 4.1, Journal of Infrastructure, Policy and Development 8 (2024) 5306. https://doi.org/10.24294/jipd.v8i8.5306.
124. O.A. Marzouk, Urban air mobility and flying cars: Overview, examples, prospects, drawbacks, and solutions, Open Engineering 12 (2022) 662–679. https://doi.org/10.1515/eng-2022-0379.
125. O.A. Marzouk, Toward More Sustainable Transportation: Green Vehicle Metrics for 2023 and 2024 Model Years, in: A.K. Nagar, D.S. Jat, D.K. Mishra, A. Joshi (Eds.), Intelligent Sustainable Systems, Springer Nature Singapore, Singapore, 2024: pp. 261–272. https://doi.org/10.1007/978-981-99-7886-1_23.
126. O.A. Marzouk, Growth in the Worldwide Stock of E-Mobility Vehicles (by Technology and by Transport Mode) and the Worldwide Stock of Hydrogen Refueling Stations and Electric Charging Points between 2020 and 2022, Key Engineering Materials 972 (2023) 89–96. https://doi.org/10.4028/p-8IMGm4.
127. O.A. Marzouk, Aerial e-mobility perspective: Anticipated designs and operational capabilities of eVTOL urban air mobility (UAM) aircraft, Edelweiss Applied Science and Technology 9 (2025) 413–442. https://doi.org/10.55214/25768484.v9i1.4156.
128. O.A. Marzouk, Expectations for the Role of Hydrogen and Its Derivatives in Different Sectors through Analysis of the Four Energy Scenarios: IEA-STEPS, IEA-NZE, IRENA-PES, and IRENA-1.5°C, Energies 17 (2024) 646. https://doi.org/10.3390/en17030646.
129. O.A. Marzouk, Reduced-Order Modeling (ROM) of a Segmented Plug-Flow Reactor (PFR) for Hydrogen Separation in Integrated Gasification Combined Cycles (IGCC), Processes 13 (2025) 1455. https://doi.org/10.3390/pr13051455.
130. A.T. Hoang, A. Pandey, E. Lichtfouse, V.G. Bui, I. Veza, H.L. Nguyen, X.P. Nguyen, Green hydrogen economy: Prospects and policies in Vietnam, International Journal of Hydrogen Energy 48 (2023) 31049–31062. https://doi.org/10.1016/j.ijhydene.2023.05.306.
131. O.A. Marzouk, Power Density and Thermochemical Properties of Hydrogen Magnetohydrodynamic (H2MHD) Generators at Different Pressures, Seed Types, Seed Levels, and Oxidizers, Hydrogen 6 (2025) 31. https://doi.org/10.3390/hydrogen6020031.
132. O.A. Marzouk, OpenFOAM computational fluid dynamics (CFD) solver for magnetohydrodynamic open cycles, applied to the Sakhalin pulsed magnetohydrodynamic generator (PMHDG), Discover Applied Sciences 7 (2025) 1108. https://doi.org/10.1007/s42452-025-07744-1.
133. [Oman Vision 2040 Implementation Follow-up Unit] Om2040U, Oman Vision 2040 | Follow-up System, (2024). https://www.oman2040.om/organization?lang=en (accessed July 30, 2024).
134. [Oman Vision 2040 Implementation Follow-up Unit] Om2040U, Oman 2040 Vision Document, Om2040U [Oman Vision 2040 Implementation Follow-up Unit], Muscat, Sultanate of Oman, 2020. https://www.oman2040.om/VisionDocument?lang=en (accessed October 6, 2023).

 doi:10.20944/preprints202605.0188.v1

135. O.A. Marzouk, Benchmarks for the Omani higher education students-faculty ratio (SFR) based on World Bank data, QS rankings, and THE rankings, Cogent Education 11 (2024) 2317117. https://doi.org/10.1080/2331186X.2024.2317117.
136. O.A. Marzouk, Status of ABET Accreditation in the Arab World, Global Journal of Educational Studies 5 (2019) 1–10. https://doi.org/10.5296/gjes.v5i1.14218.
137. O.A. Marzouk, Accrediting Artificial Intelligence Programs from the Omani and the International ABET Perspectives, in: K. Arai (Ed.), Intelligent Computing, Springer International Publishing, Cham, Switzerland, 2021: pp. 462–474. https://doi.org/10.1007/978-3-030-80129-8_33.
138. V. Bhandari, V. Mohite, Role of higher education institutions in developing digital competence in Sultanate of Oman: a step towards achieving Vision 2040, Library Hi Tech ahead-of-print (2024). https://doi.org/10.1108/LHT-12-2023-0639.
139. A. Ravikumar, S. Al Subhi, K.M. Meesala, Community Perception and Attitude towards Sustainable Tourism and Environmental Protection Measures: An Exploratory Study in Muscat, Oman, Economies 10 (2022) 29. https://doi.org/10.3390/economies10020029.
140. P. Ordoñez de Pablos, Editorial: Digital innovation, competitiveness and governments: insights from Oman and other countries in the digital era, Journal of Science and Technology Policy Management 14 (2023) 801–806. https://doi.org/10.1108/JSTPM-09-2023-218.
141. O.A. Marzouk, Globalization and diversity requirement in higher education, in: The 11th World Multi-Conference on Systemics, Cybernetics and Informatics (WMSCI 2007) - The 13th International Conference on Information Systems Analysis and Synthesis (ISAS 2007), IIIS [International Institute of Informatics and Systemics], Orlando, Florida, USA, 2007: pp. 101–106.
142. [Ministry of Energy and Minerals in the Sultanate of Oman] MEM, MEM | The Sultanate of Oman's National Strategy for an Orderly Transition to Net Zero, MEM [Ministry of Energy and Minerals in the Sultanate of Oman]], Muscat, Sultanate of Oman, 2022. https://www.ea.gov.om/media/xdvpdu1w/oman-net-zero-report-2022_screen.pdf (accessed May 13, 2024).
143. O.A. Marzouk, Portrait of the Decarbonization and Renewables Penetration in Oman's Energy Mix, Motivated by Oman's National Green Hydrogen Plan, Energies 17 (2024) 4769. https://doi.org/10.3390/en17194769.
144. S. Al. Shibli, ICAO | Oman Vision 2040: A National Blueprint for Sustainable environment and Clean Energy, in: ICAO 2025 Environmental Report - Skyward Action - Realizing Aviation's Sustainable Future, ICAO [International Civil Aviation Organization], Montreal, Canada, 2025: pp. 257–259. https://www2023.icao.int/environmental-protection/Documents/EnvironmentalReports/2025/Envreport2025_71.pdf (accessed June 28, 2025).
145. A.H. Al-Badi, A. Malik, A. Gastli, Assessment of renewable energy resources potential in Oman and identification of barrier to their significant utilization, Renewable and Sustainable Energy Reviews 13 (2009) 2734–2739. https://doi.org/10.1016/j.rser.2009.06.010.
146. A.H. Al-Badi, A. Malik, A. Gastli, Sustainable energy usage in Oman—Opportunities and barriers, Renewable and Sustainable Energy Reviews 15 (2011) 3780–3788. https://doi.org/10.1016/j.rser.2011.06.007.
147. S.J. Zarrouk, H. Moon, Efficiency of geothermal power plants: A worldwide review, Geothermics 51 (2014) 142–153. https://doi.org/10.1016/j.geothermics.2013.11.001.
148. A.E. Williams, Industrial Energy Systems Handbook, 1st ed., River Publishers, New York, USA, 2023. https://doi.org/10.1201/9781003356431.
149. I. Dincer, M.F. Ezzat, 3.4 Renewable Energy Production, in: I. Dincer (Ed.), Comprehensive Energy Systems, Elsevier, Oxford, 2018: pp. 126–207. https://doi.org/10.1016/B978-0-12-809597-3.00310-2.
150. [National Center for Biotechnology Information] NCBI, PubChem | Butane, (2025). https://pubchem.ncbi.nlm.nih.gov/compound/7843 (accessed June 28, 2025).
151. [National Center for Biotechnology Information] NCBI, PubChem | Norflurane (R134a), (2025). https://pubchem.ncbi.nlm.nih.gov/compound/13129 (accessed June 28, 2025).
152. Z. Guzović, P. Rašković, Z. Blatarić, The comparision of a basic and a dual-pressure ORC (Organic Rankine Cycle): Geothermal Power Plant Velika Ciglena case study, Energy 76 (2014) 175–186. https://doi.org/10.1016/j.energy.2014.06.005.

 doi:10.20944/preprints202605.0188.v1

153. N. Kazemi, F. Samadi, Thermodynamic, economic and thermo-economic optimization of a new proposed organic Rankine cycle for energy production from geothermal resources, Energy Conversion and Management 121 (2016) 391–401. https://doi.org/10.1016/j.enconman.2016.05.046.
154. O.A. Marzouk, E.D. Huckaby, Simulation of a Swirling Gas-Particle Flow Using Different k-epsilon Models and Particle-Parcel Relationships, Engineering Letters 18 (2010). https://www.engineeringletters.com/issues_v18/issue_1/EL_18_1_07.pdf (accessed October 1, 2024).
155. O.A. Marzouk, A.H. Nayfeh, Reduction of the loads on a cylinder undergoing harmonic in-line motion, Physics of Fluids 21 (2009) 083103. https://doi.org/10.1063/1.3210774.
156. N. Nandaliarasyad, D.T. Maulana, P.S. Darmanto, Study of Development Scenarios for Bottoming Unit Binary Cycle to Utilize Exhaust Steam from Back Pressure Turbine Geothermal Power Plant, IOP Conf. Ser.: Earth Environ. Sci. 417 (2020) 012017. https://doi.org/10.1088/1755-1315/417/1/012017.
157. G. Godard, J. Reynes, J. Bascou, R.-P. Ménot, R. Palmeri, First rocks sampled in Antarctica (1840): Insights into the landing area and the Terre Adélie craton, Comptes Rendus Geoscience 349 (2017) 12–21. https://doi.org/10.1016/j.crte.2016.12.001.
158. H.A. Kazem, Renewable energy in Oman: Status and future prospects, Renewable and Sustainable Energy Reviews 15 (2011) 3465–3469. https://doi.org/10.1016/j.rser.2011.05.015.
159. T. Umar, Geothermal energy resources in Oman, Proceedings of the Institution of Civil Engineers - Energy 171 (2018) 37–43. https://doi.org/10.1680/jener.17.00001.
160. J.L. White, J.E. Goddard, H.M. Phillips, Use of Polymers To Control Water Production in Oil Wells, Journal of Petroleum Technology 25 (1973) 143–150. https://doi.org/10.2118/3672-PA.
161. B. Bierman, H. Al-Lawatia, M. DiFilippo, J. O'Donnell, Deploying enclosed trough for thermal EOR at commercial scale, AIP Conference Proceedings 2033 (2018) 030002. https://doi.org/10.1063/1.5067018.
162. O.A. Marzouk, Hydrogen Utilization as a Plasma Source for Magnetohydrodynamic Direct Power Extraction (MHD-DPE), IEEE Access 12 (2024) 167088–167107. https://doi.org/10.1109/ACCESS.2024.3496796.
163. F. Schütz, G. Winterleitner, E. Huenges, Geothermal exploration in a sedimentary basin: new continuous temperature data and physical rock properties from northern Oman, Geotherm Energy 6 (2018) 5. https://doi.org/10.1186/s40517-018-0091-6.
164. A. Shirazi, R.A. Taylor, G.L. Morrison, S.D. White, Solar-powered absorption chillers: A comprehensive and critical review, Energy Conversion and Management 171 (2018) 59–81. https://doi.org/10.1016/j.enconman.2018.05.091.
165. [Oman Sustainability Week] OSW, Oman to study geothermal potential of hot springs, (2025). https://omansustainabilityweek.com/newfront/news/13759 (accessed February 23, 2026).
166. O.A. Marzouk, Assessment of Three Databases for the NASA Seven-Coefficient Polynomial Fits for Calculating Thermodynamic Properties of Individual Species, International Journal of Aeronautical Science & Aerospace Research 5 (2018) 150–163. https://doi.org/10.19070/2470-4415-1800018.
167. [Global Energy Monitor] GEM, GEM | Makarem Oil and Gas Field (Oman), (2025). https://www.gem.wiki/Makarem_Oil_and_Gas_Field_(Oman).
168. Offshore Technology, Oil & gas field profile: Khazzan Unconventional Gas Field, Oman, (2021). https://www.offshore-technology.com/marketdata/oil-gas-field-profile-khazzan-unconventional-gas-field-oman/ (accessed February 23, 2026).
169. [Egypt Oil & Gas] EOG, EOG | Petronas to Acquire 10% Stake in Oman's Al Khazzan Field, (2018). https://egyptoil-gas.com/news/petronas-to-acquire-10-stake-in-omans-al-khazzan-field/ (accessed February 23, 2026).
170. T. Al Hosni, Evaluating the Hot springs in north Oman, heat source and potential of geothermal energy, Sultan Qaboos University House of Expertise (2016). https://squ.elsevierpure.com/en/projects/evaluating-the-hot-springs-in-north-oman-heat-source-and-potentia-2/ (accessed February 23, 2026).
171. O.A. Marzouk, Thermoelectric generators versus photovoltaic solar panels: Power and cost analysis, Edelweiss Applied Science and Technology 8 (2024) 406–428. https://doi.org/10.55214/25768484.v8i5.1697.
172. O.A. Marzouk, Detailed Derivation of the Scalar Explicit Expressions Governing the Electric Field, Current Density, and Volumetric Power Density in the Four Types of Linear Divergent MHD Channels Under a

 doi:10.20944/preprints202605.0188.v1

Unidirectional Applied Magnetic Field, Contemporary Mathematics 6 (2025) 4060–4100. https://doi.org/10.37256/cm.6420256918.

173. [United States National Renewable Energy Laboratory] NREL, SAM (System Advisor Model) | Geothermal Power, GitHub (2025). https://sam.nrel.gov/geothermal.html (accessed May 6, 2025).
174. [United States National Renewable Energy Laboratory] NREL, NREL | About, (2025). https://www.nrel.gov/about (accessed June 29, 2025).
175. O.A. Marzouk, Solar Heat for Industrial Processes (SHIP): An Overview of Its Categories and a Review of Its Recent Progress, Solar 5 (2025) 46. https://doi.org/10.3390/solar5040046.
176. [United States National Renewable Energy Laboratory] NREL, SAM (System Advisor Model) | Welcome, (2025). https://sam.nrel.gov (accessed May 30, 2025).
177. M.S. Siddiqui, A. Rasheed, M. Tabib, T. Kvamsdal, Numerical investigation of modeling frameworks and geometric approximations on NREL 5 MW wind turbine, Renewable Energy 132 (2019) 1058–1075. https://doi.org/10.1016/j.renene.2018.07.062.
178. J.I. Rojas-Sola, M.Á.G.-E. González, E.P. Martín, Computer-aided design and engineering: A study of windmills in la Mancha (Spain), Renewable Energy 31 (2006) 1471–1482. https://doi.org/10.1016/j.renene.2006.02.002.
179. [United States National Renewable Energy Laboratory] NREL, SAM (System Advisor Model) | About, (2025). https://sam.nrel.gov/about-sam.html (accessed May 6, 2025).
180. S. Naaim, B. Ouhammou, M. Aggour, B. Daouchi, E.M. El Mers, M. Mihi, Multi-Utility Solar Thermal Systems: Harnessing Parabolic Trough Concentrator Using SAM Software for Diverse Industrial and Residential Applications, Energies 17 (2024) 3685. https://doi.org/10.3390/en17153685.
181. [United States National Renewable Energy Laboratory] NREL, NREL | Software, (2025). https://www.nrel.gov/research/software (accessed June 29, 2025).
182. [United States National Renewable Energy Laboratory] NREL, NREL | SolTrace - Software Tool, (2025). https://www.nrel.gov/csp/soltrace (accessed June 29, 2025).
183. [United States National Renewable Energy Laboratory] NREL, NREL | REopt Web Tool - Energy Integration & Optimization, (2025). https://reopt.nrel.gov/tool (accessed June 29, 2025).
184. A. Glaws, R. King, M. Sprague, Deep learning for in situ data compression of large turbulent flow simulations, Phys. Rev. Fluids 5 (2020) 114602. https://doi.org/10.1103/PhysRevFluids.5.114602.
185. M. Hassanaly, N.T. Wimer, A. Felden, L. Esclapez, J. Ream, M.T. Henry de Frahan, J. Rood, M. Day, Symbolic construction of the chemical Jacobian of quasi-steady state (QSS) chemistries for Exascale computing platforms, Combustion and Flame 270 (2024) 113740. https://doi.org/10.1016/j.combustflame.2024.113740.
186. J. Sathyaraj, V. Sankardoss, Performance Analysis of Wind Power Forecasting via System Advisor Model Software, in: R.N. Shaw, P. Siano, S. Makhilef, A. Ghosh, S.L. Shimi (Eds.), Innovations in Electrical and Electronic Engineering, Springer Nature, Singapore, 2024: pp. 189–200. https://doi.org/10.1007/978-981-99-8289-9_15.
187. S.H. H., S.K. R, A.H. R., M.K. N., Performance Analysis of Standalone PV System using System Advisor Model- A Case Study, in: 2022 IEEE International Conference on Current Development in Engineering and Technology (CCET), 2022: pp. 1–4. https://doi.org/10.1109/CCET56606.2022.10080186.
188. N.A. DiOrio, J.M. Freeman, N. Blair, DC-connected Solar Plus Storage Modeling and Analysis for Behind-The-Meter Systems in the System Advisor Model, in: 2018 IEEE 7th World Conference on Photovoltaic Energy Conversion (WCPEC) (A Joint Conference of 45th IEEE PVSC, 28th PVSEC & 34th EU PVSEC), 2018: pp. 3777–3782. https://doi.org/10.1109/PVSC.2018.8547329.
189. D. Kesseli, M. Wagner, R. Guédez, C.S. Turchi, CSP-plant modeling guidelines and compliance of the system advisor model (SAM), AIP Conference Proceedings 2126 (2019) 170006. https://doi.org/10.1063/1.5117676.
190. E.K. Ezeanya, Massiha, Gholam H., Simon ,William E., Raush ,Jonathan R., T.L. and Chambers, System advisor model (SAM) simulation modelling of a concentrating solar thermal power plant with comparison to actual performance data, Cogent Engineering 5 (2018) 1524051. https://doi.org/10.1080/23311916.2018.1524051.

 doi:10.20944/preprints202605.0188.v1

191. M. Chennaif, M. Maaouane, H. Zahboune, M. Elhafyani, S. Zouggar, Tri-objective techno-economic sizing optimization of Off-grid and On-grid renewable energy systems using Electric system Cascade Extended analysis and system Advisor Model, Applied Energy 305 (2022) 117844. https://doi.org/10.1016/j.apenergy.2021.117844.
192. X. Yang, H. Zhao, M. Zhang, C. Ji, J. Xie, Performance comparison of CSP system with different heat transfer and storage fluids at multi-time scales by means of system advisor model, Solar Energy Materials and Solar Cells 269 (2024) 112765. https://doi.org/10.1016/j.solmat.2024.112765.
193. A. Dobos, T. Neises, M. Wagner, Advances in CSP Simulation Technology in the System Advisor Model, Energy Procedia 49 (2014) 2482–2489. https://doi.org/10.1016/j.egypro.2014.03.263.
194. M. Prilliman, DOE | GETEM in the System Advisor Model (SAM), NREL [United States National Renewable Energy Laboratory], Golden, Colorado, USA, 2023. https://www.osti.gov/biblio/1922402 (accessed June 30, 2025).
195. A. Jain, P. n. b. v. Chalapathi Rao, P. Choudhury, R. Mehta, S.K. Mittal, Optimization studies for hybrid and storage designs for parabolic solar trough systems with the system advisor model, Environmental Progress & Sustainable Energy 32 (2013) 1247–1254. https://doi.org/10.1002/ep.11719.
196. O.A. Marzouk, Evolutionary Computing Applied to Design Optimization, in: ASME 2007 International Design Engineering Technical Conferences and Computers and Information in Engineering Conference (IDETC-CIE 2007), (4–7 September 2007), ASME [American Society of Mechanical Engineers], Las Vegas, Nevada, USA, 2009: pp. 995–1003. https://doi.org/10.1115/DETC2007-35502.
197. L. Guzman, A. Henao, R. Vasquez, Simulation and Optimization of a Parabolic Trough Solar Power Plant in the City of Barranquilla by Using System Advisor Model (SAM), Energy Procedia 57 (2014) 497–506. https://doi.org/10.1016/j.egypro.2014.10.203.
198. N. Franchina, O. Kouaissah, G. Persico, M. Savini, Three-dimensional modeling and investigation of the flow around a troposkein vertical axis wind turbine at different operating conditions, Renewable Energy 199 (2022) 368–381. https://doi.org/10.1016/j.renene.2022.08.130.
199. Z. Yang, T. Wang, A.E. Copping, Modeling tidal stream energy extraction and its effects on transport processes in a tidal channel and bay system using a three-dimensional coastal ocean model, Renewable Energy 50 (2013) 605–613. https://doi.org/10.1016/j.renene.2012.07.024.
200. O.A. Marzouk, A.H. Nayfeh, Loads on a Harmonically Oscillating Cylinder, in: ASME 2007 International Design Engineering Technical Conferences and Computers and Information in Engineering Conference (IDETC-CIE 2007), ASME [American Society of Mechanical Engineers], Las Vegas, Nevada, USA, 2009: pp. 1755–1774. https://doi.org/10.1115/DETC2007-35562.
201. O.A. Marzouk, A.H. Nayfeh, Fluid Forces and Structure-Induced Damping of Obliquely-Oscillating Offshore Structures, in: The Eighteenth International Offshore and Polar Engineering Conference (ISOPE-2008), ISOPE [International Society of Offshore and Polar Engineers], Vancouver, British Columbia, Canada, 2008: pp. 460–468.
202. T.V.R. Sekhar, G. Nandan, R. Prakash, M. Muthuraman, Modeling a Renewable Energy Collector and Prediction in Different Flow Regimes Using CFD, Materials Today: Proceedings 5 (2018) 4563–4574. https://doi.org/10.1016/j.matpr.2017.12.026.
203. O.A. Marzouk, A.H. Nayfeh, Characterization of the flow over a cylinder moving harmonically in the cross-flow direction, International Journal of Non-Linear Mechanics 45 (2010) 821–833. https://doi.org/10.1016/j.ijnonlinmec.2010.06.004.
204. R. Lanzafame, S. Mauro, M. Messina, Wind turbine CFD modeling using a correlation-based transitional model, Renewable Energy 52 (2013) 31–39. https://doi.org/10.1016/j.renene.2012.10.007.
205. [United States Department of Energy] DOE, DOE | Geothermal Electricity Technology Evaluation Model (GETEM), (2025). https://www.energy.gov/eere/geothermal/geothermal-electricity-technology-evaluation-model (accessed June 30, 2025).
206. D.J. Entingh, DOE Geothermal Electricity Technology Evaluation Model (GETEM): Volume I - Technical Reference Manual, DOE [United States Department of Energy], Washington, D.C., USA, 2006. https://www1.eere.energy.gov/geothermal/pdfs/getem_vol_i_technical_manual.pdf (accessed June 30, 2025).

 doi:10.20944/preprints202605.0188.v1

207. S. Hanson, Geothermal Electricity Technology Evaluation Model (GETEM) Individual Case Files and Summary Spreadsheet (GETEM version Spring 2013), (2013). https://doi.org/10.15121/1148822.
208. [Idaho National Laboratory] INL, INL | Geothermal Electricity Technology Evaluation Model (GETEM) Individual Case Files and Summary Spreadsheet (GETEM version Spring 2013), (2025). https://catalog.data.gov/dataset/geothermal-electricity-technology-evaluation-model-getem-individual-case-files-and-summary-8b58b (accessed June 30, 2025).
209. A.K. Runchal, THE FUTURE OF CFD AND THE CFD OF THE FUTURE, Comput Thermal Scien 4 (2012) 517–524. https://doi.org/10.1615/ComputThermalScien.2012006511.
210. J.D. Denton, Some Limitations of Turbomachinery CFD, in: American Society of Mechanical Engineers Digital Collection, 2010: pp. 735–745. https://doi.org/10.1115/GT2010-22540.
211. O.A. Marzouk, E.D. Huckaby, Effects of Turbulence Modeling and Parcel Approach on Dispersed Two-Phase Swirling Flow, in: World Congress on Engineering and Computer Science 2009 (WCECS 2009), IAENG [International Association of Engineers], San Francisco, California, USA, 2009: pp. 1–11.
212. L. Wesley, J. Lee, L. Rodman, R. Childs, Toward an integrated CFD expert system environment, in: 36th AIAA Aerospace Sciences Meeting and Exhibit, AIAA [American Institute of Aeronautics and Astronautics], Reno, Nevada, USA, 1998: p. AIAA-98-1005. https://doi.org/10.2514/6.1998-1005.
213. M. Cortés, P. Fazio, J. Rao, W. Bustamante, S. Vera, CFD modeling of basic convection cases in enclosed environments: Needs of CFD beginners to acquire skills and confidence on CFD modeling, Rev. Ing. Constr. 29 (2014) 22–45. https://doi.org/10.4067/S0718-50732014000100002.
214. [European Commission] EC, JRC (The Joint Research Centre: EU Science Hub) | PVGIS (Photovoltaic Geographical Information System), (2025). https://re.jrc.ec.europa.eu/pvg_tools/en (accessed May 30, 2025).
215. G.E. Beghi, A DECADE OF RESEARCH ON THERMOCHEMICAL HYDROGEN AT THE JOINT RESEARCH CENTRE - ISPRA, in: T.N. Veziroglu, Z. Yajie, B. Deyou (Eds.), Hydrogen Systems, Pergamon, 1986: pp. 153–171. https://doi.org/10.1016/B978-1-4832-8375-3.50022-9.
216. L. Topp, D. Mair, L. Smillie, P. Cairney, Knowledge management for policy impact: the case of the European Commission's Joint Research Centre, Palgrave Commun 4 (2018) 87. https://doi.org/10.1057/s41599-018-0143-3.
217. [European Commission] EC, JRC [The Joint Research Centre: EU Science Hub] | PVGIS 5.3, (2025). https://joint-research-centre.ec.europa.eu/photovoltaic-geographical-information-system-pvgis/pvgis-releases/pvgis-53_en (accessed June 29, 2025).
218. [European Commission] EC, JRC [The Joint Research Centre: EU Science Hub] | SARAH Solar Radiation, (2025). https://joint-research-centre.ec.europa.eu/photovoltaic-geographical-information-system-pvgis/pvgis-data-download/sarah-solar-radiation_en (accessed June 29, 2025).
219. W. Wang, S. Li, S. Guo, M. Ma, S. Feng, L. Bao, Benchmarking urban local weather with long-term monitoring compared with weather datasets from climate station and EnergyPlus weather (EPW) data, Energy Reports 7 (2021) 6501–6514. https://doi.org/10.1016/j.egyr.2021.09.108.
220. M.F. Jentsch, P.A.B. James, L. Bourikas, A.S. Bahaj, Transforming existing weather data for worldwide locations to enable energy and building performance simulation under future climates, Renewable Energy 55 (2013) 514–524. https://doi.org/10.1016/j.renene.2012.12.049.
221. [European Commission] EC, PVGIS | User Manual, (2025). https://joint-research-centre.ec.europa.eu/photovoltaic-geographical-information-system-pvgis/getting-started-pvgis/pvgis-user-manual_en (accessed March 1, 2025).
222. [GreenwichMeanTime.com] GMT, GMT | Time now in GMT plus 4, (2025). https://greenwichmeantime.com/time-zone/gmt-plus-4/ (accessed June 29, 2025).
223. J.D. McTigue, J. Castro, G. Mungas, N. Kramer, J. King, C. Turchi, G. Zhu, Hybridizing a geothermal power plant with concentrating solar power and thermal storage to increase power generation and dispatchability, Applied Energy 228 (2018) 1837–1852. https://doi.org/10.1016/j.apenergy.2018.07.064.
224. K. Menberg, F. Heberle, H. Uhrmann, C. Bott, S. Grünäugl, D. Brüggemann, P. Bayer, Environmental impact of cogeneration in binary geothermal plants, Renewable Energy 218 (2023) 119251. https://doi.org/10.1016/j.renene.2023.119251.

 doi:10.20944/preprints202605.0188.v1

225. D. Budisulistyo, C.S. Wong, S. Krumdieck, Lifetime design strategy for binary geothermal plants considering degradation of geothermal resource productivity, Energy Conversion and Management 132 (2017) 1–13. https://doi.org/10.1016/j.enconman.2016.10.027.
226. M. El Haj Assad, E. Bani-Hani, M. Khalil, Performance of geothermal power plants (single, dual, and binary) to compensate for LHC-CERN power consumption: comparative study, Geotherm Energy 5 (2017) 1–16. https://doi.org/10.1186/s40517-017-0074-z.
227. K.J. Beckers, K.R. Young, H. Johnston, D.M. Snyder, Analysis of Geothermal Reservoir and Well Operational Conditions using Monthly Production Reports from Nevada and California, in: Geothermal Resources Council 41st Annual Meeting - Geothermal Energy: Power To Do More (GRC 2017), Salt Lake City, Utah, USA, 2017. https://www.osti.gov/biblio/1423750 (accessed July 22, 2025).
228. D. Chandrasekharam, J. Bundschuh, Geothermal Energy Resources for Developing Countries, CRC Press, Netherlands, 2002. https://books.google.com.om/books?id=aRkBJRLV8AwC (accessed July 22, 2025).
229. S.-C. Han, N. Schmerr, G. Neumann, S. Holmes, Global characteristics of porosity and density stratification within the lunar crust from GRAIL gravity and Lunar Orbiter Laser Altimeter topography data, Geophysical Research Letters 41 (2014) 1882–1889. https://doi.org/10.1002/2014GL059378.
230. A. Aboubakar, B.I. Manefouet, L.S. Komguep, E.T. Talom, C.R. Foueze, Y.L. Djonthu, Geotechnical characterization of Beka-Gotto rock massif (Adamawa Region-Cameroon) for the use in civil engineering, Journal of Nepal Geological Society 62 (2021) 47–57. https://doi.org/10.3126/jngs.v62i0.38693.
231. L. Seyitini, B. Belgasim, C.C. Enweremadu, Thermo-physical characterisation of natural rocks and impact analysis of variations in their thermo-physical properties on thermal storage performance, Energy Storage 6 (2024) e631. https://doi.org/10.1002/est2.631.
232. Z. Wang, P. Gao, S. Hu, Y. Wang, H. Fang, Y. Shi, C. Zhang, G. Jiang, Influence of Specific Heat Capacity Variation with Temperature and Other Important Parameters on the Thermal Reservoir Performance in the Geothermal Doublet System, International Journal of Energy Research 2024 (2024) 5567936. https://doi.org/10.1155/2024/5567936.
233. E. Burlutsky, D. Balzamov, V. Bronskaya, O. Kharitonova, L. Khairullina, O. Solovyeva, Influence of Temperature on the Thermal Properties of the Core Material - the Coefficient of Temperature Conductivity, Specific Heat Capacity, Thermal Conductivity, International Journal of Technology 14 (2023) 443. https://doi.org/10.14716/ijtech.v14i2.6009.
234. B. Tang, C. Zhu, M. Xu, T. Chen, S. Hu, Thermal conductivity of sedimentary rocks in the Sichuan basin, Southwest China, Energy Exploration & Exploitation 37 (2019) 691–720. https://doi.org/10.1177/0144598718804902.
235. R.K. Ramstad, K. Midttømme, H.T. Liebel, B.S. Frengstad, B. Willemoes-Wissing, Thermal conductivity map of the Oslo region based on thermal diffusivity measurements of rock core samples, Bull Eng Geol Environ 74 (2015) 1275–1286. https://doi.org/10.1007/s10064-014-0701-x.
236. C. Chen, C. Zhu, B. Zhang, B. Tang, K. Li, W. Li, X. Fu, Effect of Temperature on the Thermal Conductivity of Rocks and Its Implication for In Situ Correction, Geofluids 2021 (2021) 6630236. https://doi.org/10.1155/2021/6630236.
237. S. Fuchs, A. Förster, Rock thermal conductivity of Mesozoic geothermal aquifers in the Northeast German Basin, Geochemistry 70 (2010) 13–22. https://doi.org/10.1016/j.chemer.2010.05.010.
238. W. Ricks, J.D. Jenkins, Pathways to national-scale adoption of enhanced geothermal power through experience-driven cost reductions, Joule 9 (2025). https://doi.org/10.1016/j.joule.2025.101971.
239. C.E. Clark, C.B. Harto, J.L. Sullivan, M.Q. Wang, Water use in the development and operation of geothermal power plants., Argonne National Laboratory (ANL), Argonne, IL (United States), 2010. https://doi.org/10.2172/1013997.
240. EBARA Corporation, EBARA | BSP SS - Stainless steel submersible pumps - Databook 50Hz, EBARA Corporation, Tokyo, Japan, 2022. https://www.ebaraeurope.com/wp-content/plugins/woocommerce-onpage/storage/cache/7a0d95d557c48ca65284221151f5e797861e3caf.pdf/BSP%20SS%20Data%20book%2050Hz.pdf (accessed July 21, 2025).
241. J. McTigue, D. Wendt, K. Kitz, N. Kincaid, J. Gunderson, G. Zhu, Hybridizing Solar Heat with a Geothermal Binary Power Plant Using a Solar Steam Topping Turbine, in: Geothermal Resources Council Transactions

 doi:10.20944/preprints202605.0188.v1

Volume 42, Geothermal Rising, Reno, Nevada, USA, 2018: pp. 1985–2002. https://www.proceedings.com/42374.html (accessed July 22, 2025).

242. G.V. Tomarov, A.A. Shipkov, E.V. Sorokina, Investigation of a binary power plant using different single-component working fluids, International Journal of Hydrogen Energy 41 (2016) 23183–23187. https://doi.org/10.1016/j.ijhydene.2016.09.165.
243. A. Franco, M. Villani, Optimal design of binary cycle power plants for water-dominated, medium-temperature geothermal fields, Geothermics 38 (2009) 379–391. https://doi.org/10.1016/j.geothermics.2009.08.001.
244. M.A. Ehyaei, A. Ahmadi, M.A. Rosen, A. Davarpanah, Thermodynamic Optimization of a Geothermal Power Plant with a Genetic Algorithm in Two Stages, Processes 8 (2020) 1277. https://doi.org/10.3390/pr8101277.
245. M.A. Al-Weshahi, F. Latrash, A. Anderson, B. Agnew, Working fluid selection of low grade heat geothermal Organic Rankine Cycle (ORC), International Journal of Thermal Technologies 4 (2014) 6–12.
246. Y.S.H. Najjar, Comparison of performance for cogeneration systems using single- or twin-shaft gas turbine engines, Applied Thermal Engineering 17 (1997) 113–124. https://doi.org/10.1016/S1359-4311(96)00028-2.
247. I. Kocabas, Geothermal reservoir characterization via thermal injection backflow and interwell tracer testing, Geothermics 34 (2005) 27–46. https://doi.org/10.1016/j.geothermics.2004.09.003.
248. W. Ping, P. Wenqing, L. Shiyin, G. Baozhu, X. Chang, C. Lei, Optimization technology and application of horizontal well trajectory drilled in ultra-deep carbonate reservoirs in Tazhong area, Tarim Basin, China Petroleum Exploration 24 (2019) 123–128.
249. A. Ewusi, J.S. Kuma, H.J. Voigt, Utility of the 2-D Multi-Electrode Resistivity Imaging Technique in Groundwater Exploration in the Voltaian Sedimentary Basin, Northern Ghana, Nat Resour Res 18 (2009) 267–275. https://doi.org/10.1007/s11053-009-9102-4.
250. D. Luo, A. Maheshwari, A. Danielescu, J. Li, Y. Yang, Y. Tao, L. Sun, D.K. Patel, G. Wang, S. Yang, T. Zhang, L. Yao, Autonomous self-burying seed carriers for aerial seeding, Nature 614 (2023) 463–470. https://doi.org/10.1038/s41586-022-05656-3.
251. H. Wang, M. Sharma, A Rapid Injection Flow-Back Test RIFT to Estimate In-Situ Stress and Pore Pressure in a Single Test, in: OnePetro, 2020. https://doi.org/10.2118/199732-MS.
252. B. Stenger, T. Pham, N. Al-Afaleg, P. Lawrence, Tilted original oil/water contact in the Arab-D reservoir, Ghawar field, Saudi Arabia, GeoArabia 8 (2003) 9–42. https://doi.org/10.2113/geoarabia080109.
253. B. Radmehr, UNU | Preliminary Design of a Proposed Geothermal Power Plant IN NW-Sabalan Area, Azerbaijan-Iran, UNU [United Nations University], Reykjavík, Iceland, 2005. https://rafhladan.is/bitstream/handle/10802/23505/UNU-GTP-2005-15.pdf (accessed July 22, 2025).
254. C. Risch, E. Eastham, Marshall University | Geothermal EnergyThe Economics of West Virginia's EGS Potential, Marshall University, Huntington, West Virginia, USA, 2012. https://www.marshall.edu/cber/files/2021/04/2012_06_XX_GeothermalEGS.pdf (accessed July 22, 2025).
255. [International Energy Agency - Energy Technology Systems Analysis Program] IEA ETSAP, IEA-ETSAP | Geothermal Heat and Power - Technology Brief E07, IEA-ETSAP [International Energy Agency - Energy Technology Systems Analysis Program], Paris, France, 2010. https://iea-etsap.org/E-TechDS/PDF/E07-geoth_energy-GS-gct_ADfinal_gs.pdf (accessed July 22, 2025).
256. L. Al-Ghussain, T. Johnson, J. Martinek, Z. Ma, Techno-Economic Feasibility Analysis of Solar Industrial Process Heat Using Particle Thermal Energy Storage, in: American Society of Mechanical Engineers Digital Collection, 2024. https://doi.org/10.1115/ES2024-131139.
257. S. Günhan, D. Arditi, Budgeting Owner's Construction Contingency, Journal of Construction Engineering and Management 133 (2007) 492–497. https://doi.org/10.1061/(ASCE)0733-9364(2007)133:7(492).
258. J.N.T. Addo, Determination Of Contingency Sum For Building Projects In Ghana, AFRICAN JOURNAL OF APPLIED RESEARCH 1 (2015). https://ajaronline.com/index.php/AJAR/article/view/152 (accessed July 22, 2025).
259. D. Baccarini, P.E.D. Love, Statistical Characteristics of Cost Contingency in Water Infrastructure Projects, Journal of Construction Engineering and Management 140 (2014) 04013063. https://doi.org/10.1061/(ASCE)CO.1943-7862.0000820.

 doi:10.20944/preprints202605.0188.v1

260. R.A. Jimoh, S.M. Adama, Assessment of Contingency Sum in Relation to the Total Cost of Renovation Work in Public Schools in Abuja, Nigeria, International Journal of Managerial Studies and Research 2 (2014) 55–63.
261. R. Westaway, Deep Geothermal Single Well heat production: critical appraisal under UK conditions, Quarterly Journal of Engineering Geology and Hydrogeology 51 (2018) 424–449. https://doi.org/10.1144/qjegh2017-029.
262. E.D. Mattson, G. Neupane, INL | LCOH Estimated from Existing Geothermal District Heating Systems in the U.S., INL [Idaho National Laboratory], Idaho Falls, Idaho, USA, 2017. https://www.osti.gov/biblio/1402044 (accessed July 22, 2025).
263. D. Saner, R. Juraske, M. Kübert, P. Blum, S. Hellweg, P. Bayer, Is it only CO_2 that matters? A life cycle perspective on shallow geothermal systems, Renewable and Sustainable Energy Reviews 14 (2010) 1798–1813. https://doi.org/10.1016/j.rser.2010.04.002.
264. J.W. Tester, K.F. Beckers, A.J. Hawkins, M.Z. Lukawski, The evolving role of geothermal energy for decarbonizing the United States, Energy Environ. Sci. 14 (2021) 6211–6241. https://doi.org/10.1039/D1EE02309H.
265. T. Agemar, J. Weber, I.S. Moeck, Assessment and Public Reporting of Geothermal Resources in Germany: Review and Outlook, Energies 11 (2018) 332. https://doi.org/10.3390/en11020332.
266. Argaam Investment, Argaam | Fed's preferred inflation gauge slows to 2.5% in April, (2025). https://www.argaam.com/en/article/articledetail/id/1818027 (accessed July 22, 2025).
267. Eurostat, Eurostat | Annual inflation up to 2.5% in the euro area, (2025). https://ec.europa.eu/eurostat/web/products-euro-indicators/w/2-24022025-ap (accessed July 22, 2025).
268. [Oman News Agency] ONA, ONA | Inflation Rate in Oman Reaches 1.27% by September 2023, (2023). https://omannews.gov.om/topics/en/80/show/114671 (accessed July 22, 2025).
269. TRADING ECONOMICS, TRADING ECONOMICS | Oman Inflation Rate, (2025). https://tradingeconomics.com/oman/inflation-cpi (accessed July 22, 2025).
270. [National Bank of Oman] NBO, NBO | Currency Converter, (2025). https://www.nbo.om/en/Pages/Tools/Currency-Converter.aspx (accessed June 29, 2025).
271. Bank Muscat, Bank Muscat | Currency Rates, (2025). https://www.bankmuscat.com/en/Pages/marketrates.aspx (accessed June 29, 2025).
272. O.A. Marzouk, Facilitating Digital Analysis and Exploration in Solar Energy Science and Technology through Free Computer Applications, Engineering Proceedings 31 (2022) 75. https://doi.org/10.3390/ASEC2022-13920.
273. E.M. Tonita, A.C.J. Russell, C.E. Valdivia, K. Hinzer, Optimal ground coverage ratios for tracked, fixed-tilt, and vertical photovoltaic systems for latitudes up to 75°N, Solar Energy 258 (2023) 8–15. https://doi.org/10.1016/j.solener.2023.04.038.
274. S. Sinha, S.S. Chandel, Analysis of fixed tilt and sun tracking photovoltaic–micro wind based hybrid power systems, Energy Conversion and Management 115 (2016) 265–275. https://doi.org/10.1016/j.enconman.2016.02.056.
275. J. Anderson, Introduction to Flight, 7th edition, McGraw-Hill Education, New York, 2009.
276. O.A. Marzouk, Coupled differential-algebraic equations framework for modeling six-degree-of-freedom flight dynamics of asymmetric fixed-wing aircraft, International Journal of Applied and Advanced Sciences 12 (2025) 30–51. https://doi.org/10.21833/ijaas.2025.01.004.
277. D. Divakar, R.S. B L, Simulation of The International Standard Atmosphere for Flight Reference, in: 2022 International Interdisciplinary Humanitarian Conference for Sustainability (IIHC), 2022: pp. 65–68. https://doi.org/10.1109/IIHC55949.2022.10060718.
278. O.A. Marzouk, InvSim algorithm for pre-computing airplane flight controls in limited-range autonomous missions, and demonstration via double-roll maneuver of Mirage III fighters, Scientific Reports 15 (2025) 23382. https://doi.org/10.1038/s41598-025-07639-6.
279. K.E. Trenberth, Seasonal variations in global sea level pressure and the total mass of the atmosphere, Journal of Geophysical Research: Oceans 86 (1981) 5238–5246. https://doi.org/10.1029/JC086iC06p05238.

 doi:10.20944/preprints202605.0188.v1

280. H. Struchtrup, Thermodynamics and Energy Conversion, 1st ed., Springer-Verlag, Berlin, Germany, 2014. https://link.springer.com/book/10.1007/978-3-662-43715-5 (accessed August 21, 2021).
281. J. Spurk, N. Aksel, Fluid Mechanics, 2nd ed., Springer Science & Business Media, Leipzig, Germany, 2007. https://books.google.com.om/books?id=MZH8j-2U4zkC (accessed June 30, 2025).
282. D.J. Vecellio, S.T. Wolf, R.M. Cottle, W.L. Kenney, Evaluating the 35°C wet-bulb temperature adaptability threshold for young, healthy subjects (PSU HEAT Project), Journal of Applied Physiology 132 (2022) 340–345. https://doi.org/10.1152/japplphysiol.00738.2021.
283. R. Davies-Jones, An Efficient and Accurate Method for Computing the Wet-Bulb Temperature along Pseudoadiabats, (2008). https://doi.org/10.1175/2007MWR2224.1.
284. [United States National Weather Service] NWS, NWS | Temperature - Dry Bulb/Web Bulb/Dew Point, (2025). https://www.weather.gov/source/zhu/ZHU_Training_Page/definitions/dry_wet_bulb_definition/dry_wet_bulb.html (accessed June 30, 2025).
285. [Holiday Weather Limited] HWL, Holiday Weather Limited | Muscat, Oman Average Weather, (2025). https://www.holiday-weather.com/muscat/averages (accessed July 21, 2025).
286. B. Buckley, MLA | Detailed Temperature and Humidity Climatology for Middle East Ports, MLA [Meat & Livestock Australia], North Sydney, NSW, Australia, 2009. https://www.mla.com.au/contentassets/5ff22da6b93d4ab5b51b0b429b8887eb/w.liv.0267_final_report.pdf (accessed July 21, 2025).
287. O.A. Marzouk, A.H. Nayfeh, Mitigation of Ship Motion Using Passive and Active Anti-Roll Tanks, in: ASME 2007 International Design Engineering Technical Conferences and Computers and Information in Engineering Conference (IDETC-CIE 2007), ASME [American Society of Mechanical Engineers], Las Vegas, Nevada, USA, 2009: pp. 215–229. https://doi.org/10.1115/DETC2007-35571.
288. O.A. Marzouk, A.H. Nayfeh, New Wake Models With Capability of Capturing Nonlinear Physics, in: ASME 2008 27th International Conference on Offshore Mechanics and Arctic Engineering (OMAE 2008), ASME [American Society of Mechanical Engineers], Estoril, Portugal, 2009: pp. 901–912. https://doi.org/10.1115/OMAE2008-57714.
289. S. Bhatti, A.R. Khan, A. Zoha, S. Hussain, R. Ghannam, A Machine Learning Frontier for Predicting LCOE of Photovoltaic System Economics, Advanced Energy and Sustainability Research 5 (2024) 2300178. https://doi.org/10.1002/aesr.202300178.
290. P. Dumas, M. Antics, P. Ungemach, GeoElec Project | Report on Geothermal Drilling, 2013. http://www.geoelec.eu/wp-content/uploads/2011/09/D-3.3-GEOELEC-report-on-drilling.pdf (accessed July 21, 2025).
291. S. Ba Saloom, M. Ba Geri, M. Suhail, X. Ge, Advancements in Drilling Fluid Optimization for Enhanced Geothermal Energy Extraction, in: SPE Eastern Regional Meeting, OnePetro, Wheeling, West Virginia, USA, 2024. https://doi.org/10.2118/221370-MS.
292. M.Y. Amer, A.M. Salem, M.S. Farahat, S.K. Elsayed, Reducing Drilling Cost in Geothermal Wells by Drilling Technology Optimization, Journal of Mining and Environment 16 (2025) 767–788. https://doi.org/10.22044/jme.2025.14206.2647.
293. B.M. Sveinbjornsson, S. Thorhallsson, Drilling performance, injectivity and productivity of geothermal wells, Geothermics 50 (2014) 76–84. https://doi.org/10.1016/j.geothermics.2013.08.011.
294. Sulzer, Sulzer | Production pump for geothermal plants, (2025). https://www.sulzer.com/en/shared/applications/production-pump-for-geothermal-plants (accessed July 21, 2025).
295. A. Colin Cameron, F.A.G. Windmeijer, An *R*-squared measure of goodness of fit for some common nonlinear regression models, Journal of Econometrics 77 (1997) 329–342. https://doi.org/10.1016/S0304-4076(96)01818-0.
296. O.A. Marzouk, Benchmarking Retention, Progression, and Graduation Rates in Undergraduate Higher Education Across Different Time Windows, Cogent Education 12 (2025) 2498170. https://doi.org/10.1080/2331186X.2025.2498170.

 doi:10.20944/preprints202605.0188.v1

297. A.S. Malik, S. Al-Zubeidi, Electricity tariffs based on long-run marginal costs for central grid system of Oman, Energy 31 (2006) 1703–1714. https://doi.org/10.1016/j.energy.2005.11.010.
298. [Omani Authority for Public Services Regulation] APSR, APSR | Electricity and Water Tariffs in Oman, (2025). https://apsr.om/en/tariffs (accessed June 30, 2025).
299. [Omani Authority for Public Services Regulation] APSR, APSR | Applying Cost Reflective Tariffs (CRT) in Oman to Large Electricity Consumer with More Than 100 MWh Annual Consumption (in Arabic), APSR [Omani Authority for Public Services Regulation], Muscat, Sultanate of Oman, 2021. https://apsr.om/pdfs/crt/CRT-Customer2021AR.pdf (accessed June 30, 2025).
300. [Omani Authority for Public Services Regulation] APSR, APSR | Statement of Charges Cost Reflective Tariffs (CRT) in Oman 2025, APSR [Omani Authority for Public Services Regulation], Muscat, Sultanate of Oman, 2025. https://apsr.om/pdfs/crt/CRT-2025-EnglishVersionleaflet%28002%29.pdf (accessed May 31, 2025).
301. F. Simões, C. Henriques, N.C. Figueiredo, P.P. da Silva, Efficient power purchase agreement structures for meeting corporate electricity needs with solar energy, Energy 322 (2025) 135651. https://doi.org/10.1016/j.energy.2025.135651.
302. A. Thumann, E. Woodroof, Energy Project Financing: Resources and Strategies for Success, CRC Press, Gistrup, Denmark, 2021. https://books.google.com.om/books?id=vXQWEAAAQBAJ (accessed June 30, 2025).
303. J. Burdick, P. Schmidt, Install Your Own Solar Panels: Designing and Installing a Photovoltaic System to Power Your Home, Storey Publishing, North Adams, Massachusetts, USA, 2017. https://books.google.com.om/books?id=rsUpDwAAQBAJ.
304. A. Saidi, C. Benachaiba, Comparison of IC and P&O algorithms in MPPT for grid connected PV module, in: 2016 8th International Conference on Modelling, Identification and Control (ICMIC), 2016: pp. 213–218. https://doi.org/10.1109/ICMIC.2016.7804300.
305. S. White, Solar Photovoltaic Basics: A Study Guide for the NABCEP Associate Exam, 2nd ed., Routledge, London, UK, 2018. https://doi.org/10.4324/9781315103396.
306. [Global Energy Monitor] GEM, Ibri 2 Solar - Global Energy Monitor Profile, (2024). https://www.gem.wiki/Ibri_2_Solar (accessed August 7, 2024).
307. [Sultanate of Oman Minister of Energy and Minerals] MEM, MEM | Ibri 2 Solar IPP, (2025). https://mem.gov.om/en-us/Our-Business/Renewable-Energy-and-Hydrogen/Renewable-Energy-and-Hydrogen-Projects/ArtMID/732/ArticleID/1324/Ibri-2-Solar-IPP (accessed June 9, 2025).
308. ENF Ltd., ENF | Solar System Installers in Oman - PV Companies List, (2025). https://www.enfsolar.com/directory/installer/Oman (accessed June 30, 2025).
309. [Xiamen Universe Solar Technologies Co. UNISOLAR Ltd.], UNISOLAR | Oman 100kw Solar Carport Mounting System, (2020). https://www.uisolar.com/oman-100kw-solar-carport-mounting-system_n22 (accessed July 22, 2025).
310. M.A. Rodrigues, J.U. Junior, Performance Analysis through Merit Indexes of a Carport located in Neoville campus of the Federal University of Technology of Paraná, in: 2024 16th Seminar on Power Electronics and Control (SEPOC), 2024: pp. 1–7. https://doi.org/10.1109/SEPOC63090.2024.10747485.
311. O.A. Marzouk, Recommended LEED-Compliant Cars, SUVs, Vans, Pickup Trucks, Station Wagons, and Two Seaters for Smart Cities Based on the Environmental Damage Index (EDX) and Green Score, in: M. Ben Ahmed, A.A. Boudhir, R. El Meouche, İ.R. Karaș (Eds.), Innovations in Smart Cities Applications Volume 7, Springer Nature Switzerland, Cham, Switzerland, 2024: pp. 123–135. https://doi.org/10.1007/978-3-031-53824-7_12.
312. A. Gonzalez Gonzalez, J.V. Alvarez Cabal, V. Rodríguez Montequin, J. Villanueva Balsera, R. Peón Menéndez, CSP Quasi-Dynamic Performance Model Development for All Project Life Cycle Stages and Considering Operation Modes. Validation Using One Year Data, Energies 14 (2021) 14. https://doi.org/10.3390/en14010014.

 doi:10.20944/preprints202605.0188.v1

313. L. Khalvati, G. Camacho, R. Rodrigues, S. Parkinson, Designing Sustainable and Eco-Friendly Lighting Solutions for Campus Safety: The Role of Concentrated Solar-powered Light Poles, in: 2023 International Conference on Computational Intelligence and Sustainable Engineering Solutions (CISES), 2023: pp. 61–65. https://doi.org/10.1109/CISES58720.2023.10183540.
314. S. Roga, A. Lokesh, S. Jain, A.A.N. Vinay, R. Chauhan, C. Karthik, S. Das, Y. Kumar, Assessment of Sessional Solar Energy Using PVsyst and SAM, in: A. Khosla, M. Kolhe (Eds.), Renewable Energy Optimization, Planning and Control, Springer Nature, Singapore, 2023: pp. 103–110. https://doi.org/10.1007/978-981-19-8963-6_10.
315. J.M. Freeman, NREL | Improvement and Validation of the System Advisor Model, NREL [United States National Renewable Energy Laboratory], Golden, Colorado, USA, 2018. https://www.osti.gov/servlets/purl/1495693 (accessed July 22, 2025).
316. A. Boretti, J. Nayfeh, W. Al-Kouz, Validation of SAM Modeling of Concentrated Solar Power Plants, Energies 13 (2020) 1949. https://doi.org/10.3390/en13081949.
317. [United States National Renewable Energy Laboratory] NREL, SAM (System Advisor Model) | GitHub - SAM Simulation Core (SSC) - geothermal_costs_common_data.h, GitHub (2025). https://github.com/NREL/ssc/blob/patch/test/input_cases/geothermal_costs_common_data.h (accessed July 19, 2025).
318. [United States National Renewable Energy Laboratory] NREL, SAM (System Advisor Model) | GitHub - SAM Simulation Core (SSC) - geothermal_common_data.h, GitHub (2025). https://github.com/NREL/ssc/blob/patch/test/input_cases/geothermal_common_data.h (accessed July 19, 2025).
319. [United States National Renewable Energy Laboratory] NREL, SAM (System Advisor Model) | GitHub - SAM Simulation Core (SSC) - cmod_geothermal_costs.cpp, GitHub (2025). https://github.com/NREL/ssc/blob/patch/ssc/cmod_geothermal.cpp (accessed July 19, 2025).
320. [United States National Renewable Energy Laboratory] NREL, SAM (System Advisor Model) | GitHub - SAM Simulation Core (SSC) - cmod_geothermal_costs_eqns.cpp, GitHub (2025). https://github.com/NREL/ssc/blob/patch/ssc/cmod_geothermal.cpp (accessed July 19, 2025).
321. [United States National Renewable Energy Laboratory] NREL, SAM (System Advisor Model) | GitHub - SAM Simulation Core (SSC) - lib_geothermal.cpp, GitHub (2025). https://github.com/NREL/ssc/blob/patch/shared/lib_geothermal.cpp (accessed July 19, 2025).
322. [United States National Renewable Energy Laboratory] NREL, SAM (System Advisor Model) | GitHub - SAM Simulation Core (SSC) - cmod_geothermal.cpp, GitHub (2025). https://github.com/NREL/ssc/blob/patch/ssc/cmod_geothermal.cpp (accessed July 19, 2025).
323. [United States National Renewable Energy Laboratory] NREL, SAM (System Advisor Model) | GitHub - SAM Simulation Core (SSC), GitHub (2025). https://github.com/NREL/ssc/tree/patch/ssc (accessed July 19, 2025).
324. T.S. Lowry, J.T. Finger, C.R. Carrigan, A. Foris, M.B. Kennedy, T.F. Corbet, C.A. Doughty, S. Pye, E.L. Sonnenthal, GeoVision Analysis: Reservoir Maintenance and Development Task Force Report (GeoVision Analysis Supporting Task Force Report : Reservoir Maintenance and Development), SNL [Sandia National Laboratories], Albuquerque, New Mexico, USA, and Livermore, California, USA, 2017. https://doi.org/10.2172/1394062.
325. World Bank, World Bank | The World by Income and Region, (2025). https://datatopics.worldbank.org/world-development-indicators/the-world-by-income-and-region.html (accessed July 18, 2025).